Doctoral thesis

mgr inż. Piotr Osiński

The influence of water saturation state of soil on slopes stability conditions

Wpływ stanu nasycenia gruntu wodą na warunki stateczności skarp

Dyscyplina: Inżynieria lądowa, geodezja i transport

Supervisor:
Prof. dr hab. inż. Eugeniusz Koda

Institute of Civil Engineering
Warsaw University of Life Sciences

Co-Supervisor:
Professor David Toll FICE FLSW Eur Ing

Department of Engineering
Durham University, UK

Reviewers:

Prof. dr. hab. inż. Katarzyna Zabielska-Adamska

Faculty of Civil Engineering and Environmental Sciences
Bialystok University of Technology

Dr hab. inż. Jędrzej Wierzbicki, prof UAM

Faculty of Geographical and Geological Sciences
Adam Mickiewicz University

Warsaw, 2024

**WARSAW
UNIVERSITY
OF LIFE SCIENCES**

Oświadczenie promotora rozprawy doktorskiej

Oświadczam, że niniejsza rozprawa została przygotowana pod moim kierunkiem i stwierdzam,
że spełnia warunki do przedstawienia jej w postępowaniu o nadanie stopnia naukowego doktora.

Data ....12.10.2024.................... Czytelny podpis promotora ....

Oświadczenie autora rozprawy doktorskiej

Świadom/a odpowiedzialności prawnej, w tym odpowiedzialności karnej za złożenie fałszywego oświadczenia, oświadczam, że niniejsza rozprawa doktorska została napisana przez mnie samodzielnie i nie zawiera treści uzyskanych w sposób niezgodny z obowiązującymi przepisami prawa, w szczególności z ustawą z dnia 4 lutego 1994 r. o prawie   autorskim
i prawach pokrewnych (tj. z dnia 28 października 2022 r., Dz.U. z 2022 r. poz. 2509 ze zm.)

Oświadczam, że przedstawiona rozprawa nie była wcześniej podstawą żadnej procedury związanej z uzyskaniem stopnia naukowego doktora.

Oświadczam ponadto, że niniejsza wersja rozprawy jest identyczna z załączoną wersją elektroniczną.

Przyjmuję do wiadomości, że rozprawa doktorska poddana zostanie procedurze antyplagiatowej.

Data 12.10.2024.................................. Czytelny podpis autora rozprawy ....

Acknowledgements

In memory of Anna and Leszek Data

Abstract

The influence of water saturation state of soil on slopes stability conditions

Climate change has been recently recognized as a one of the factors that could affect the safety of engineering structures all around the world. One of the nowadays geotechnical scientific challenges is the assessment of long-term earth structures stability and safety, in terms of climate change influences. For the purpose of eliminating severe effects of environmental conditions impact on infrastructure there is an urgent need to develop an interdisciplinary approach that would help identifying vulnerable elements of the earth infrastructure. It is strongly believed that the approach should be based on prediction of failures that could link both hydrological and geotechnical issues. This will not only help to increase the long-term safety but also could significantly reduce potential repair costs of earth infrastructure. The climate change is expected to affect the long-term stability of geotechnical safety of engineered slopes (e.g. road and railway embankments, earth dams or levees) through transient soil modifications. Extreme events, such as precipitation peaks and droughts, are at core of this. It is a result of several types of impacts such as: changing the slope's soil-water pressure and probably soil evolution, changing the slope's vegetation cover characteristics, causing surface and internal erosion of the slope through water flow and tension cracks, due to desiccation. Those processes affects and usually increase the permeability and hence groundwater regime significantly. It has the potential to affect road or railway embankments and cuttings built with soil material in an unsaturated state that is exposed to the climate. The present thesis aims to investigate how continuously changing atmospheric condition (mainly precipitation) will affect the serviceability and safety of earth structures. The main part of the research was to perform the the studies on the fill material used in the construction of the experimental embankment (BIONICS), and the material of which the properties had to be investigated as a part of the MUMOLADE project. The tests were carried out to understand the hydro-mechanical behaviour of the soil, which is a sandy clay of medium plasticity and granular material of fine sand. The research is divided into 3 group of tests. The first group involved the determination of the soil water retention behaviour and the mechanical behaviour under unsaturated conditions for cohesive soil samples. Soil water retention curves (SWRC) were determined by a series of tests performed on compacted samples comprising various techniques (high capacity suction probe and pressure plate). Total and matric suction SWRC following primary drying paths from 26% of water content were determined for

sandy clay. In addition, a series of tests of continuous drying and wetting, reflecting changing atmospheric conditions (moisture content) were performed using a newly developed research stage, at Durham University. The SWRC determination tests revealed that the stress state and history have a significant impact on the hydraulic behaviour of tested material. For continuous wetting and drying method it is shown that the major differences occur in the first cycle and smaller differences are seen in subsequent scanning curve paths. For the investigation of the mechanical behaviour cohesive samples a series of constant water content triaxial tests were carried out in double cell triaxial rig on as-compacted samples, and also samples wetted and dried from as-compacted conditions of 15%, and 20%. The mechanical behavior of the sandy clay soil was found to be governed by the initial conditions, the as-compacted conditions. Although the critical state stress ratio, was not affected by the initial water content, the differences in volumetric behavior led to differences for samples subjected to wetting and drying after compaction. Samples that were dried back to a particular water content had a higher strength than samples compacted at that water content. Since specimens were at high degrees of saturation, calculations based on effective stress showed a reasonable interpretation of the data. The second group of tests involved determination of hydro-mechanical behaviour of granular soil samples. They comprise the SWRC determination using modified suction probe and axis translation method using triaxial cell equipped with ceramic porous disc, allowing multistage wetting and drying method application. The mechanical behaviour of tested granular soil samples was determined using modified Bishop and Wesley triaxial rig, allowing applying and controlling the soil suction during the entire test. The tests revealed that for multiplied cycles of wetting and drying the shear strength changes in a certain pattern. The shear strength was observed to increase significantly for the first drying cycle while for the further commencing cycles the changes were not as much obvious. The third group of analyses were focused on analysing the stability of slope filled with the soil material examined in laboratory tests. The numerical modelling of a slope that was exposed to modelled rainfall events allowed the identification of exact changes in factor of safety depending on the pore water pressures fluctuations and geotechnical parameters, that were adopted from the hydro-mechanical test performed in laboratory conditions.

Key words: Unsaturated soil mechanics, soil suction, laboratory tests, mechanical behavoir, soil water retention curves

Streszczenie

Wpływ stanu nasycenia gruntu wodą na warunki stateczności skarp

Zmiany klimatyczne uznawane są za jeden z czynników znacząco wpływających na bezpieczeństwo obiektów inżynierskich na całym świecie. Jednym z obecnych wyzwań współczesnej geotechniki jest ocena długoterminowej stateczności i bezpieczeństwa konstrukcji ziemnych ze względu na wpływu zmian klimatycznych. W celu eliminacji dotkliwych skutków oddziaływania warunków atmosferycznych na infrastrukturę istnieje pilna potrzeba opracowania interdyscyplinarnego podejścia, które pomogłoby zidentyfikować wrażliwe elementy infrastruktury i konstrukcji inżynierskich. Podejście to powinno opierać się na przewidywaniu awarii, które mogą łączyć zarówno kwestie hydrologiczne, jak i geotechniczne. Główną przyczyną obserwowanych zagrożeń osuwiskowych są zjawiska ekstremalne, takie jak deszcze nawalne i susze. Utrata stateczności skarp jest wynikiem kilku rodzajów oddziaływań, takich jak: zmiana ciśnienia wody w porach gruntu i postępująca zmiana struktury gruntu, zmiana charakterystyki okrywy roślinnej zbocza, oddziaływanie erozji powierzchniowej i żłobinowej skarp na skutek filtracji wody i spękań gruntu, będących efektem wysychania. Procesy te zwykle znacznie zwiększają przepuszczalność, powodując zwiększony reżim wód gruntowych. Niniejsza praca ma na celu zbadanie, w jaki sposób stale zmieniające się warunki atmosferyczne (opady) będą miały wpływ przekroczenia stanów granicznych i bezpieczeństwo konstrukcji ziemnych. Zasadniczą częścią badań było wykonanie analiz laboratoryjnych gruntu wykorzystanych do budowy nasypu doświadczalnego (BIONICS) oraz materiału gruntowego, którego właściwości należało zbadać w ramach projektu MUMOLADE. Badania przeprowadzono w celu poznania hydromechanicznego zachowania się dwóch rodzajów gruntów, tj. glina piaszczysta oraz grunt niespoisty w postci piasku drobnego. Badania podzielone zostały na 3 grupy analiz laboratoryjnych. Pierwsza grupa obejmowała określenie zachowania się przepływu wody w gruncie oraz parametrów mechanicznych w warunkach nienasyconych próbek analizowanego gruntu. Krzywe retencji gruntu (SWRC) wyznaczono na drodze serii testów przeprowadzonych na zagęszczonych próbkach różnymi technikami (tensjometry o wysokiej zdolności pomiaru ciśnienia ssania oraz komory talerzy ciśnieniowych). Dla próbek gruntu gliny piaszczystej o wilgotności początkowej 26% wyznaczono całkowite i matrycowe ciśnienie ssania po głównych ścieżkach wysychania. Dodatkowo przeprowadzono szereg badań metodą ciągłego wysuszania i nawadniania, uwzględniających zmieniające się warunki

atmosferyczne (zmiana wilgotności imitującej opad atmosferyczny), wykorzystując nowo opracowane stanowisko badawcze stworzone na Uniwersytecie w Durham, Wielka Brytania. W celu zbadania właściwości mechanicznych próbek gruntów spoistych przeprowadzono serię testów trójosiowych przy stałej wilgotności w dwukomorowym aparacie trójosiowym na zagęszczonych próbkach, a także próbkach zwilżonych i wysuszonych po zagęszczeniu przy wilgotności początkowej gruntu 15%, 20% i 22%. Badania wykazały, że mechaniczne zachowanie gliny piaszczystej w dużej mierze zależy od warunków początkowych, czyli warunków po zagęszczeniu. Próbki wysuszone do określonej wilgotności miały wyższą wytrzymałość na ścinanie niż próbki zagęszczone przy tej samej wilgotności. Ponieważ próbki charakteryzowały się wysokim stopniem nasycenia, obliczenia naprężeń efektywnych pozwoliły na wtórną interpretację danych. Druga grupa badań polegała na określeniu zachowania hydromechanicznego próbek gruntów niespoistych. Obejmowały one wyznaczanie SWRC zmodyfikowanym na potrzeby badań tensjometrem oraz metodą translacji osi z wykorzystaniem aparatu trójosiowego wyposażonego w dysk ceramiczny, umożliwiających wieloetapowe zastosowanie metody zwilżania i suszenia. Do określenia parametrów mechanicznych badań gruntów niespoistych wykorzystano zmodyfikowany aparat trójosiowy Bishopa-Wesleya, umożliwiający zastosowanie i kontrolę ciśnienia ssania w trakcie całego badania. Badania wykazały, że dla wielokrotnych cykli zwilżania i suszenia wytrzymałość na ścinanie zmienia się według określonego wzorca. Zaobserwowano znaczny wzrost wytrzymałości na ścinanie dla pierwszego cyklu suszenia, natomiast w kolejnych rozpoczynających się cyklach zmiany nie były już tak oczywiste. Trzecia grupa analiz skupiała się na analizie stateczności skarpy wypełnionej materiałem gruntowym badanym w badaniach laboratoryjnych. Modelowanie numeryczne skarpy narażonej na zamodelowaną wielkość opadu atmosferyczne pozwoliło na identyfikację dokładnych zmian współczynnika bezpieczeństwa w zależności od wahań ciśnień wody w porach oraz parametrów geotechnicznych, które przyjęto z badań hydromechanicznych przeprowadzonych w warunkach laboratoryjnych.

Słowa kluczowe: Mechanika gruntów nienasyconych, ciśnienie ssania, badania laboratoryjne, właściwości mechaniczne, krzywa retencji gruntu

Table of Content

1. Introduction

1.1. Climate change and infrastructure

Although the fact of climate change is already established, it is still challenging to assess how it can affect the slopes of engineered transport infrastructure (e.g. Dijkstra & Dixon 2010; Glendinning et al. 2015). The following are important headline messages regarding climate change (IPCC 2014):

- The warming of the climate system is undeniable, and since the 1950s, many of the documented changes have been unprecedented throughout decades to millennia, with far-reaching effects on human and ecological systems.
- Climate change has affected human and environmental systems across all continents and oceans in the last few decades. Impacts result from observed climate change, regardless of the cause, demonstrating how vulnerable human and environmental systems are to climate change.
- In all evaluated emission scenarios, an increase in surface temperature is anticipated during the 21st century. Extreme precipitation events are predicted to become more powerful and frequent in many locations, while heatwaves are likely to occur more frequently and last longer.
- Natural and human systems will be more vulnerable to new and increased threats as a result of climate change.

The effects of climate change are predicted to be considerably more severe and widespread in the future for the European environment (EEA 2015a). Global average temperatures are expected to rise by 0.3–1.7°C under the lowest emission scenario and 2.6–4.8°C under the maximum emission scenario during the 21st century (IPCC 2013, 2014). Over Europe, annual average land temperatures are expected to rise at a faster rate than the average global temperature. According to projections, summer temperatures in southern Europe will rise more than winter temperatures in eastern and northern Europe (Fig. 1.1). The general expectation is that annual precipitation will rise in northern Europe and fall in southern Europe (Fig. 1.2), intensifying the contrasts between the regions that are now wetter and those that are currently dryer. It is also anticipated that extreme weather events would become more frequent and intense in many areas, and that sea level rise will speed dramatically (EEA, 2012). Significant regional variations underpin global trends, and it is necessary to take into account the impact

of slopes on the resilience of transport infrastructure at the regional level. There have been some seasonal and geographical differences in the frequency and/or intensity of heavy precipitation throughout Europe. Europe has had a greater rate of increase in temperature than the rest of the world between 2002 and 2011, with land area temperatures rising by an average of 1.3°C over pre-industrial levels (EEA 2015a).
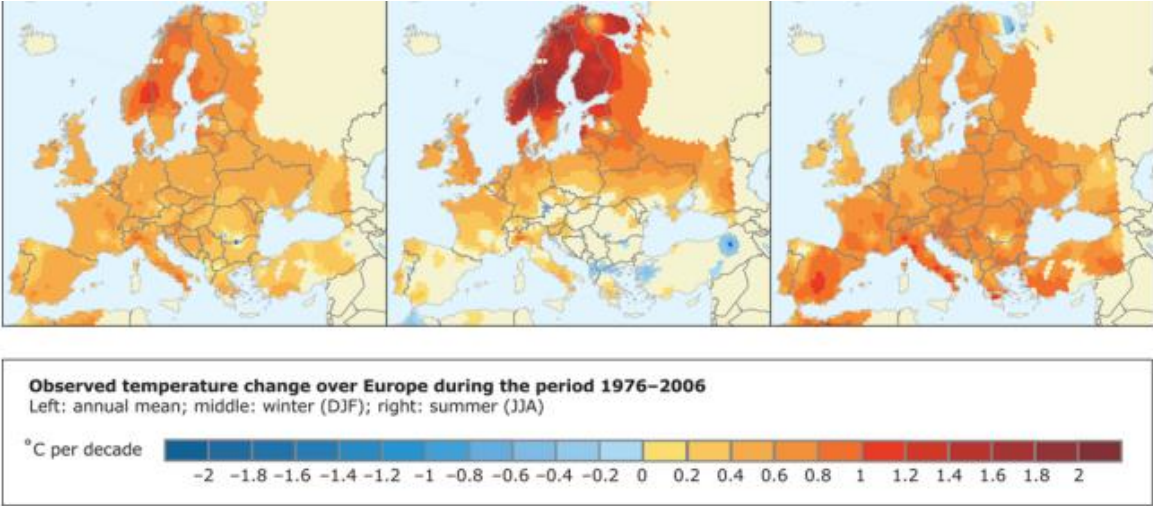
Figure 1.1 Temperature changes observed in 1976 – 2006 (from EEA 2012).
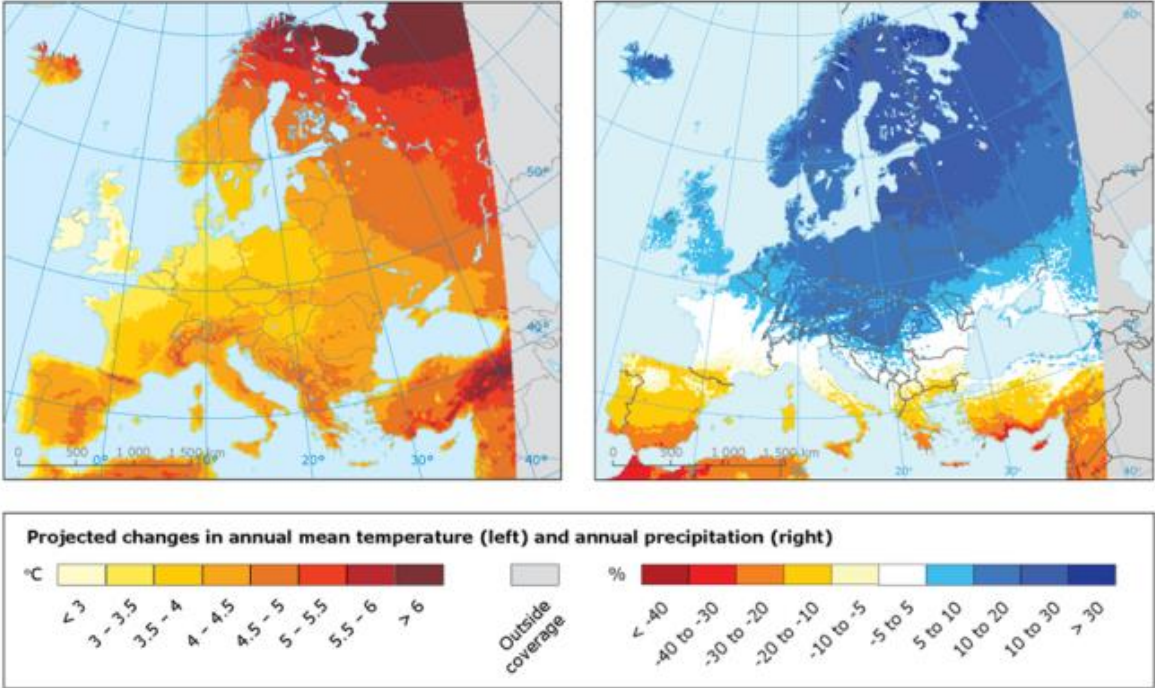
Figure 1.2 Temperature and precipitation projections for the years 2071–2100 in comparison to 1971–2000, derived from a collection of regional climate model simulations made available by the EURO-CORDEX project (EEA 2015b).

When predicting the effects of climate change at the local level, national climate forecasts such as UKCIP (Jenkins et al. 2008) and KNMI scenarios (Van den Hurk et al. 2006) can be highly useful. Because climate influences have varying effects in different places, a more thorough examination of the specific infrastructure network is necessary for a climate change assessment. The KNMI scenarios were specifically designed to gather accurate meteorological data over both space and time, and they were utilised in a recent case study for the Netherlands' railway network (Stipanovic-Oslakovic et al. 2012). Several research (Glendinning et al. 2014; Sayers et al. 2015; Briggs et al. 2016) have made use of UKCIP scenarios.

It is crucial to understand that while developing new infrastructure and choosing operating and maintenance techniques, a steady state cannot be expected due to the dynamic environment that climate change causes (Dijkstra & Dixon 2010). Regional differences in the kind and degree of climate change that is occurring or will occur must also be taken into account. The intensification of heavy precipitation and the rising water table in northern Europe will lower the ground's ability to absorb water. Therefore, it is expected that there would be more surface and interior erosion as well as rainfall-induced slope instability. Furthermore, frost action associated with freeze-thaw cycles is another factor that is anticipated to harm designed slopes when snow, lake, and river ice cover diminish in northern Europe. Lastly, it is projected that vegetation regimes on currently constructed slopes in northern Europe would shift. The stability of engineered slopes must be evaluated taking into account all of the previously mentioned procedures and variables. Table 1.1 and Figure 1.3 provide an overview of the variety of effects of climate change.

The effects for the various European regions varied slightly. The predicted effects of climate change will likewise be less significant, even though its features are more moderate for northwest Europe. It is anticipated that summer precipitation will decrease and heated temperature extremes will increase throughout central and eastern Europe. The average soil water content and water level will consequently drop. Other destabilising forces, such as desiccation cracking, will come into play even if the reduction of water content (and related reduction of porewater pressure) may imply that the risk of possible collapse of constructed slopes will be reduced. In the Mediterranean region, annual precipitation is likely to be lower and temperatures are expected to climb more than the average for all of Europe. This implies that a decline in the water table level and average soil water content is reasonable.

Table 1.1 Possible effects of climate change on European infrastructure (Tang et al., 2018).

	Climate change features	Potential impacts	Potential failure modes	Processes and parameters to be considered
Northern Europe	Temperature rise much larger than global average	Snow, lake and river ice cover (−)	Damage risk from winter storms (+)	Drainage system
	Heavy precipitation (+) in winter and summer	River flows (+)	Rainfall-induced slope instability (++)	Shrink−swell of clay soil
		Evapotranspiration (++)	Surface and internal erosion (++)	Surface and internal erosion
		Infiltration capacity (−−)	Differential settlement (++)	Change of soil suction
		Average soil water content (++)	Crack development (++)	Vegetation
		Water table level (++)		Freeze−thaw cycles (only for northern Europe)
		Erosion (+)		
		Modification of vegetation (++)		
NW Europe	Annual mean temperature (+)	River flow (+)	Risk of river and coastal flooding (+)	
	Winter precipitation (+)	Evapotranspiration (+)	Rainfall-induced slope instability (+)	
		Infiltration capacity (−)	Surface and internal erosion (+)	
		Average soil water content (+)	Differential settlement (+)	
		Water table level (+)	Crack development (+)	
		Erosion (+)		
		Modification of vegetation (+)		
Central and eastern Europe	Warm temperature extremes (+)	Water temperature (+)	Rainfall-induced slope instability (+)	
	Summer precipitation (−)	Evapotranspiration (++)	Crack development (+)	
		Infiltration capacity (+)		
		Average soil water content (−)		
		Change in water table (−)		
		Erosion (−)		
Mediterranean Europe	Temperature rise larger than European	Annual river flow (−) average	Crack development (+)	
	Annual precipitation (−)	Evapotranspiration (++)		
		Infiltration capacity (+)		
		Average soil water content(−)		
		Water table level (−)		

However, as previously mentioned, any benefit from lower porewater pressures must be weighed against the emergence of desiccation cracks and preferential seepage pathways that allow for the quick creation of high porewater pressures during episodes of exceptionally heavy summer rainfall. Because of this, there is still a chance of landslides brought on by rain, though they might happen less frequently and with greater potential damage. Below are more specifics on these processes that are influenced by the climate. These make up a sizable portion of any network of transportation. Making sure the infrastructure is capable of handling future climatic events is necessary to prevent losses in terms of society and economy (Tang et al., 2018).

Scientific projects such as BIONICS (BIOlogical and eNgineering Impacts of Climate change on Slopes), iSmart (Infrastructure slopes Sustainable Management And Resilience Assessment), COST action TU1202 (Impact of climate change on engineered slopes for infrastructure), and MUMOLADE (Multiscale Modelling of Landslides and Debris Flows) have been completed recently in order to investigate the implications of climate change on slopes. All of them sought to determine if earth structures—such as cuts, embankments, and naturally occurring slopes—were safe and able to withstand changing climatic circumstances. They were all involving different institutions from all around Europe, which were represented by the expert who concentrated their research on pertinent subjects. A portion of the results of all those initiatives is included in the current thesis.

1.2. Aims and hypothesis

The aim of the present study is to investigate the impact of changing atmospheric conditions, particularly precipitation, on the long-term serviceability and safety of earth structures, with a focus on understanding the hydro-mechanical behavior of the fill material used in construction under unsaturated conditions. This will aid in the prediction and prevention of climate change-related failures in earth infrastructure.

The hypothesis that was formulated and explored throughout the research process was: *Variable soil properties in various saturation states determine the selection of geotechnical parameters for the slope stability analyses.* A complimentary hypothesis supporting the research study was that *an interdisciplinary approach to stability analysis, which considers the interactions between climate change, geotechnical parameters and the soil saturation condition, is crucial to understand the behavior of slopes experiencing different weather events.*
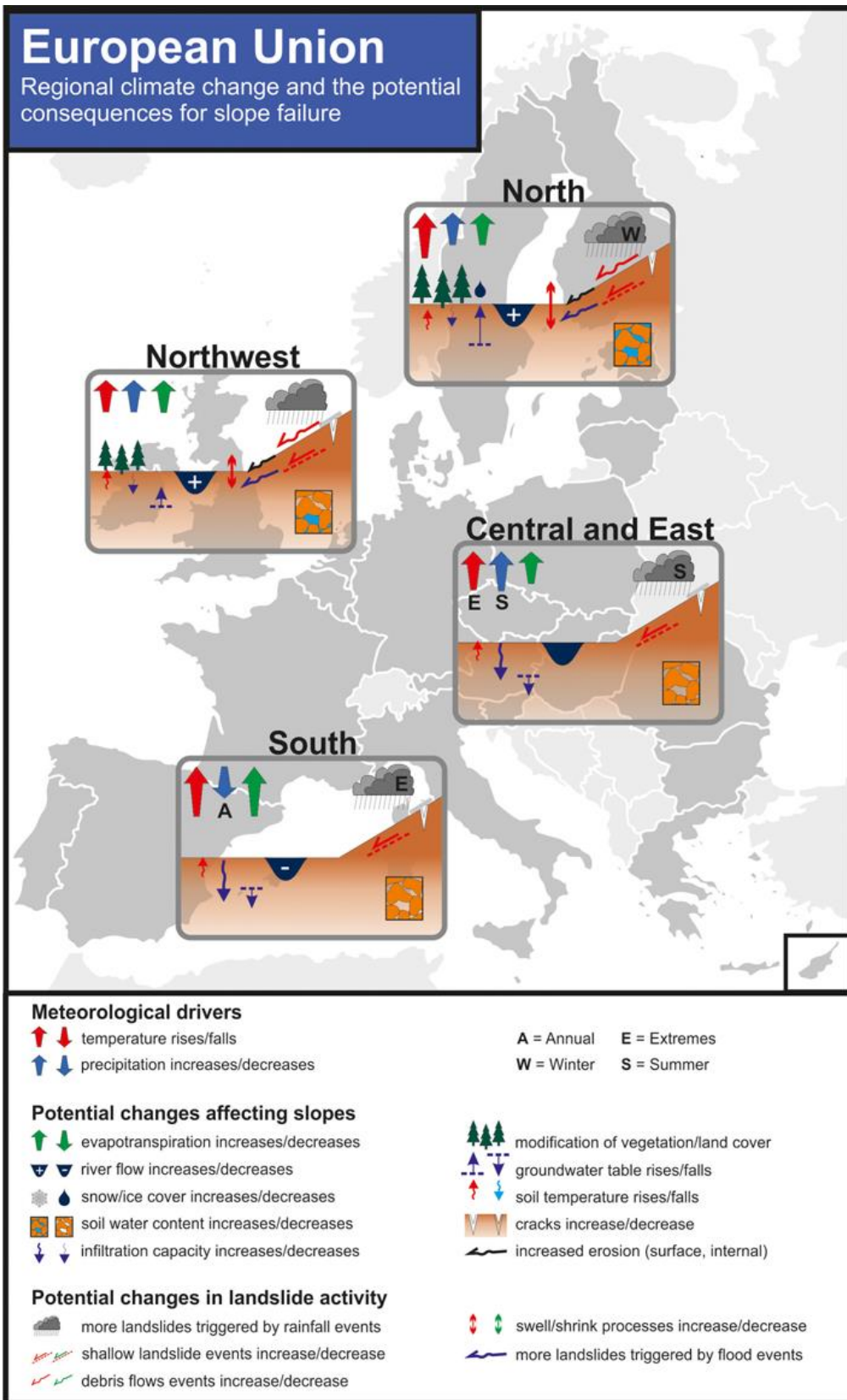
Figure 1.3 European Union regional climate change and the potential consequences for slope failure (Tang et al., 2018).

The objectives helping meet the aim of the thesis and to verify the hypotheses are:

- To assess the effect of climate change on the stability of engineered earth structures such as road and railway embankments, earth dams, and levees, particularly under extreme weather events like heavy precipitation.

- To investigate the hydro-mechanical behavior of fill materials, specifically sandy clay and fine sand, used in earth structures through laboratory testing under unsaturated conditions.

- To evaluate soil water retention characteristics (SWRC) for cohesive and granular soils, analyzing the effect of wetting and drying cycles on soil suction and mechanical strength.

- To determine the mechanical behavior of soils under unsaturated conditions, examining how factors like initial compaction, drying/wetting cycles, and water content affect shear strength and volumetric changes.

- To conduct numerical computations of slope stability under simulated rainfall events, using data from laboratory tests to predict changes in the factor of safety and pore water pressures in reliable scenarios.

- To contribute towards an interdisciplinary approach for predicting geotechnical failures, incorporating both hydrological and geotechnical insights to enhance the long-term safety and cost-effectiveness of earth infrastructure under changing climatic conditions.

1.3. Thesis scope and structure

There are ten chapters in the thesis. The background of the work is introduced in Chapter 1. The introduction of unsaturated soils and their typical behaviour opens Chapter 2, which is then followed by an examination of the experimental methods available for examining the behaviour of unsaturated soils in terms of water retention in both laboratory and field settings. There are also some global field studies of unsaturated soils that are presented. The available constitutive models for unsaturated soils round off the chapter, which then moves on to discuss the most widely used methods for mechanical testing of unsaturated soils and numerical constitutive models used slope stability analyses applying the approaches based on definitions of net stresses and soil suction.

Chapter 3 introduces the tested cohesive and granular soil material properties. The sample preparation methods for both soil types are presented in Chapter 4, which aims to demonstrate samples preparation for laboratory examinations.

Chapters 5 and 6 present procedures and determination of soil water retention curves (SWRC) for sandy clay and fine sand. Total and matric suction SWRC are displayed, and the measurement quality is assessed by comparing data obtained from different approaches.

Chapter 7 discusses the mechanical behaviour of the sandy clay in saturated and unsaturated conditions. A two cell triaxial system was used for the mechanical testing. It included triaxial tests on materials obtained from as-compacted conditions that overcame wetting and drying cycles before testing, all while maintaining a constant water content at different confining pressures. The materials were examined under various initial conditions.

Chapter 8 covers the mechanical testing of granular material of fine sand samples. The material was tested in saturated conditions applying standard triaxial approach using Bishop - Wesley cell, to establish the as the reference condition. The major part of the testing was focused on applying various suction values to evaluate the mechanical behaviour in unsaturated conditions. The chapter also discusses the potential issues of laboratory tests deriving from characteristics of used equipment, this mostly concerns the temperature affected readings of the porewater transducer.

The numerical computations investigating the slope stability of an experimental slope is presented in Chapter 9. The parameters of slope filling material used in the analyses are based on the laboratory testing performed within the scope of the present research. The conditions investigated in the laboratory were reflected in the modeling. Such an approach allowed for determining the influence and the importance of parameters used in stability analyses that actually reflect the potential climate scenarios.

The thesis ends with Chapter 10 with conclusions and recommended future work that would allow to deepen the understanding of the coupled phenomenon of landslides and slope failures.

2. Literature review

2.1. Unsaturated soil and soil suction

When constructing earth structures like road and railway embankments, dams, dykes, understanding of the behavior of soil behaviour in unsaturated or partially saturated conditions are crucial. Unsaturated soils are typically built in the vadose zone, which is where the phenomenon known as negative pore water pressure manifests itself (Fig. 2.1). The hydraulic alterations brought on by the various climate events affect their mechanical qualities. Studying the hydraulic behaviour of the soil is essential for determining its geotechnical properties, particularly when analysing slope failures caused by rainfall.

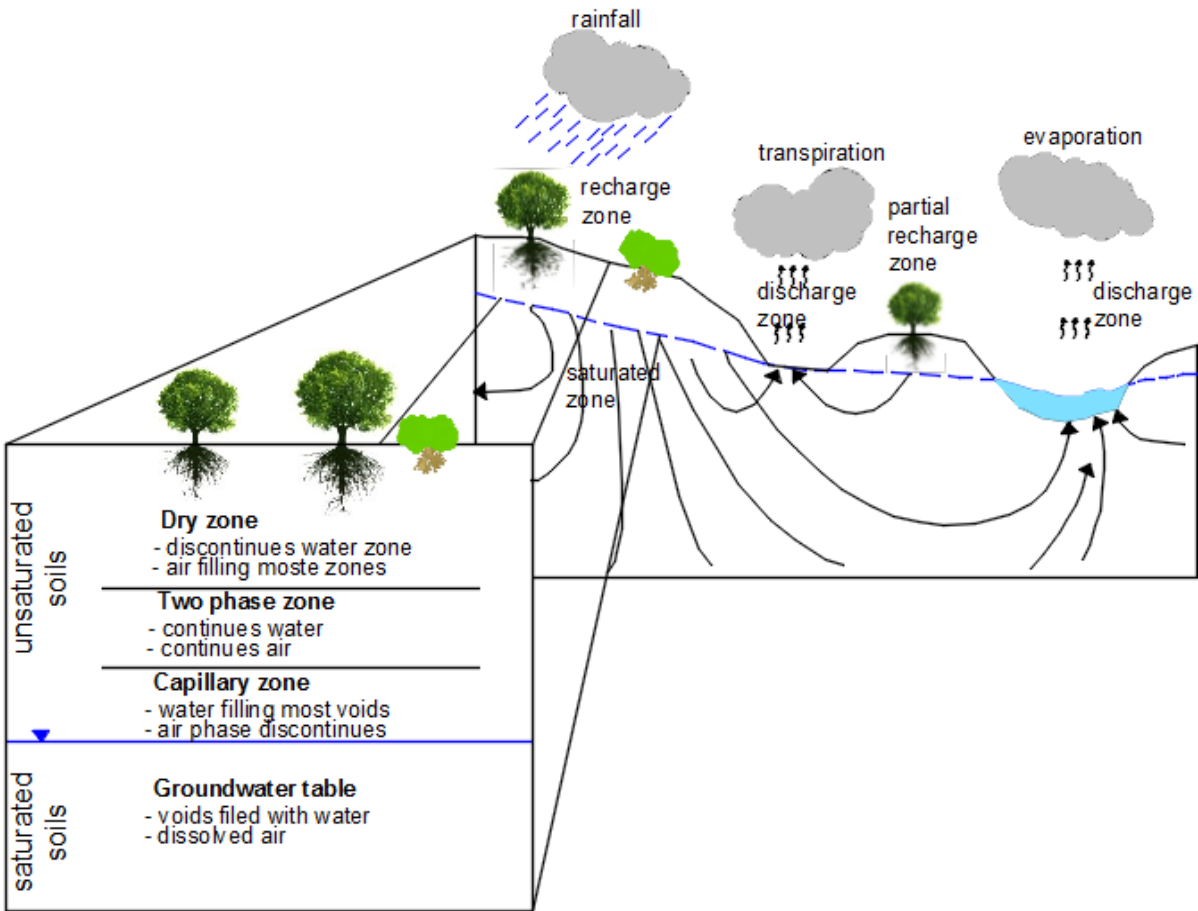**Figure 2.1**. Unsaturated soil zone location.

While Terzaghi's equation for effective stress can be used to explain the mechanical behaviour in saturated soils, it is considerably more difficult to comprehend the mechanical behaviour in unsaturated soils since the spaces are filled with both water and air. There hasn't been much consensus on the best stress state variables to employ in unsaturated soils until late

70's (Fredlund and Rahardjo, 1993). According to Fredlund and Morgenstern (1977), the relevant stress state variables for unsaturated soils are net normal stress and soil matric suction. The term "three-phase mixture" refers to a mixture of solids, air, and water. However, there is a compelling argument to include a fourth independent phase known as the contractile skin or the air-water interface. The contractile skin serves as a barrier between the water and air phases of the soil, resembling a thin membrane woven throughout the soil's cavities. An unsaturated soil changes in volume and shear strength due to the interaction of the contractile skin with the soil structure. The position of the contractile skin, or the degree of saturation, affects the characteristics of the unsaturated soil (Fredlund and Morgenstern, 1977). Prior to delving into the hydro-mechanical behaviour of unsaturated soil, it is necessary to ascertain the force responsible for soil suction. The attraction that the soil has for free water when the two come into contact is known as soil suction. If the water inside the voids begins to evaporate, this "pull" force may get greater. Matrix suction and osmotic suction are the two components of total suction, expressed as soil suction. The following formula can be used to define total suction:

$$\psi = (u_a - u_w) + \pi \qquad (2.1)$$

where:

ψ – total suction;

$(u_a - u_w)$ – matric suction, pore air pressure (u_a) and pore water pressure (u_w);

π – osmotic suction, equivalent suction associated with osmotic potential of the pore water.

The capillarity phenomenon, which is linked to surface tension between the water and air phases inside the soil pores, creates the matric suction. Because the pore size distribution of the soil influences matric suction, matric suction depends on the soil structure. A soil with a finer grain size may withstand a greater matric suction value than one with a coarser grain size. When the water content of the soil decreases, the matric suction rises, and this is where the water content of the soil also plays a part. The amount of salt present in the pore water is related to the osmotic suction. Although osmotic suction can have a considerable impact on volume change behaviour (shrinkage and swelling), changes in osmotic suction are typically less significant than changes in matric suction for the majority of engineering challenges.

2.2. Soil water retention curve

SWRC frequently reflects the behaviour of soil throughout the adsorption and desorption processes. It is typically expressed as a relationship between the soil suction, which is indicated in kPa, and the degree of saturation or water content (gravimetric or volumetric). Three main steps can be recognised in order to obtain the SWRC. When the drying process first begins, the soil could be almost completely saturated. As the soil dries out, air starts to seep into its pores, creating suction and reaching the soil's air entrance value. The phase of the desorption process that is find to be beyond the air entrance value is known as the transition zone, and here is where the majority of desaturation takes place. The following phenomenon, known as relative suction, shows that the only water present in the soil is that which is firmly attached to soil particles. Although all of these stages can be found in different kinds of soils, the shapes of the SWRC and suction values can differ significantly. This is due to the fact that there are additional factors that impact soil suction and they include void ratio, soil structure, stress history, and stress state. Equation 2.2 shows that they are closely related:

$$\psi = - \frac{RT}{\nu_{wo}\omega_v} \ln\left(\frac{\bar{u}_v}{\bar{u}_{v0}} \right)$$

(2.2)

where:

ψ – total suction (kPa)

R – universal gas constant ($8.31432 \, m^3 \cdot Pa \cdot K^{-1} \cdot mol^{-1}$)

T – absolute temperature (273.16 + t) (K):

    t – temperature (°C)

υ_{wo} – specific volume of water ($1/\rho_w$) (m^3/kg)

    ρ_w – density of water (kg/m^3)

ω – molecular mass of water vapour (kg/mol)

Figure 2.2 shows the normal behaviour of an SWRC along a drying path. At first, the suction rises while the boundary effect zone (the saturation level) is kept near to 100%. The soil's air entry value (AEV) is attained when the suction value is high enough to begin pore-draining. Air begins to fill the pores and bulk water begins to be drawn out of the larger ones once the AEV is reached. The soil is deemed desaturated at this point, and until a residual degree of saturation is established (transition zone), the amount of suction required to remove water from the pores may not need to be increased much.
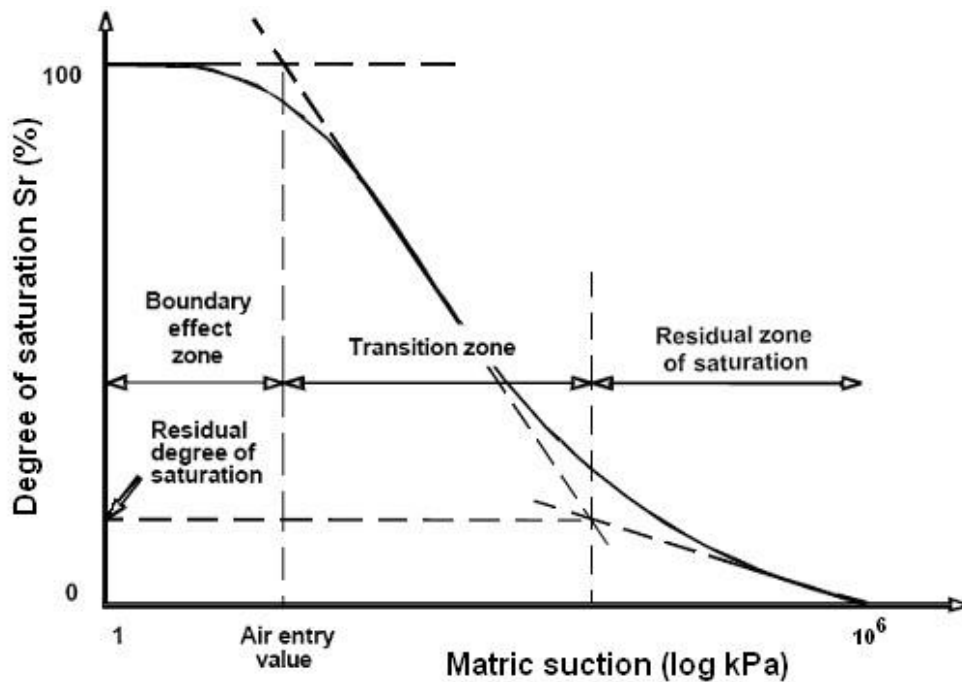
Figure 2.2. Soil Water Retention Curve example, and zones identification.

The procedure used to obtain the SWRC affects its shape as well. The resulting curves display distinct curves depending on whether the soil is exposed to drying or wetting routes. Hydraulic hysteresis is typically blamed for this hysteretic tendency (Croney, 1952). The effects of pore entrapment, or "ink-bottle pores," are frequently used to explain hydraulic hysteresis. Because of the distinctive shrink and swell behaviour of these materials, clayey soils pose an extra challenge. The rearranging of the pores, including changes in pore size, makes the observed hysteresis even more complex. A soil may not transition smoothly from a completely dry state to a completely wet one. Soils at an intermediate stage, where the direction of the change in water content is inverted, are fairly prevalent. Scanning curves are SWRC obtained at intermediate phases. A couple of different types of scanning curves are shown as basic examples in Figure 2.2 an ascending scanning curve where the initial condition was reached while following a drying path and then wetted, and a descending scanning curve where the intermediate stage begins on the SWRC's wetting path and the material dries gradually until it reaches the drying path of the SWRC. The SWRC exhibits extreme hysteria. The Primary Drying Curve will be followed if the soil is subjected to drying after beginning in a saturated state. The Primary Wetting Curve (Figure 2.3) will be followed when soil is wetted after being oven dried. The ultimate volumetric water content may be less than the original saturated value when the suction is decreased to zero. This could be due to air bubbles that were still trapped in the soil or because the soil experienced irreversible shrinkage.
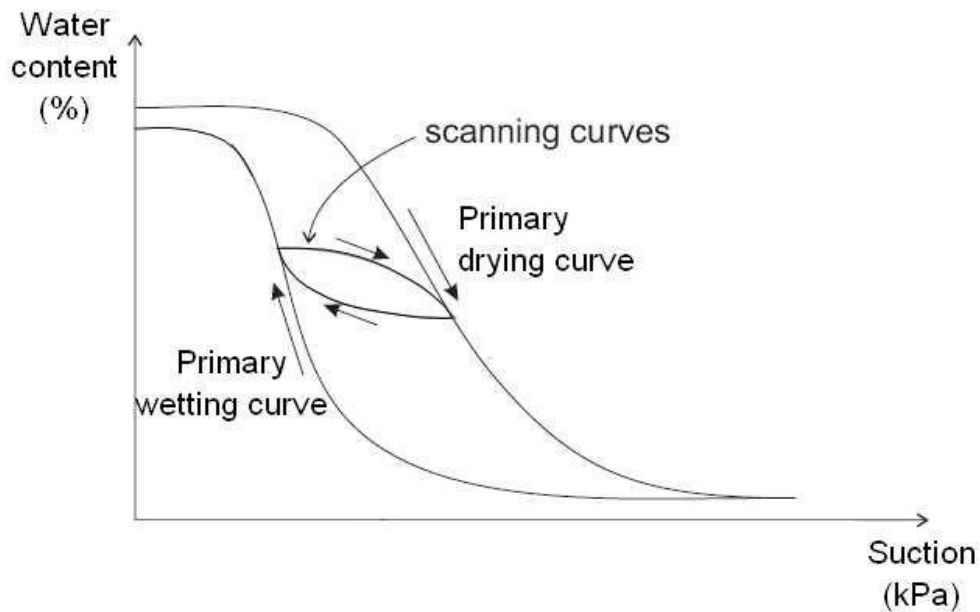
Figure 2.3 Hysteretic characteristics of SWRC (after Toll et al., 2017).

2.3. Soil suction determination

2.3.1. High capacity suction probe

A summary of the different approaches that can be used to assess soil suction can be found in the following publications: Rahardjo and Leong (2006), Bulut and Leong (2008), Delage et al. (2008), Lee and Wray (1995), Ridley and Wray (1996), and Fredlund and Rahardjo (1993). There are several different suction measurement systems and techniques on the market. Nevertheless, only the apparatus and techniques employed in this study are detailed, including the high capacity tensiometer, the pressure plate technique, the modified pore water pressure (PWP) transducer created at the University of Nottingham, and the axis translation method (using a ceramic disc) in a Bishop-Wesley triaxial cell. Table 2.1 lists the measuring ranges for the most popular methods for calculating the SWRC.

High capacity suction probes are referred to by different names by different inventors. They are sometimes called tensiometers or suction probes. It is distinguished from other tensiometers on the market by its "high capacity", which allows it to measure suction pressures lower than the typical cavitation limit of 100 kPa. At Imperial College London, Ridley and Burland (1993) created the first high capacity suction probe. This high capacity suction probe was made up of an Entran Ltd EPX series electronic pressure transducer (3.5 MPa capacity) as the measuring device and a small water reservoir (3 mm^3) as a filter between the measuring device and the soil sample.

Table 2.1 Suction range and equilibration time for methodologies used in the study to determine SWRCs, based on researcher's experience.

Methodology	Suction Range (kPa)	Equilibration Time
Axis translation in triaxial cell	0-120	Days
Modified PWP transducer	0-130	Hours
Tensiometer	0 – 1600	Hours
Pressure Plate	0 – 1500	Days

The pressure transducer registers zero suction when the ceramic high air entrance disc and water reservoir are entirely saturated. The water in the high capacity suction probe begins to be dragged towards the soil until equilibrium is attained when it comes into contact with a soil sample with a specific suction value. The matric suction of the soil causes a deflection on the pressure transducer as a result. Since then, other reports of high capacity suction probes have emerged, with differences in the ceramic disc, water reservoir, pressure transducers, or size but essentially the same operating principle. Table 2.2 presents a comprehensive overview of the majority of large capacity suction probes currently available, as provided by Delage et al. (2008).

Table 2.2 Effect of the pre-pressurisation pressure on the maximum sustained tension (after Delage et al, 2008).

Authors	Ceramic AEV (MPa)	Max positive pressure (MPa)	Max tension water (MPa)
Ridley and Burland (1993)	1.5	6	1.37
Ridley and Burland (1995)	0.1	4	0.164
	0.5	4	0.74
	1.5	4	1.8
Guan and Fredlund (1997)	1.5	12	1.25
Meilani et al. (2002)	0.5	0.8	0.495
Tarantino and Mongiovi (2002)	1.5	4	2.06
Take and Bolton (2003)	0.3	1	0.53
Chiu et al. (2005)	0.5	0.7	0.47
Lourenco et al. (2006)	1.5	1	1.23
He et al. (2006)	0.5	2	0.55
Mahler and Diene (2007)	0.5	0.6	0.8
	1.5	0.6	1.4
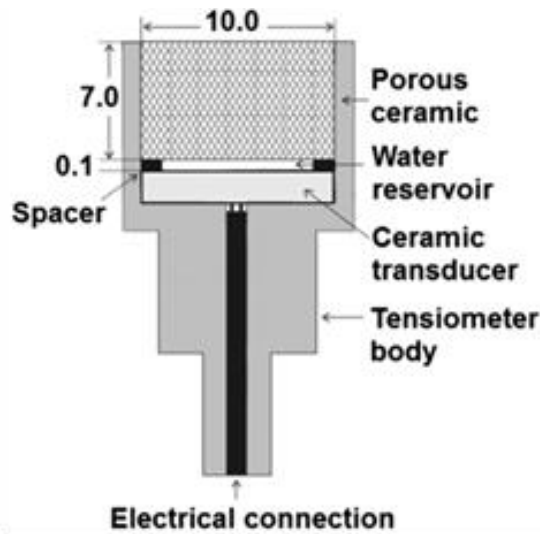
Figure 2.4 Schematic of the DU-WF high capacity suction probe (after Lourenço, 2008).

The Durham University – Wykeham Farrance (DU-WF) large capacity suction probe was the one employed in the present investigation. There are some internal modifications and differences in the production process between this probe and the Ridley and Burland (1993) probe. The high capacity suction probe measures 35 mm by Ø14 mm and has a volume of 5 mm^3. It employs a ceramic pressure transducer that is soldered to a ceramic disc with a thickness of 10 mm that is 1.5 MPa high AEV, as shown in Figure 2.4. The development of these devices has focused mostly on improving the measuring range and measurement stability, but the saturation process of the probes is a critical component for any device that aims to produce a trustworthy measurement.

Saturation of high suction probe

According to Lourenço (2008), the DU-WF high capacity suction reached saturation through water infiltration under vacuum and subsequent pressurisation of 1.5 MPa inside a saturation manifold created by Donohgue (2006). This occurred after the suction was initially dry. The majority of high capacity suction probes go through this saturation phase. In the event that the probe has become desaturated due to cavitation, re-saturation should occur within 24h under wet conditions.

Calibration

The calibration of the pressure transducers in these types of probes is often done in the positive range and extrapolated to the negative range. However, the desired measured value, or negative pore water pressure, is suction. According to Tarantino and Mongiovi (2003), it was thought to be adequate to obtain an error of 1 to 1.5% in the measurement when

extrapolating the positive to the negative range. Lourenço (2008) examined the DU-WF large capacity suction probe's extrapolation from the positive to the negative range. Extrapolation calibrations were performed in comparison to a standard pressure transducer. Through his investigation, he demonstrated how the probe's calibration technique affected accuracy. The external forces from the probe's holding mechanism affected the calibration when it was performed inside the saturation manifold. He came to the conclusion that the calibration should be carried out in the same circumstances as the anticipated conditions of use in order to get a more accurate calibration through extrapolation. By using the axis translation technique and isotropic unloading, Lourenço et al. (2008) verified the extrapolated calibrations against known values of suction imposed by soil samples. Both approaches showed good agreements. However, isotropic unloading produced a superior agreement. By applying negative pore water pressures down to -100 kPa with a vacuum pump, he was also able to establish a good agreement for the calibrations.

Advantages and disadvantages

The direct measurement of matric suction, small equipment size, and quick measurement time (less than an hour) are the main benefits of utilising large capacity suction probes. The measurements taken from the probes are accurate and dependable when the device is properly calibrated and able to saturate. The device's capacity to measure in both the positive and negative range is also significant. These probes' primary drawbacks are their zero suction value and cavitation potential. When these probes are utilised for extended periods of time in the negative pressure region, drifting of the zero suction value is typically noticed. The reported variances with the DU-WF high capacity suction probe have been minimal, up to 5 kPa; this can cause some inaccuracies while operating in the tiny suction range.

2.3.2. Pressure plate method

The pressure plate method, which is frequently used to generate SWRCs, is different from the other procedures in that it applies suction on the soil sample instead of measuring it. The matric suction is defined by the differential between the pore air and pore water pressures, which are controlled in order to apply suction to the soil samples. Saturated high air entry value (HAEV) porous ceramic discs are housed inside a pressure chamber in the pressure plate apparatus utilised for the investigation. During testing, the soil sample is positioned at top of the HAEV. Durham University devised a technique that enabled independent examination of three different samples.
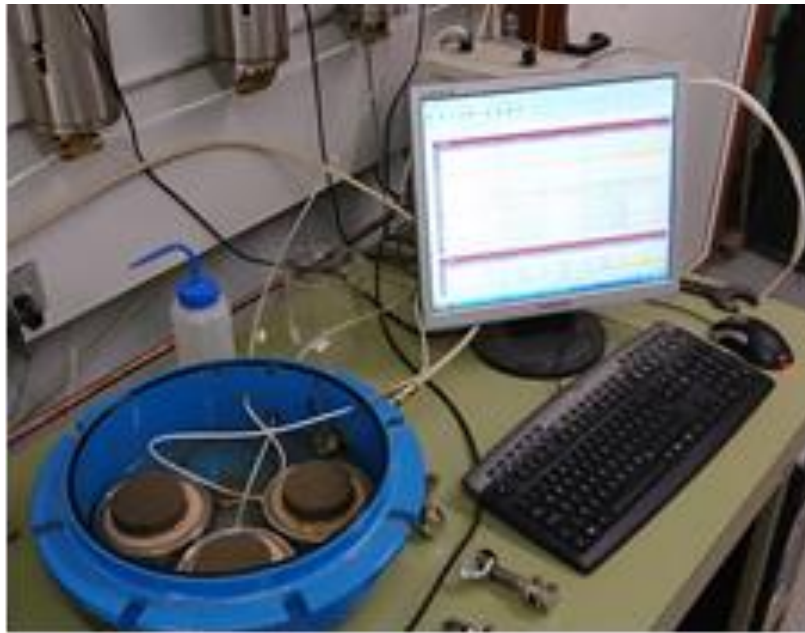
Figure 2.5 Pressure plate apparatus used in the study.

This type of device's maximal differential pressure is limited by the AEV of the porous ceramic disc inside the chamber. The air pressure maximum that can be applied to the chamber before air entry, sometimes known as "bubbling," takes place—that is, before air begins to flow through the HAEV porous ceramic disc—is known as the AEV value. The AEV values of the most popular ceramic discs are 500 kPa or 1500 kPa.

The standard procedure used in this technique is to seal the chamber, maintain atmospheric pore pressure, and raise pore air pressure to level that is higher than atmospheric one. After the air and water pore pressures reach their target values, the soil sample is allowed to stabilise. Water is released from the pores in the soil sample, travels via the porous disc of the HAEV, and then flows into a burette. In this instance, the burette is used to measure the amount of water that exits the sample, which can be connected to the water content at this specific suction value. Balance is only reached when the water flow is stopped. To create the SWRC, this procedure is repeated while applying varying suction values (raising the pore air pressure). The ultimate water content can be ascertained following the suction stage, and this information can be utilised to confirm the burette's indirect measurements of water content.

Vaquero (2007) at Durham University created an alternative way for this technique using an already-existing pressure plate equipment made by Soil Moisture Corp. of Santa Barbara, California. Multi sample testing was made possible by substituting four independent porous discs (diameter of 100 mm) with an AEV value of 1500 kPa for the standard single HAEV porous disc. The second change concerned the burette, where a separate volume gauge, one

for each porous disc, was used to accomplish the measurement. The automatic data acquisition system, which is linked to a computer for measurement scanning and recording, has a transducer fastened to the volume gauge (Figure 2.6).
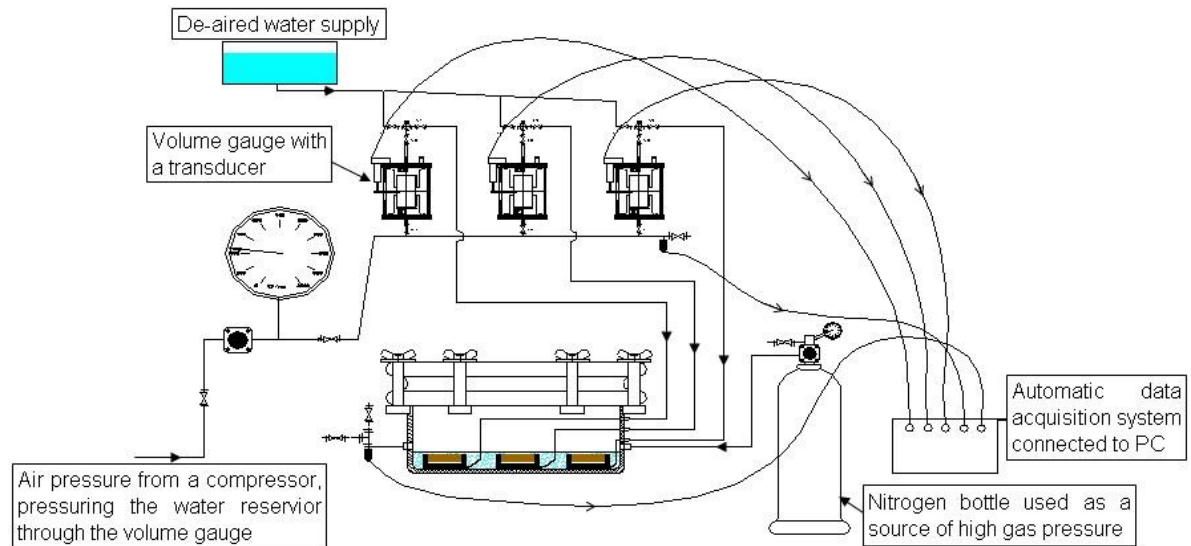
Figure 2.6 Setup of the pressure plate apparatus (After Vaquero 2007).

2.3.3. Axis translation method using triaxial cell

Determining the test specimen's overall volume change is essential for evaluating unsaturated soils. The following methods can be employed to do this:

- Directly regulate/measure the volume changes and air and water pressures inside the test specimen. This entails controlling the air pressure and air volume change in the test specimen with a specialised pressure/volume controller. The volume change and pore-water pressure are managed by a second controller. The overall volume change in the test specimen is determined by adding the volume changes from the two controllers. This approach was also adopted in the current study, which was a component of the Mumolade project's research program, to analyse the mechanical and hydraulic behaviour of granular material at University of Nottingham.

- Use a low range, high accuracy differential pressure transducer to measure the change in head of water between an inner cell surrounding the sample (as the sample deforms) and a reference tube.

- Determine the overall specimen volume change by measuring the cell volume change. Because the cell stiffness is finite and variations in specimen loading and cell pressure result in a volumetric change in the cell, this technique is typically not very

satisfactory. Nonetheless, the internal cell wall can be made to be endlessly rigid by employing a double cell and applying the same pressure to the exterior and internal cells (i.e., a cell within a cell). The thermal stability of this system must be quite high. The amount of the cell water can vary significantly even with little temperature variations.

- Use Hall Effect or LVDT local strain transducers to measure the local diameter and axial deformation directly on the test specimen. It is feasible to calculate the test specimen's overall volume change based on the local strain data.

In order to determine the hydraulic behaviour of granular soil, specifically the SWRC, a modified Bishop-Wesley cell was employed in this work (together with newly develop and modifies pore water pressure transducer). Using an extra pressure/volume controller that is directly attached to the specimen is the alteration. The back pressure, also known as the pore water pressure, is normally applied to the specimen through the base pedestal, as illustrated in Figure 2.7, whereas the pore air pressure is typically applied through the top-cap. Though it is housed in a single wall Triaxial chamber, the technique is essentially based on the pressure plate apparatus. This arrangement is employed because a high air entry porous disc, or HAEPD, is most suited to be housed on the base pedestal. To sustain matric suction within the test specimen, the HAEPD is necessary to separate the pore air and pore water. The HAEPD ceramic material's ability to sustain pore air pressure on its top that is higher than the pore water pressure applied to its base, even when completely saturated, is what allows for this. Additionally, the material stops air from leaving the specimen up to a pressure differential that matches a predetermined air-entry value. Keep in mind that the usual range of air-entry values for HAEPDs is 300–1500 kPa. The Bishop Wesley cell, which is described in more detail later in the thesis, is the triaxial rig to which the complete setup is attached in the investigation.

2.3.4. Modified pore water pressure transducer

It is well known that soil suction tests take a lot of time and sometimes produce findings that are a little bit inflated (Osinski et al 2016, Toll et al, 2015). Therefore, as part of the Mumolade project, which was focused on assessing the granular material samples, it was decided to adapt the pore water transducer available at the University of Nottingham in order to compare the SWRC curve and make the testing more efficient. The PPT was utilised to measure the specimen's matric suction directly during the soaking and drying phases. The

PPT needed to be changed into a tensiometer in order for it to function as intended (Toll et al. 2013). The transducer, 12 mm in length and 6 mm in diameter, is a smaller version of Druck PDCR81 Pore Pressure Transducer, (König et al. 1994) (Figure 2.8).
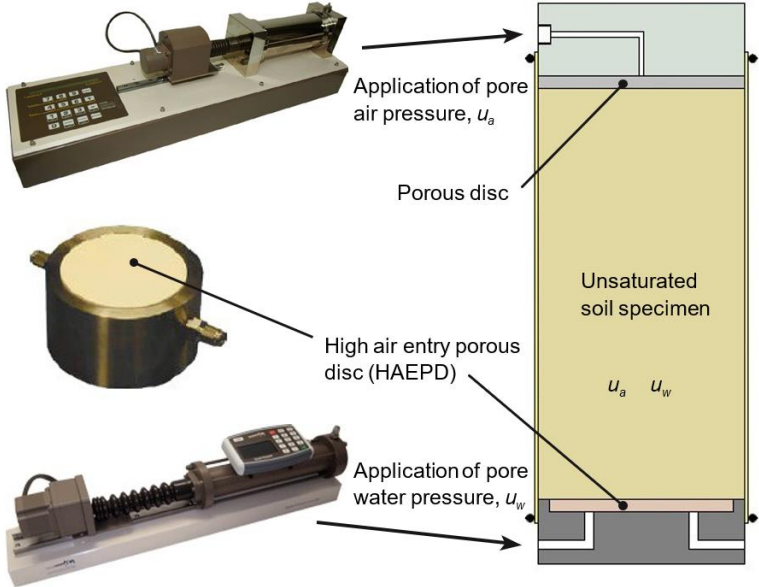
Figure 2.7 Unsaturated soil specimen set up used in Bishop Wesley cell (GDS, 2016).
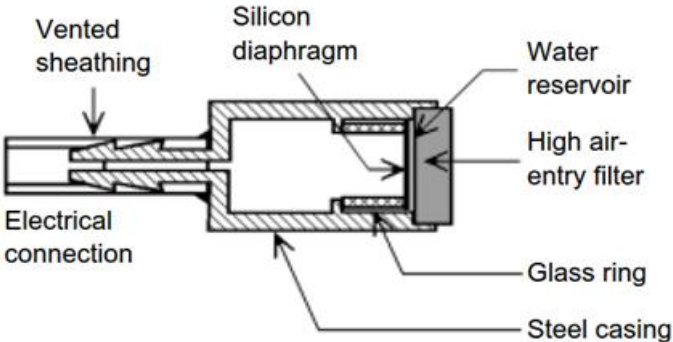
Figure 2.8 Pore Pressure Transducer, fitted with high air entry value disc (Matziaris et al, 2015).

It is made out of a diaphragm that generates an electrical signal when it deforms due to pore water pressure. The diaphragm and the filter are separated by a little water reservoir. The calibration process was carried out to establish a correlation between the real pressure and the electrical signal that the sensor produced when it was subjected to pressure variations. By putting a high air entry porous disc in front of the diaphragm, PPT was adjusted to precisely detect negative pore pressure, or suction. Prior to testing, the porous disc was sufficiently saturated following the method outlined by Matziaris et al. (2015). The removal of air bubbles from water reservoir and disk made sure that the pore water was in contact with the diaphragm and that the suction readings were accurate (discussed in the Chapter 6).

2.4. Mechanical testing of unsaturated soils

It is crucial to comprehend the mechanical behaviour of unsaturated soils in order to comprehend the soil strength variations that may result in landslides. Different types of soil samples, such as compacted samples (Toll, 1990; Wheeler and Sivakumar, 1995), reconstituted samples (Cunningham et al., 2003), and intact samples (Futai and Almeida, 2005), have been examined in order to study the mechanical behaviour of unsaturated soils. For the study of the mechanical behaviour in unsaturated conditions, supporting methods such as axis translation (Toll, 1990, Wheeler and Sivakumar, 1995), relative humidity (Olecop and Alonso, 2000), osmotic (Dineen and Burland, 1995), and more recently a computer controlled technique based on the use of high capacity suction probes (Jotisankasa, 2005) are typically used in conjunction with known methods for saturated soils, such as the triaxial apparatus. Using a triaxial cell, one of the most popular methods used by researchers to examine the mechanical behaviour of unsaturated soils is the axis translation approach. The Axis Translation Technique was first described by Hilf (1956), who found that raising the air pressure would also raise the pore water pressure by the same amount, assuming that there were no changes in suction or water content. Conventional pressure transducers can read pore water pressure when the pore air pressure rises to a level higher than the pore water pressure's initial negative value. After that, the pore water pressure turns positive. In order to manage suction during the test, Bishop and Donald (1961) created a double wall triaxial cell that could independently control both air pressure and water pressure. The greatest suction value obtainable in the axis translation technique depends on several components of the triaxial apparatus: the achievable air pressure, the air entry value of the porous stone (which isolates the sample from the pore water pressure mechanism), and the stiffness of the cell. The lengthy test period and the potential for air diffusion through the porous stone are two more drawbacks of this methodology. Al Mukhtaret al. (1993) applied the relative humidity control system to geotechnics, mainly for evaluating soils at suctions above 1 MPa. It started out as a soil science system, primarily focused on regulating the air surrounding the soil sample's relative humidity. In this way, the relationship between the total suction and relative humidity can also be regulated. However, in order to ensure the suction balance, an independent suction measurement is required. Blatz and Graham (2003) made strides in this independent suction measurement when they tested a high plasticity clay and used a thermocouple psychometer to measure suction.

Since its creation by Zur in 1966, the osmotic system has been extensively employed in a variety of works, including those by Cui and Delage (1996), Dineen (1997), and Colmenares (2002). The sample is separated from a solution of a large molecular weight material (often polyethylene glycol, or PEG) in the osmotic system using a semi-permeable membrane. Water moves from the soil across the membrane to the PEG solution through osmosis since this membrane is permeable to water but not to PEG. This process continues until the soil suction equalises the osmotic potential of the PEG solution. As a result, the suction is dependent on the PEG solution's concentration; as a result, the suction increases as the PEG solution's concentration does, and vice versa. More recently, Cunningham (2000) at Imperial College created a suction measurement method that takes into account the movement of dry air across the soil sample's surface. This air-regulated system uses dry air flowing across the base of the soil sample to dry it out and therefore boost suction. It also includes suction probes for independent suction monitoring. Cunningham utilised this technique during test loading and shearing phases, when suction typically drops. His goal was to maintain a consistent suction value, thus he used the suction probe measurements to regulate the air flow and maintain a constant suction value.

2.5. Rainfall triggered landslides

Landslides, which are defined as the deformations of slope-forming materials like rock, soil, or its mixture, are serious natural disasters that occur frequently throughout the world and cause significant property damage as well as fatalities. According to the United Nations Office for Disaster Risk Reduction, landslides rank as the fifth most common natural disaster globally, with over 380 occurrences documented in the 20 years between 1995 and 2015 (UN, 2016). It has been estimated that landslides causes \$2 to \$4 billion (in 2010 USD) in annual financial damages and 25 to 50 human fatalities in the United States alone (Shuster, 1996; US Geologocal, 2016). Therefore, significant losses can be avoided with early landslip prediction. The equilibrium of forces operating on a naturally occurring soil slope results in its stability. Landslides can be caused by a variety of triggers, including seismic activity, rainfall, volcanic eruptions, and wildfires. Since rainfall is the most frequent of these triggering causes (Polemio and Petrucci, 2000), the main focus of this research is on identifying the mechanical and hydraulic characteristics of soil that is subjected to pore water pressure changes that cause landslides. Rainfall-caused landslides typically happen in areas with residual soil slopes that are naturally stabilized by negative pore water pressure or matric suction. Rainwater

infiltration raises the soil's moisture content, which damages the matric suction. Slope instability is caused by this phenomena, which also results in lower effective stress, increased soil weight, and decreased soil shear strength. It is, therefore, realised that the accuracy of predicting rainfall-triggered landslides can be increased if the soil moisture content can be employed as a direct factor in assessing landslide dangers.

In the past, specified threshold rainfall intensities and durations at selected landslip areas have been used to predict rainfall-triggered landslides. However, the primary cause of slope failure is the increase in porewater pressures brought on by rising soil moisture levels (Weerasinghe et al, 2011; Dahigamuwa et al, 2018). Previous studies have tried to quantify the risk of landslides using in situ soil moisture measurements (Ray and Jacobs, 2007; Ray et al, 2010; Brocca et al, 2017). However, because of the complex apparatus needed and the unpredictability of instrument findings, measuring soil moisture in situ can be an expensive undertaking. However, instead of using direct ground soil moisture measurements, the majority of current landslip prediction methods use indirect methods to assess the increases in moisture. Examples of these methods include the use of hydrological conditioning factors, such as drainage density, distance to drainage, and the Topographic Wetness Index, or other similar water-drainage based variables. An alternative to in situ soil moisture measurements and other variables dependent on water drainage is the use of remotely sensed soil moisture. Regularly obtained soil moisture records from satellites are thought to be very useful for these kinds of evaluations. On the other hand, site-scale landslide hazard assessment also frequently uses physically-based models, such as numerical and analytical models with the ability to simulate the subsurface processes that cause landslides (Hong et al., 2006; Simmon, 2012; Chatterjea, 1994; Lim, 1995; Lim et al, 1996; Gasmo, 1997). By simulating the temporary seepage caused by rainwater penetration in the unsaturated zone of the soil, these models seek to measure the variation in pore pressure during rainfall. The Richards equation is commonly used to predict the temporary seepage in soil following rainfall and the ensuing loss of matric suction. In order to calculate the slope's factor of safety against failure, the slope stability is lastly evaluated using a limit equilibrium analysis with soil shear strength reduction owing to rainfall that is normally predicted by the extended Mohr-Coulomb criterion. Nevertheless, when modelling the infiltration of water into soil as a result of rainfall, the current numerical and analytical models rarely take into account the interaction between surface and subsurface water flows. This is frequently a crucial element that controls how quickly water penetrates the earth, particularly after strong storms when landslides are most common. Additionally,

Darcy's law is used to create the Richards equation, which is used in current models to estimate transient seepage caused by rainfall, under the pseudo-steady state assumption. As a result, while modelling seepage in the aforementioned research, the inertial components of flow are frequently disregarded. To get real-time subsurface pore pressure variations, a physically-based numerical technique can be calibrated using remotely observed surface soil moisture content. Thus, an enhanced real-time landslip hazard assessment approach will result from integrating remote sensing with numerical modelling in this way.

2.6. Constitutive models

2.6.1. Introduction

Constitutive models have been discussed to explain the mechanical behaviour of unsaturated soils based on experimental research. As an extension of the saturated effective stress, Bishop (1959) attempted to characterise the mechanical behaviour of unsaturated soils using a single effective stress variable by integrating pore air pressure and pore water pressure as shown in equation 2.4. Bishop's formulation contained a parameter, X, that corresponded to the saturation level, or the amount of air or water that contributed to the voids.

$$\sigma' = \sigma - X.u_w - (1 - X).u_a$$

(2.4)

Jennings and Burland (1962) discouraged characterising the behaviour of unsaturated soils by a single stress variable. The inability of a single stress variable to replicate the behaviour of collapsable soils is the problem with employing it. In their experiment, Jennings and Burland demonstrated this by reducing the volume of silt samples under continuous applied stress during inundation, all the while maintaining an increase in pore water pressure. More recent constitutive models incorporate two or more variables to describe the behaviour of unsaturated soils, overcoming the drawback of using only one stress variable. These distinct stress variables include matric suction (u_a - u_w) and net stress in the two conceivable forms of (σ - u_a) and (σ - u_w). Two variables are sufficient to satisfactorily represent the volumetric response of unsaturated soils (Fredlund and Morgenstern, 1978). A tensorial variable, the net stress is represented as follows:

$$\bar{\sigma} = \begin{bmatrix} (\sigma_x - u_a) & \tau_{yx} & \tau_{zx} \\ \tau_{xy} & (\sigma_y - u_a) & \tau_{zy} \\ \tau_{xz} & \tau_{yz} & (\sigma_z - u_a) \end{bmatrix}$$

(2.5)

The matric suction is, instead, a scalar variable, expressed as:

$$s = u_a - u_w \qquad (2.6)$$

The most common and recent constitutive models for unsaturated soils are described below.

2.6.2. Critical state framework for saturated soils

The critical state framework for saturated soils serves as the basis for the majority of modern constitutive models that explain the mechanical behaviour of unsaturated soils. The critical state hypothesis emphasises the idea that, under stress, a soil eventually attains a state of plastic behaviour that is marked by constant deformation without experiencing more stress, idealising the range of states at which the soil may reside. The behaviour of shear and volume changes in saturated soils under external loading can be explained using the critical state framework. Cam clay (Schofield and Wroth, 1968) was the first elasto-plastic critical state model; however, a second model, called Modified Cam clay (Roscoe and Burland, 1968), later appeared. A few presumptions that aid in understanding the behaviour of stress and strain and take into account the complexity of soils simplify the elasto-plastic critical state models (Kurtay and Reece, 1970). It is believed that soil is homogenous and isotropic:

- There are no time-dependent elements to the mechanical behaviour.
- The behaviour may be stated in terms of appropriate stress state variables.
- A macroscopic continuum mechanics model describes the behaviour.
- And lastly, the soil is not viscous.

Under the presumptions made, the effective mean effective stress (p'), deviatoric stress (q), and specific volume (v), which are defined as follows, are the state variables to characterise the mechanical behaviour:

$$p' = \frac{\sigma_1 + \sigma_2 + \sigma_3}{3} - u_w = \frac{\sigma'_1 + \sigma'_2 + \sigma'_3}{3} = p - u_w \qquad (2.7)$$

$$q = \sigma_1 - \sigma_3 = \sigma'_1 - \sigma'_3 \qquad (2.8)$$

$$v = 1 + e \qquad (2.9)$$

where:

p – mean stress,

e – void ratio,

σ_1, σ_2, σ_3 – principal stresses,

σ'_1, σ'_2, σ'_3 – principal effective stresses,

Under triaxial conditions where σ_2 is equal to σ_3, equation 2.7 takes the form of equation 2.10.

$$p' = \frac{\sigma_1 + 2\sigma_3}{3} - u_w \tag{2.10}$$

Or in terms of principal effective stresses:

$$p' = \frac{\sigma'_1 + 2\sigma'_3}{3} \tag{2.11}$$

Two two-dimensional planes can be used to define the critical state: the first unique line is defined in the stress plane (q-p' plane), which is the plane where there are no volume changes, and the second unique line is defined in the specific volume – effective stress plane (v-p' plane), which is the plane without shear stresses. It is possible to derive new parameters to characterise the critical state line from the two-dimensional planes:

$$v = \Gamma - \lambda \ln p' \qquad \text{in the v-p' plane} \tag{2.12}$$

$$q = Mp' \qquad \text{in the q-p' plane} \tag{2.13}$$

where:

λ – slope of critical state line on the v-p' plane,

Γ – intercept of the critical state line on the v axis,

M - slope of critical state line on the q-p' plane,

M can be interpreted as a friction parameter, and equation 2.16 can be used to calculate the internal friction angle at the critical state from M. It is possible to calculate the internal effective friction angle ($\emptyset$) from:

$$\sin \emptyset' = \frac{\sigma'_1 - \sigma'3}{\sigma'_1 + \sigma'3} \tag{2.14}$$

Following the derivation from equation 2.14, where:

$$\frac{\sigma'_1 - \sigma'_3}{\sigma'_1 + \sigma'_3} = \frac{3(\sigma'_1 - \sigma'_3)}{3(\sigma'_1 + \sigma'_3)} = \frac{3(\sigma'_1 - \sigma'_3)}{(\sigma'_1 - \sigma'_3) + 2(\sigma'_1 + 2\sigma'_3)} = \frac{3}{3} \times \frac{3(\sigma'_1 - \sigma'_3)/(\sigma'_1 + 2\sigma'_3)}{(\sigma'_1 - \sigma'_3)/(\sigma'_1 + 2\sigma'_3) + 2} = \frac{3M}{M + 6} \tag{2.15}$$

This provides the opportunity to determine the critical state friction angle using equation 2.16:

$$\emptyset' = \arcsin \left(\frac{3M}{M + 6} \right) \tag{2.16}$$

2.6.3. The Barcelona Basic Model

Alonso et al. (1990) introduced the Barcelona Basic Model (BBM), which is an expansion of the Modified Cam Clay (MCC) framework (Burland, 1965a; Roscoe and Burland, 1968) designed for partially saturated cases. This model involves several primary stress variables, which are as follows:

Mean net stress(tensor)
$$p'' = p - u_a = \frac{1}{3}(\sigma_1 + 2\sigma_3) - u_a \qquad (2.17)$$

Deviatoric stress (tensor)
$$q = (\sigma_1 - u_a) - (\sigma_3 - u_a) = \sigma_1 - \sigma_3 \qquad (2.18)$$

Matric suction (scalar)
$$s = (u_a - u_w) \qquad (2.19)$$

A yield line, often referred to as the Load Collapse (LC) yield curve, represents the location of volumetric yield points in the s: p'' plane in the BBM and divides a zone of quasi-elastic behaviour from a zone where plastic compression occurs along the s - p'' space. This model states that a decrease in matric suction or an increase in mean net stress can both lead to yield. Regardless of the stress path causing the irreversible compressive phenomena, the yield line itself indicates when they begin to occur. However, the mechanical response of the soil remains essentially the same whether yield is induced through loading or soaking. The BBM also says that any path will result in recoverable elastic volumetric strains inside the quasielastic area. This strain-hardening type of model, called the BBM, says that plastic deformations cause the quasi-elastic region to expand, which moves the LC yield line to the right in the s:p'' space. Nevertheless, the LC yield line moves in response to both loading and wetting, and its movement indicates the same amount of volumetric stresses.

Additionally, the model suggests that a soil is saturated when the matric suction equals zero, which may not always be the case. On the other hand, it has also been demonstrated that partially saturated soils can have null matric suction. Saturated soil can exhibit suction values. One of the primary motivations for some researchers' attempts to enhance this model is that it captures fundamental ideas about the mechanical behaviour of partially saturated soils, specifically:

- the elevated pressures caused by the collapse as the load increases steadily
- the collapse under continuous load while wetting
- while loading at constant suction, the growing yield stress with increasing suction.

Using two distinct modified stress variables, new forms of elasto-plastic models have been given (Gallipoli et al., 2003a; Wheeler et al., 2003) to address the concerns raised by BBM.

The final two models, which will be discussed later, have effectively replicated key ideas regarding the behaviour of partially saturated soils (concepts that were not replicated by previous models like BBM). These models include the history of suction (i.e., a soil response to compression at constant suction will depend on the previous history of suction) and present smooth transitions from fully saturated to partly saturated behaviours in addition to accounting for irreversible changes of the void ratio during the wetting-drying cycle.

The primary goal of these models is to disentangle the two mechanical effects that a partially saturated soil encounters: the impact of the soil's saturation level and its water distribution, which would change the two stress variables included in the Wheeler and Gallipoli models.

The first variable, which relates to the distribution of water in soil, is expressed as an equation 2.20, which is based on equation 2.4 and is a function of the effective stress placed on the soil skeleton and the bulk water in the soil (Bishop's average skeleton stress; Jimmi, 2000):

$$p^* = p - [\, Sr \times u_w + (\, 1 - Sr \,) \times u_a] \tag{2.20}$$

where:

p^* - Bishop's average stress skeleton,

p – total stress,

Sr – degree of saturation,

u_w – pore water pressure,

u_a – pore air pressure

The second variable has to do with the water menisci, or more specifically, the stabilisation that these water menisci offer at the soil's inter-particle interactions, even though Wheeler and Gallipoli interpret it differently. In the end, the degree of saturation, porosity, and suction are what account for this impact. Because of their realistic methods to predicting partly saturated soils and their capacity to incorporate significant impacts on soil behaviour, the models put forth by Wheeler and Gallipoli are shown below.

2.6.4. Wheeler model

Wheeler et al. (2003) provide a model that takes hydraulic hysteresis into account and assumes that soil stability reflects the fluctuation of stabilising forces at interpaticle contacts. The Soil Water Retention Curve (SWRC), which illustrates the phenomena of hydraulic hysteresis, explains why two soils may exhibit comparable matric suction values yet differ in the amount of fluid present in their pores. Wheeler's differentiation of bulk and meniscus pore

fluid allowed him to take this effect and its impact on the mechanical behaviour of soil into account. It is therefore possible to say that two samples with similar matric suction and dry density values, subjected to the same external load, but presenting different degrees of saturation, represent two different states of a soil. Soil behaviour is therefore dependent on the proportion of meniscus and pore fluid within the soil skeleton, or, in other words, the degree of saturation of the soil. The degree of saturation has an impact on soil behaviour since samples with only menisci present exhibit different contact forces than those with fluid-filled pores. An extra stabilising force is present during interparticle interactions when menisci are present. Volumetric deformations may potentially have an impact on the SWRC's location. The SWRC will move to the right during compression as smaller voids necessitate greater suction levels to maintain the saturation degree. Because elasto-pastic processes can be used in both mechanical and hydraulic processes, the Wheeler et al. model can couple both processes. These two distinct phenomena allow for this linkage to occur:

- elasto-plastic deformation of the soil skeleton by loading

- elasto-plastic inflow and outflow of fluid from interparticle pores.

Two independent stress variables are considered to control the behaviour of the soil: s*, also known as modified suction, and p*, also known as Bishop's stress, which represents the stabilising effect of menisci at interparticle contacts and total stress, pore fluid pressure, and gas pressure effect on the soil skeleton. Regarding strain variables, Wheeler et al. offer two conjugate strain variables: the degree of saturation (dSr) and volumetric strains ($d\varepsilon_V$). A Load Collapse (LC) yield line can be used to simulate plastic volumetric deformations, just like in the Alonso et al. (1990) model. Wheeler, however, asserts that this line is vertical and straight in the s*:p* plane and that this is because the stabilising force acting on the menisci is continuous and unaffected by suction. The amount of interparticle connections showing menisci determines soil stability, not the matric suction value. The soil sample undergoes compressive plastic volumetric strains when the LC yield line is crossed during loading, which causes the LC yield line to shift. The number of menisci at interparticle contacts changes when the soil sample is wetted or dried to the point where plastic changes in the degree of saturation occur. As a result, the LC yield line also shifts—either to the left, contracting the yield locus on wetting, or to the right, expanding it, on drying. The scanning curve meets the main branches of the SWRC when either a Suction Decrease (SD) or a Suction Increase (SI) line is crossed, resulting in irreversible changes in the degree of saturation (see Figure 2.9).
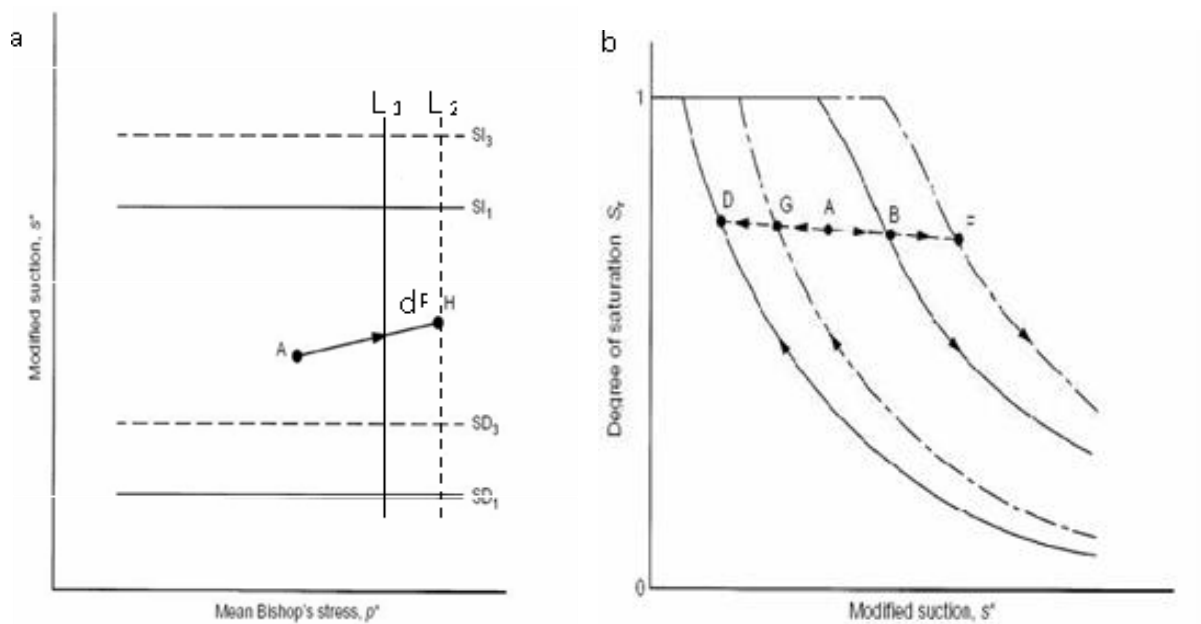
Figure 2.9 Coupled movement of the SI and SD caused by plastic volumetric yielding: **a)** Stress path **b)** SWRC (after Wheeler et al., 2003).

The SWRC position moves, the SI and SD yield lines move in tandem, and plastic volumetric strains develop if the LC yield line is crossed during loading (Figure 2.9). This model states that elastic behaviour is that which is contained inside the $s^*:p^*$ space's SI, SD, and LC lines; any path that crosses any of these lines will lead to either irreversible changes in the degree of saturation or plastic volumetric strains. As a result, the Wheeler et al. model can replicate a number of significant features of soil behaviour, including the following:

- the expansion or contraction upon wetting - the change in a soil's saturation level from partially saturated to saturated
- compression of plastic throughout the wetting-drying cycle
- variations in saturation level brought on by hydraulic hysteresis
- how wetting-drying cycles affect a soil's future mechanical reactions when it is loaded.

A single LC yield line (or curve) or removing the impact of hydraulic hysteresis cannot adequately represent the majority of the aforementioned aspects. Another benefit of Wheeler's model is that it makes it possible to forecast a behaviour that smoothly shifts from unsaturated to saturated. Nevertheless, thus far, only qualitative predictions have been realised, and certain model assumptions still need to be confirmed and validated by experiments.

2.6.5. Gallipoli model

While Gallipoli et al. (2003a) take a somewhat different tack and concentrate on soil factors such as stress, pore gas pressure, pore fluid pressure, and degree of saturation, Wheeler et al. (2003)'s model focuses on the distinct behaviours of fluid- and gas-filled pores.

A model with two independent stress factors is also presented by Gallipoli et al. (2003a), but it specifically takes into consideration how plastic variations in saturation degree affect the behaviour of partially saturated soils under stress. The stress variables that Gallipoli included in his model are: Menisci bonding effect at interparticle contacts is explained by the bonding variable σ*, also called average skeleton stress, which is equal to Bishop's stress ξ.

Gallipoli proposed that the primary cause of the void ratio increase with increasing suction of samples that yield along a typical compression line is the presence of menisci and the bonding effect these give. Gallipoli found a relationship between the void ratio of the partially saturated samples (θ) and the saturated samples (θs) yielding along a normal compression line of constant suction and subjected to the same skeleton stress (Figure 2.10b) by comparing the normal compression lines at constant suction of soil samples with different values of matric suction (Figure 2.10a).

This relationship is associated with the bonding variable ξ and the bonding effect of menisci. Despite the fact that the authors have discovered that the bonding variable ξ and the ratio e/e_s hold true for both isotropic and anisotropic loading, the mathematical formulation has only been provided for the isotropic stress space up to this point.

In order to describe plastic volumetric compression, a normal compression state surface is defined in the e: p*: ξ space. Like the models mentioned above, the normal compression state surface indicates yielding states; pathways along it represent elasto-plastic changes in the void ratio, while paths below it are associated with fully elastic processes. The normal compression lines for various values of ξ are straight since the ratio e/es is constant for a given value of ξ (Figure 2.11a). Elastic variations in the void ratio are independent of ξ and rely on variations in p*. Gallipoli proposed that the mechanical formulation he had developed be used in conjunction with models like those by Vaunat et al. (2000) or Gallipoli et al. (2003b) in order to incorporate the effects of hydraulic hysteresis and plastic changes in void ratio on the variation of the degree of saturation.
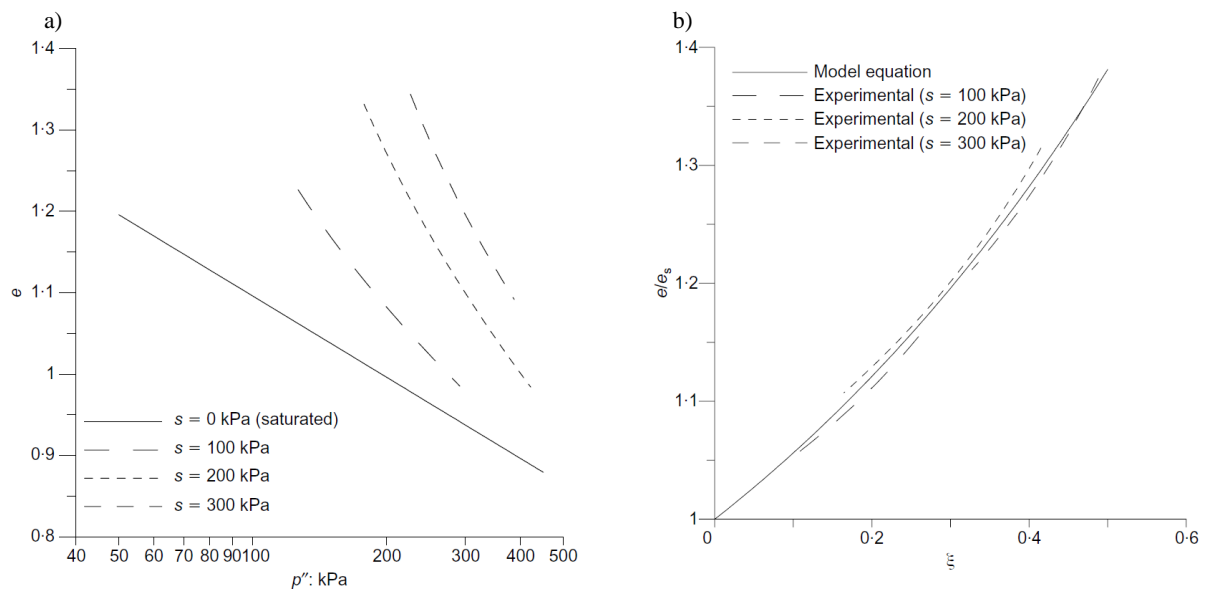
Figure 2.10 a) Normal Compression Line at constant suction b) Relationship between ratio e/e_s and bonding factor ξ during isotropic virgin loading at constant suction (Gallipoli et al., 2003a, experimental data from Sharma, 1998).

However, the latter work only addresses changes in the SWRC as a result of void ratio variations, not hydraulic hysteresis specifically. Furthermore, Gallipoli's model does not differentiate between expansive and non-expansive soils. Nevertheless, it makes it possible to forecast certain significant features of soil behaviour, such as partially saturated soil behaviour and expansive and non-expansive soils. Some of these aspects, such as the development of plastic compressive strains during a wetting-drying cycle and the significance of suction history on stress-strain behaviour during isotropic loading at constant matric suction along the normal compression line, cannot be replicated with a single LC yield line as previous models advocate.

2.6.6. Toll framework for unsaturated soil behaviour

Toll (1990) tested a framework on lateritic gravel known as Kiunyu gravel, which attempted to explain the behaviour of unsaturated soils in terms of total stresses and suction operating within compacted soils. This framework, like the BBM, was based on the critical state model for saturated soils, where the unsaturated behaviour was described by taking suction and total loads into distinct considerations. In contrast to the BBM, Toll's method placed more emphasis on the soil fabric, which is mostly reliant on the saturation level and expresses the contributions of suction and total stress to shear strength as two distinct stress ratios.
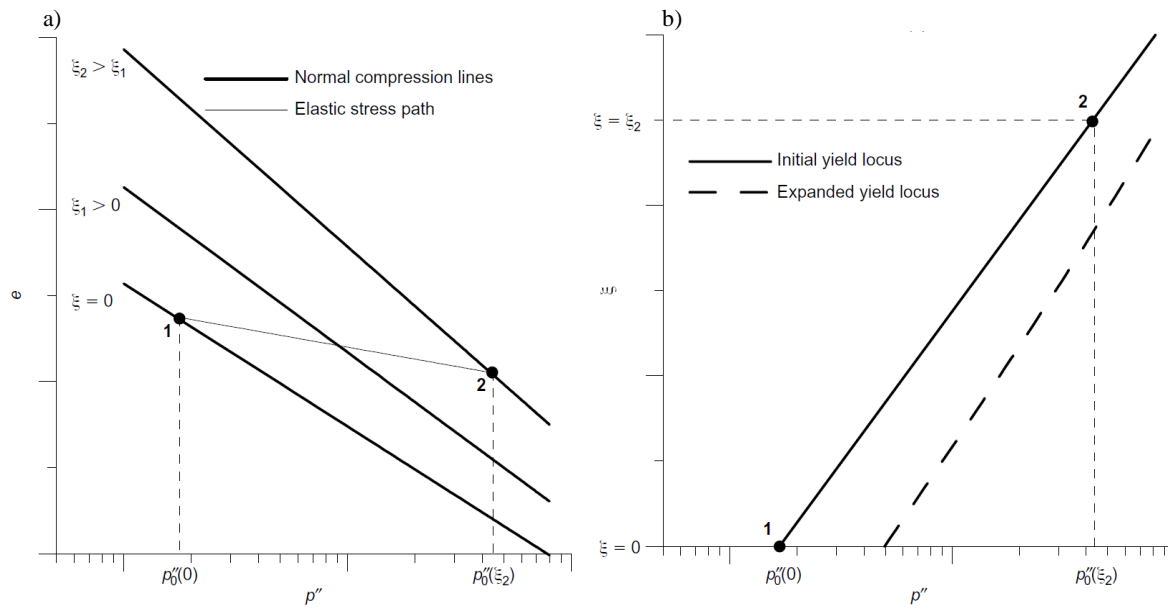
Figure 2.11 Yield locus derivation in the isotropic plane for the Gallipoli et al. (2003a) model: **a)** change of void ratio; **b)** stress path (Gallipoli et al., 2003a).

Toll (1990) discusses the significance of the soil fabric in compacted clays, using the findings of Croney et al. (1958) who defined the fabric of compacted clays as aggregates of clay particles (or clay plackets) divided by relatively large air gaps. According to Brackley (1980), air fills the gaps between the aggregates while the voids within the clay aggregates are saturated. The behaviour of a compacted soil is influenced by the size and distribution of the clay aggregates, which also affects the interaggregational void space. The aggregates of clay particles might act as single, larger particles and behave as soils with coarser grading if suction was strong enough in the inter-aggregate gaps. Conversely, if the suction was decreased, the aggregates may become unstable and there's a chance that their volume would decrease (collapse). The behaviour of unsaturated compacted soils at the critical stage is described by the Toll framework, which is stated as follows:

$$q = M_a(p - u_a) + M_w(u_a - u_w) \tag{2.21}$$

$$v = \Gamma_{aw} - \lambda_a \ln(p - u_a) - \lambda_w \ln(u_a - u_w) \tag{2.22}$$

where:

q − deviator stress

 p − total stress

u_a - u_w − matric suction

u_a − pore air pressure

u_w − pore water pressure

47

M_a – total stress ratio

M_w – suction ratio

ν – specific volume

Γ_{aw} – intercept in the ν space

λ_a – slope of the critical state derived from the total stress

λ_w – slope of the critical state derived from suction

In equations 2.21 and 2.22 the parameters M_a, M_w, λ_a, λ_w, and Γ_{aw} are functions of the degree of saturation and fabric of the soil. It is necessary to conduct an experimental analysis to ascertain how these parameters depend on the saturation level. Within this perspective, the saturation level serves as a useful, but limited, fabric indication. Five dimensions are needed in order to adequately describe the behaviour of unsaturated soil at the critical condition using this framework, these are: p-u_a, u_a – u_w, q, ν and Sr (degree of saturation).

Toll and Ong (2003) also used this framework on a residual sandy clay soil from Singapore and discovered that, when normalised, the functions linking Ma and Mw to saturation degree were comparable to those for lateritic gravel.

2.7. Chapter summary

Understanding the behaviour of unsaturated soils, various research approaches, mechanical and hydraulic properties, and some of the frameworks available in the literature for presenting and interpreting such data are some of the subjects covered.

It is essential to comprehend the fundamental ideas discussed in the opening sections of this chapter in order to comprehend the behaviour of unsaturated soils. These include the nature of unsaturated soils, their phases (soil, water, air, and air-water), and the behaviour of soil suction and water retention. There are several methods for determining soil suction, however only the approaches utilised in this study, high capacity suction probe, and pressure plate technique, axis translation, were discussed. The idea behind the measurement, benefits, and drawbacks were discussed for each technique. Major findings and methods from other researchers' work were provided, as part of this research also involved monitoring suction outside of a controlled environment. The hydro-mechanical testing of unsaturated soils was deemed significant, and various approaches were presented, including osmotic, axis translation, relative humidity, and a computer-controlled approach utilising high-capacity suction probes. These methodologies were identified in the literature.

The last section of this chapter presents a few of the frameworks that have been developed in the literature to describe and explain the behaviour of unsaturated soils. These frameworks include the Wheeler model, the Gallipoli model, the Barcelona basic model, or BBM, and the Toll framework.

3. Soil materials used in the study

3.1. Cohesive soil

The cohesive soil material investigated in the present study was collected from a purpose built experimental embankment located near Newcastle, UK. The embankment itself was constructed as a part of the international scientific project called BIONICS and ISmart, in which the author of the thesis was involved thanks to participation in TU1202 - Impact of climate change on engineered slopes for infrastructure (EC founded project).

According to Hughes et al. (2005), the glacial till that was utilised as a filling material of slope, that was purchased from a stock pile in County Durham. Its composition was determined to be 12% gravel, 16% sand, 35% silt, and 37% clay. The material is categorised as sandy clay soil due to the high percentage of clay minerals present. Table 3.1 displays the Atterberg limits obtained by the rolled thread test for the Plastic Limit (PL) and the cone penetrometer test for the Liquid Limit (LL). Based on the Casagrande plasticity chart, the fill material is classified as intermediate plasticity.

Table 3.1 Atterberg Limits for the cohesive soil samples used in the study.

Water content Wn (%)	Liquid limit LL (%)	Plastic Limit PL (%)	Plasticity Index PI	Liquidity Index LI
22.6	43.3	23.7	19.6	-0.05

By dividing the PI by the percentage of clay material, one can calculate the Activity (A) of the clay minerals in the fill material (Skempton, 1953). According to Skempton's categorisation, the clay minerals in this fill material are deemed inactive since A=0.53, which is less than 0.75.

To lessen density variance, the initial material that was gathered from the embankment was sieved through a 2.80mm mesh. Figure 3.1 displays the soil's sieved particle size distribution. Four particle size distribution curves were plotted. The first portion of each curve in Figure 4.1 was derived from a single test in which 3000g of material was dry-screened through sieves ranging in size from 2.80 mm to 0.063 mm. The pipette method was used to analyse the material that passed through this sieve utilising pipette sedimentation. Four separate samples

underwent sedimentation analysis experiments, yielding the four particle size distribution curves shown in Figure 3.1. These test findings will be identical to the non-sieved material since the Atterberg limits (liquid limit, plastic limit, plasticity index, and liquidity index) and specific gravity are obtained on material passing 425µm. The sieved material's clay activity (A) of 1.3, determined by calculating the PI/Clay fraction, indicates that the laboratory material is classified as normal, based on activity. This increase in activity when compared to the unsieved material was caused by the sieved material's higher percentage of clay particles.
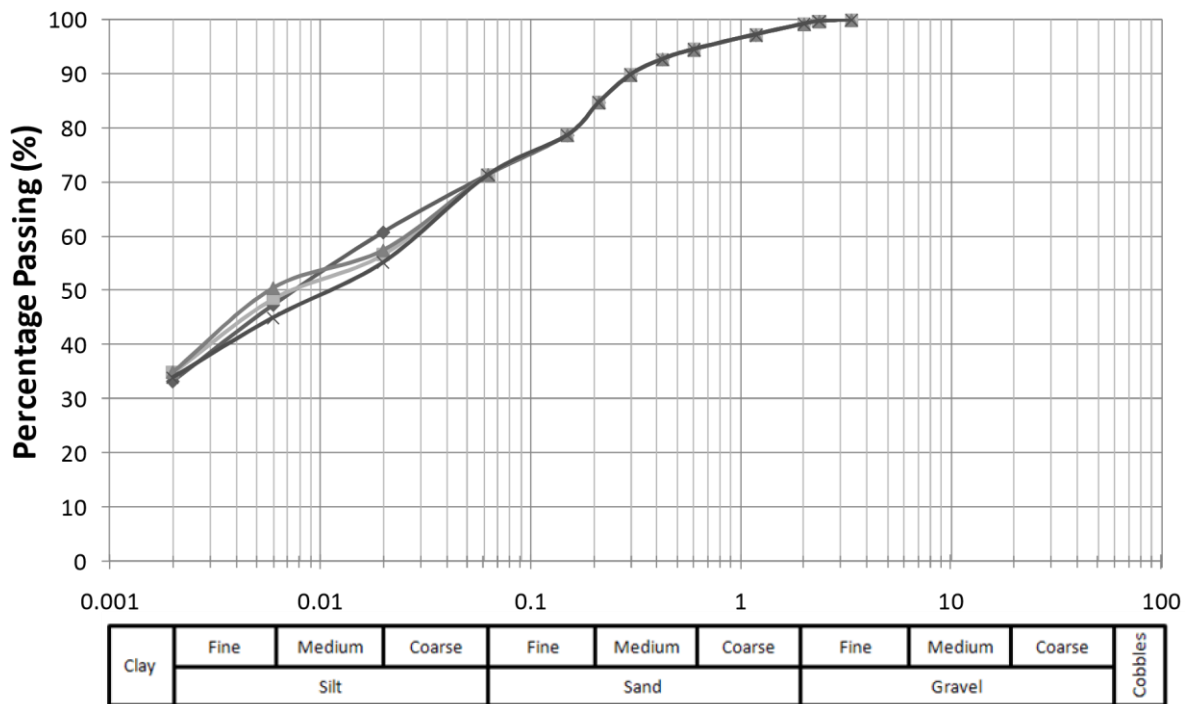

Figure 3.1 Particle distribution curves for the sieved cohesive soil.

Various compaction curves were derived for distinct samples and varying compaction efforts. Each compaction curve was designated based on the applied compaction effort and the height of the compacted sample. In this context, BS denotes British Standard, L (light) or H (heavy) indicates the compaction effort, while the numbers 100 and 200 signify the height of the compacted sample. The letter S was appended to the label of the compaction curve derived from the sieved material. Figure 3.2 presents the compaction curves for the original material, utilising the BS1377 process (BSL100 and BSH100) and the updated procedure for the 200mm high mould (BSL200 and BSH200). A test on the sieved material is also shown (BSL200 S). A significant decrease in dry density is evident when comparing the compaction curves of the original material (BSL200) and the sieved material (BSL200 S). The optimal water content and maximum dry density for the BSL200 S test were W_{opt} = 15% and

$\gamma_{d\ max}$ = 1.719 Mg/m³. Another observation is the close proximity of BSL200 S to the light proctor compaction curve BSL100. The BSL200 S compaction curve used as the baseline for all subsequent tests. The compaction curves BSL200 S and BSL100 exhibit a favourable correlation with data recorded during the construction of the BIONICS embankment (Hughes, 2005), as illustrated in Figure 3.3. Consequently, the sample preparation methods yield material with a density closely resembling that observed in the BIONICS embankment.
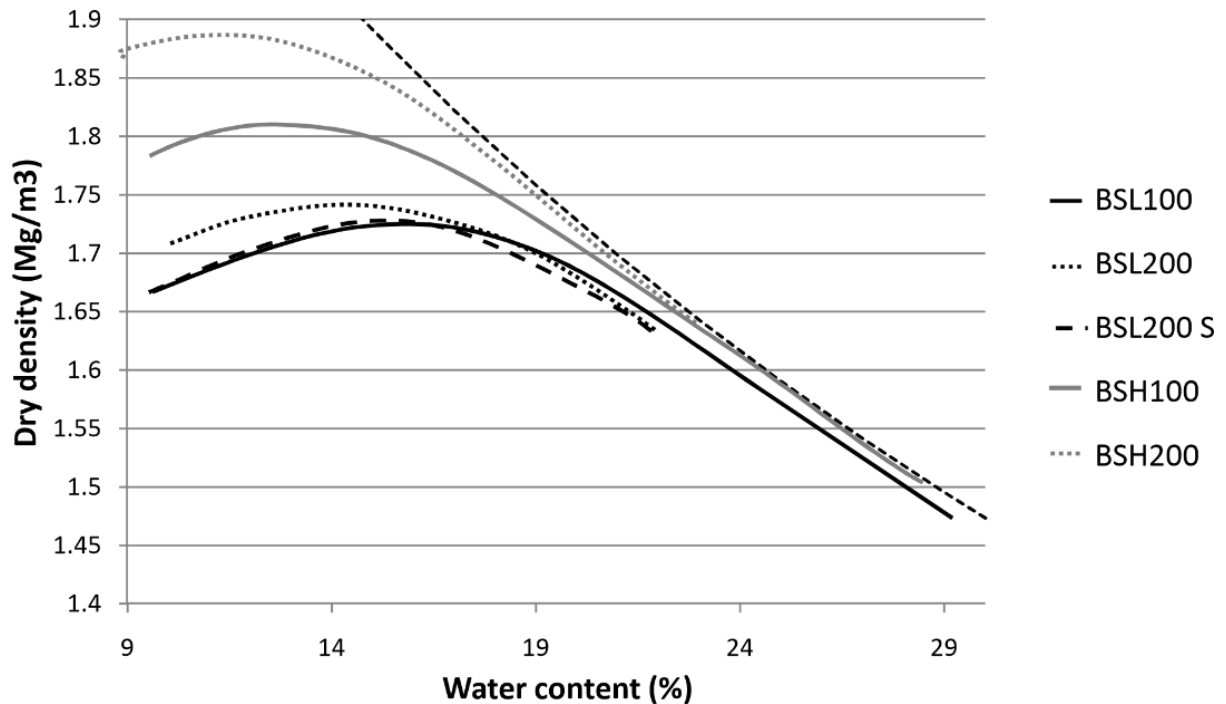

Figure 3.2 Results obtained for the compaction curves.

3.2. Granular soil

The second type of soil material of which hydraulic-mechanical parameters were examined within the present research was granular soil in a form of fine sand particles. This was the material provided for the purpose of delivering the millstones of international project MUMOLADE (Multiscale Modelling of Landslides and Debris Flows, within the framework of Marie Curie ITN) that the author was a participant of.

The soil was classified as a fine and uniform uncrushed silica sand. It is deposited near Bedfordshire in the east of England and it supplied by the David Ball Group, Cambridge, U.K. The particle size distribution of the material is presented on Figure 3.4. The curve was determined using the dry sieve method. In the same figure, the grading curves of the different fractions are also shown, using data from Cavarretta (2009).

The specific gravity of the anlysed sand is 2.65. The maximum and minimum void ratios are found to be 0.99 and 0.65, respectively. The coefficient of permeability is $1.44*10^{-4}$ m/s. All the main physical parameters are presented in Table 3.2.
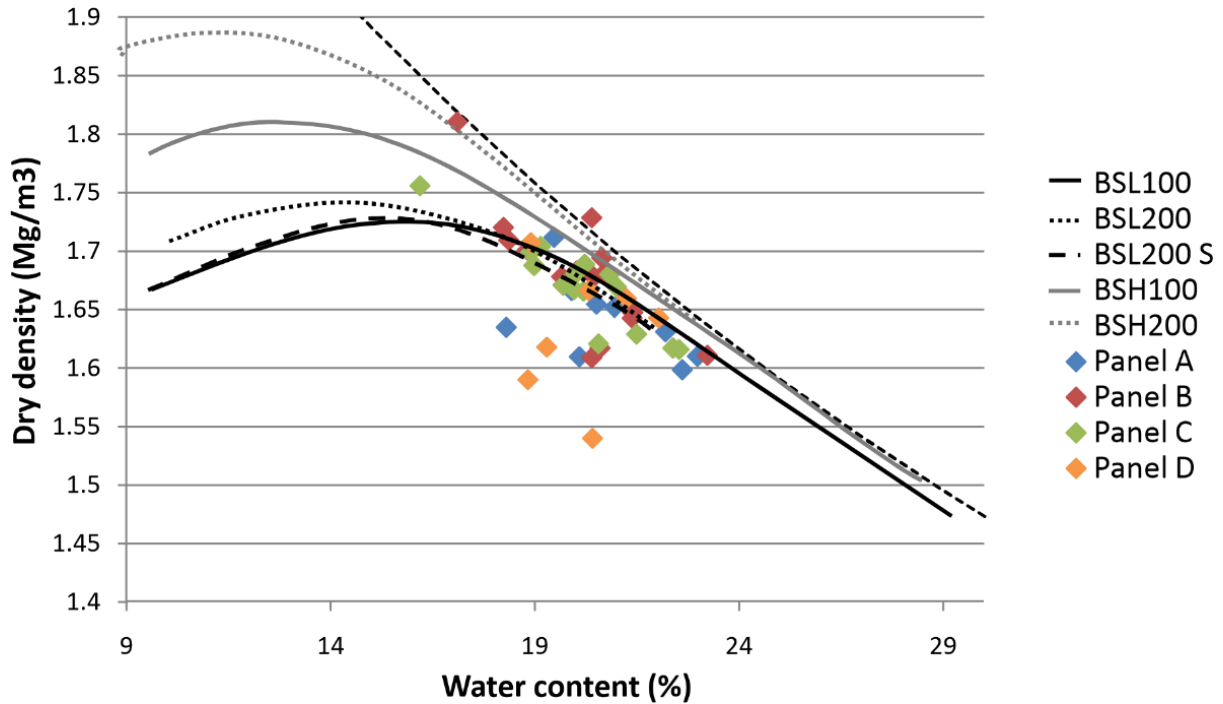

Figure 3.3 Different compaction curves related with field measurements obtained for the experimental embankment.
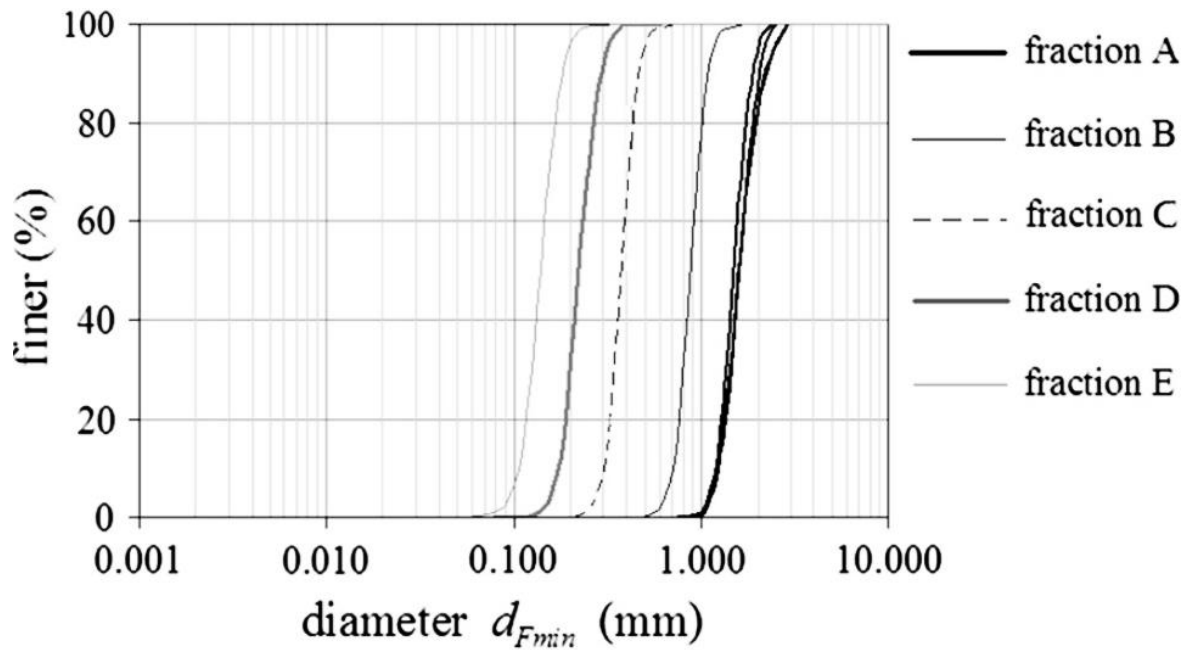

Figure 3.4 Grain size distribution curves for sand provided by the manufacturer, fraction E represents the find sand used in the study (Lanzano et al. 2016).

Table 3.2 – Fine sand, fraction E– soil characteristics.

Parameter	Unit	Value
Permeability, k	(m/s)	$1.44*10^{-4}$
Dry density maximum, ρ_{dmax}	(Mg/m^3)	1.61
Dry density minimum, ρ_{dmin}	(Mg/m^3)	1.33
Optimum moisture content, W_{opt}	(%)	11
e_{max}	–	0.90
e_{min}	–	0.52
G	–	2.65
D_{10}	(mm)	0.095
D_{50}	(mm)	0.12
E	–	0.735

The compaction test was performed using light 2.5 kg rammer sliding freely from 300 mm. The soil is compacted into three layers, each receiving 27 blows from the falling rammer. The test was performed according to light compaction test. The results of bulk density against moisture content are presented on Figure 3.5.
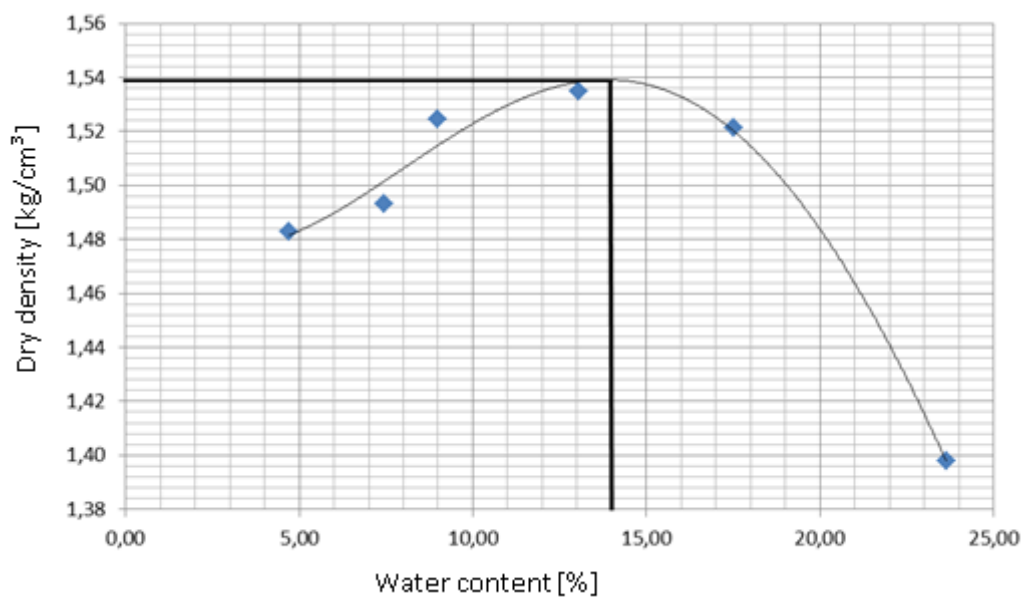

Figure 3.5 Results obtained for the compaction curve of fine sand.

4. Laboratory sample preparation methodology

4.1. Introduction

The chapter outlines the methodology required to conduct tests that characterise the hydromechanical behaviour of two soil types: cohesive and granular materials, as detailed in the preceding chapter. The primary focus was on cohesive material, specifically sandy clay, as the studied materials were reconstituted and required preparation prior to conducting hydraulic-mechanical tests. The technique employed and the challenges faced during the testing procedure and their corresponding solutions are described. A critical aspect of soil testing is the implementation of effective and dependable sample preparation protocols. This facilitates replication and makes the results reliable. Nonetheless, the challenges in acquiring adequate specimens and maintaining repeatability limited the use of such method. Consequently, dynamic (drophammer) compaction was implemented. Constant water content tests were conducted in the triaxial cell apparatus to elucidate the mechanical behaviour and gain insight into the hydraulic behaviour. During testing, suctions were quantified utilising high-capacity suction probes. A distinct approach was implemented for granular material (fine sand) since this material was supplied by a manufacturer under the specified conditions.

4.2. Cohesive soil sample preparation for the hydraulic-mechanical behaviour testing

Samples were compacted with drop-hammer (dynamic) compaction to achieve densities that mimic building circumstances (as will be proved subsequently). A mould of 115 mm in height and 105 mm in diameter was utilised for standard compaction testing (BS 1377: Part 4, 1990). Specimens having a height-to-diameter ratio of 2:1 were prepared for triaxial testing. To get a more accurate portrayal of field circumstances, a sample diameter of 100mmx200mm was selected. The compaction level was sustained at the equivalent of BS Light (Proctor) compaction, used a split mould with a diameter of 100mm and a height of 200mm. Consequently, the soil was compacted in six levels, each roughly 33mm thick, in contrast to three layers of 38mm used in standard compaction tests. Table 4.2 presents the outcomes of compaction tests conducted in the 200mm high mould utilising the compaction effort given in Table 4.1.

The tested samples were the actual material received from the BIONICS experimental embankment site, utilised without any prior sifting before testing. Repetitive tests were conducted at two moisture levels (15% and 20%). The results for dry density at 15% water

content for the original material indicate a variation of 0.075 Mg/m^3, whereas at 20% water content, the difference was reduced to 0.016 Mg/m^3. The density change of 0.075 Mg/m^3 (equal to 4%) was excessive and attributable to the presence of bigger particles. To mitigate this difference in the measured densities, the material was subjected to sieving using a 2.8mm screen to eliminate bigger particles, which constituted 11.5% of the total material.

Table 4.1 Compaction procedures adopted for sample preparation.

Specifics	Light compaction	Heavy compaction	Compaction procedure adopted
Height (mm)	115	115	200
Diameter (mm)	105	105	100
Nr. of blows per layer	27	27	27
Nr. of layers	3	3	6
Ram weight (kg)	2.5	4.5	2.5

Consequently, all subsequent testing was conducted on material filtered through a 2.8mm sieve. The approach for sample preparation is summarised as follows:

- The soil was desiccated to ambient conditions;
- The soil was subjected to sieving through a 2.80 mm mesh to exclude bigger particles;
- The soil underwent oven drying for a minimum duration of 24 hours.
- Four bags, each containing 1000 g of soil, were constructed to facilitate calculations for the required amount of water.
- Water was incorporated to attain the requisite moisture level.
- The bags were allowed to equilibrate for 24 hours to achieve homogenisation of the water content within the soil.
- The soil was densified via a drop-hammer compaction apparatus.

An effective sample preparation protocol was established, enabling the replication of samples with identical dry density for the same water content.

To accomplish this, the maximum particle size of the soil was decreased by screening through a 2.8 mm mesh. The sieved substance was categorised as sandy clay. A strong correlation was noted between the laboratory densities) and the values obtained from field measurements.

4.3. Granular soil sample preparation

Preparing granular soil samples for hydraulic-mechanical testing is always a challenging task as its loose structure and lack of cohesion do not provide stable conditions when working on any research stage. The methodology needs to differ depending on type of a test and achieving required physical soil parameters. The fine sand was provided by the manufacturer in 25 kg paper bags. The granular material for testing, in comparison to the cohesive soil did not have to go through the entire procedure of sieving and compaction (using Proctor test). All the samples for triaxial testing and Soil Water Retention Curve determination were prepared at the research stage, hovered before providing desired moisture content, the material prior the testing was always oven dried in 105°C, and left to equalize for 24h. Due to the complexity and specific characteristics of granular samples preparation for unsaturated hydro-mechnical testing, the procedure for each tests, depending whether it was triaxial or soil suction measurement will be described later in the text, when each hydraulic-mechanical test is described. This is to make the understating of the testing approach easier to follow.

5. Soil Water Retention Curve determination for sandy clay

5.1. Introduction

Unsaturated soil mechanics are crucial in the design of earth structures such as railway and road embankments, dams, dykes, and shallow foundations. They are often constructed in the vadose zone. Their mechanical qualities are influenced by hydraulic variations resulting from diverse climatic occurrences. The measurement of Soil Water Retention Curves (SWRC) is essential for analysing the geotechnical properties of soil, particularly in the context of rainfall-induced slope failures (Hughes et al., 2009). This research analyses the Soil Water Retention Curve (SWRC) for compacted clay soil samples generated at varying moisture contents and exposed to wetting and drying cycles. The application of hydrological cycles aimed to represent various climate scenarios (Tang et al., 2018). Given that soil suction influences the mechanical strength of fill material in earth structures, it is essential to ascertain and comprehend the hydraulic behaviour of the soil. SWRC typically represents soil behaviour regarding adsorption and desorption processes. The link between water content (gravimetric or volumetric) or degree of saturation and soil suction, given in kPa, is typically presented. Three primary stages can be identified in the acquisition of the SWRC. Initially, the soil may be nearly fully saturated during the drying process. As drying progresses, resulting in heightened suction, air begins to infiltrate

the soil's pores, establishing the air entry value of the soil. Beyond the air entrance value, the desorption process enters a transition zone, where the majority of desaturation occurs. This is succeeded by residual suction, indicating that the sole water present in the soil is that which is tightly adhered to soil particles (Lourenco, 2008). All three stages can be observed across all soil types; however, the morphologies of the Soil Water Retention Curve (SWRC) and suction values may differ.

5.2. Measurement techniques of soil suction used in the study

5.2.1. Pressure Plate

The pressure plate apparatus employed in this work was a Soil Moisture Corp. pressure chamber with a range of 1500 kPa, configured as shown in Figure 2.5. Alterations to the initial configuration were implemented to facilitate independent multi-sample testing by replacing the original porous ceramic disc with three distinct ceramic discs, each possessing an air entry value comparable to the original disc (1500 kPa), and each connected to a separate volume gauge in lieu of the burette. As depicted in Figure 2.5, nitrogen cylinders supplied the air instead of the laboratory air compressor, facilitating the application of elevated air pressures within the chamber. Prior to testing, the ceramic discs were fully wet. This step is essential for this testing approach, as the removal of all air bubbles from ceramic discs is necessary for accurate measurements. The implemented saturation technique involved positioning the ceramic discs within the pressure plate apparatus, which was submerged in deaired water, with the water level maintained at 2 cm above the discs. Upon securely sealing the lid of the pressure plate, air pressure was incrementally elevated to propel water through the discs. The operation continued until no air bubbles were detected rising from the discs. This process was conducted before any testing in the pressure plate device. The sandy clay specimen prepared as detailed in Chapter 3. The samples utilised for the SWRC determination were made "as compacted" at 25% water content. The soil was initially oven-dried and sieved to attain a density that was as uniform as feasible. Subsequently, soil samples were transferred into plastic bags, and water was introduced. The prepared soil was allowed to rest for 24 hours to facilitate uniform moisture distribution throughout the sample. The samples were reconstituted in a split mould of 100 mm in diameter and 200 mm in height, then compacted by light compaction Proctor testing (Figure 5.1). The soil core was extruded and cut to the specified dimensions. Following the trimming of each sample, specimens for water content analysis were obtained to verify uniformity of water content across the soil sample profile.

Figure 5.1 Sample preparation and trimming to desired size: a) sample core extruded after Proctor test; b) stainless still ring; c) soil specimens, size of 20/75 mm.

The sample was subsequently positioned on the saturated porous ceramic plate within a Soil Moisture Corp. pressure chamber operating at 1500 kPa, ensuring close contact between the sample and the plate. The chamber was partially filled with water beneath the ceramic plate to humidify the air within, preventing excessive desiccation of the sample. The chamber was securely sealed; internal air pressure and external water pressure were utilised to achieve the specified matric suction on the sample, defined as the differential between air and water pressure. Pressure was exerted on the water reservoir beneath the plate using a volume gauge to quantify the volume of water entering or exiting the specimen as the suction varied. Exerting pressure on the water reservoir effectively inhibits the release of dissolved air from the solution after traversing the ceramic plate. The elevated air pressure within the chamber ensures that the water, while passing through the ceramic plate, retains a significant concentration of dissolved air. Without this underlying pressure, the dissolved air could escape from the solution, potentially disrupting the water flow. In this case, exerting pressure on the water reservoir mitigates an erroneous measurement of the water volume fluctuation in the gauge. The volume change indicated by the gauge is influenced by both air diffusion and water flow within the ceramic plate. In certain casess, the air diffusion rate of the porous ceramic plate is minimal, yet it can occasionally be substantial enough to affect the resulting Soil Water Retention Curve (SWRC) (Vaquero, 2007). Despite attempts to theoretically predict the volume of diffused air, the numerous factors influencing diffusion rates render these predictions unreliable (Fredlund and Rahardjo, 1993). It is prudent to ascertain the air diffusion rate through the ceramic plate, particularly when the volume gauge measurement is the sole method available for assessing water volume change in a soil sample, to rectify the volume change values in the gauge. A computer utilising TRIAX data collecting software (Toll, 1999) was employed to monitor gauge volume changes and applied pressures, recording data at 30-

minute intervals during the experimental duration. When the gauge indicated a volume change of less than 0.35 cm^3/day, the sample was deemed to have achieved equalisation (Vaquero, 2007). Subsequent to equalisation, the sample was extracted from the pressure chamber and assessed: weight was recorded to the nearest 0.01g, and dimensions were measured with an accuracy of 0.01mm by vernier callipers. Subsequent to the measurements, the soil sample was returned to the plate, and the procedure was reiterated for ascending pressures. The maximum suction exerted was 1100 kPa, associated with an air pressure of 1310 kPa and a water pressure of 210 kPa. Upon completion of the experiment, the soil sample was subjected to oven drying to ascertain its dry mass, and the water content at various suction stages was subsequently back-calculated.

5.2.2. DU-WF High capacity suction probe

Stage Wetting and Drying

The tensiometer utilised in the investigation was the model developed at Durham University by Lourenço et al. (2011). Since Ridley and Burland's first development of a high suction probe in 1993, numerous enhancements and adjustments have been implemented. The primary distinguishing characteristic of pore pressure transducers is the air entrance value of the ceramic disc and the manufacturing design. Figure 4 illustrates the apparatus employed in the investigation, comprising (from the top): a 1500 kPa porous stone, a tiny water reservoir, a spacer, a ceramic transducer, and an electrical connection. All components are encased in a stainless steel housing. Tarantino and Mongiovì (2003) described another effective device that utilised a strain gauged diaphragm rather than a ceramic transducer. The primary benefit of the high suction probe is its nearly instantaneous reaction when assessing suction levels. The prevention of cavitation is accomplished by utilising a small water reservoir. The highest negative pore water pressure recorded with the tensiometer developed at Durham University was 2.1 MPa (Lorenco et al., 2011).

The initial method employed for ascertaining the Soil Water Retention Curve (SWRC) via the high suction probe was a sequential drying and soaking process. The samples were crushed using light Proctor testing at an initial water content of 25%. The samples were cut to the specified dimensions of 20 mm in height and 50 mm in diameter. The sample was thereafter positioned on a pedestal, with the tensiometer fixed to the base of the supporting plate and secured with an O-ring. To maintain continuous contact with the instrument, the sample was delicately pressed down. The sample was enclosed in a sealed

container and allowed to attain equilibrium of suction measurement. Subsequent to documenting the suction value, the sample was extracted from the pedestal, and measurements including weight and dimensional alterations were recorded manually. In the subsequent phase, based on the hydraulic path assessment, the sample was either desiccated (exposed to the atmosphere) or saturated (by employing a syringe to introduce water) to achieve the targeted water content. The sample was encased in cling film, sealed in an airtight container, and allowed to equilibrate for 24 hours before measuring the suction again. The method was done for various water amounts ranging from 25% to 16%. The suction measurements were conducted in phases.

Continuous drying and wetting approach

In contrast to the stage approach, for this method all the measurements such as mass, volume and suction changes are recorded continuously. All the readings are digitally recorded by the data acquisition system supplied with TRIAX software (Toll, 2001). The major component of the system is a PCV framework with high suction probe fixed at the bottom of the supporting plate, and six local small strain transducers (LVDT) attached to each side of the frame. Two of them are vertically placed at the top of the specimen and 4 at the side walls in the horizontal direction. The entire system rests on the digital balance as presented on Figure 5.2.
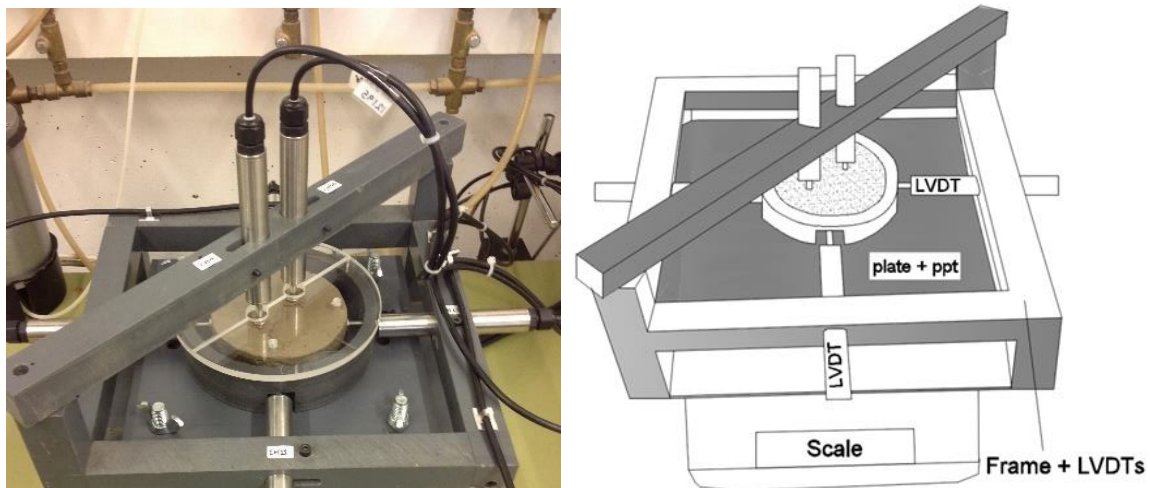

Figure 5.2 The laboratory set up for SWRC determination applying continuous hydraulic path changes (with tensiometer attached at the bottom).

The system is also equipped with a portable, split cover to avoid too rapid evaporation or drying of a sample during the measurement. The sample preparation procedure is the same as the one proposed for stage approach, however, the diameter was larger (20/75 mm).

When the hydraulic path followed is drying the sample is simply left on the pedestal and enclosed within the split cover. When the procedure is reversed for the wetting path, water drops are applied by using a syringe through holes drilled in the Perspex cover.

5.3. SWRCs obtained by the different methods and approaches

The results presented below focus on determination and evaluation of SWRC obtained by the pressure plate system (applying axis translation technique) and direct suction measurement by using high suction probe. The results are plotted as a function of gravimetric water content and suction (Figure 5.3), but also the SWRCs are presented in terms of changes in volumetric water content (Figure 5.4) and degree of saturation (Figure 5.5). This is to give a wider picture of the hydraulic behaviour of the tested sandy clay material.
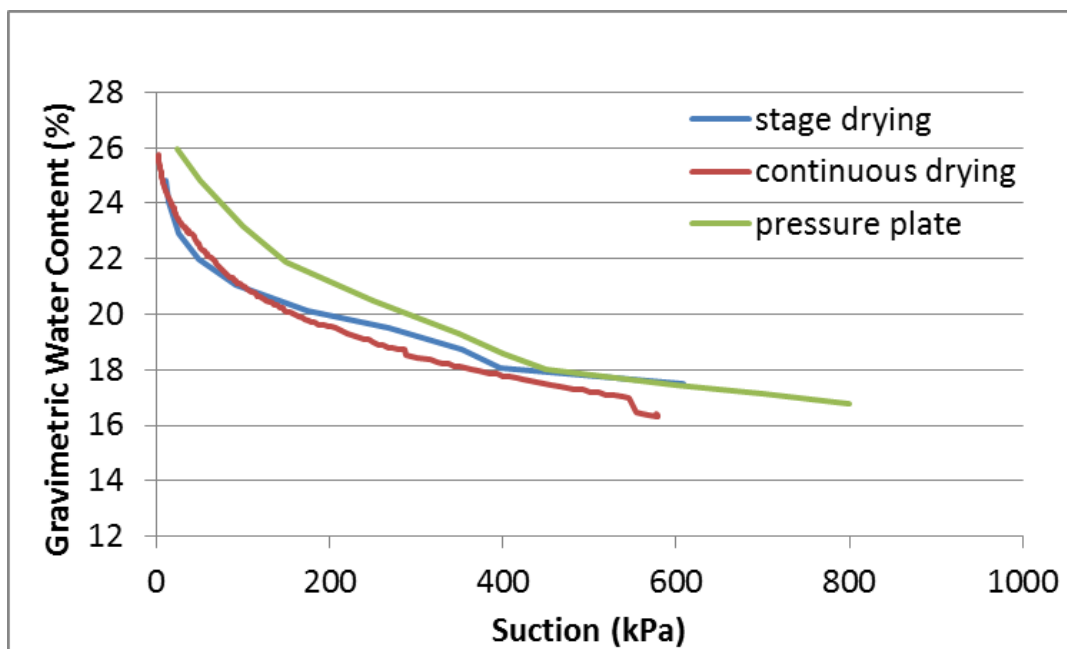

Figure 5.3 SWRC for different testing methods used, presented as gravimetric water content against suction.

From the graph (Figure 5.3) it can be seen that that suction measurements for the stage and continuous drying match each other, especially at the initial stage. The line inclination for the continuous approach is more consistent, which could be the effect of simultaneous reading of mass losses with suction increase.

The readings could also be influenced by the differences in sample dimensions. The second graph (Figure 5.4) presents SWRC as a function of volumetric water content.
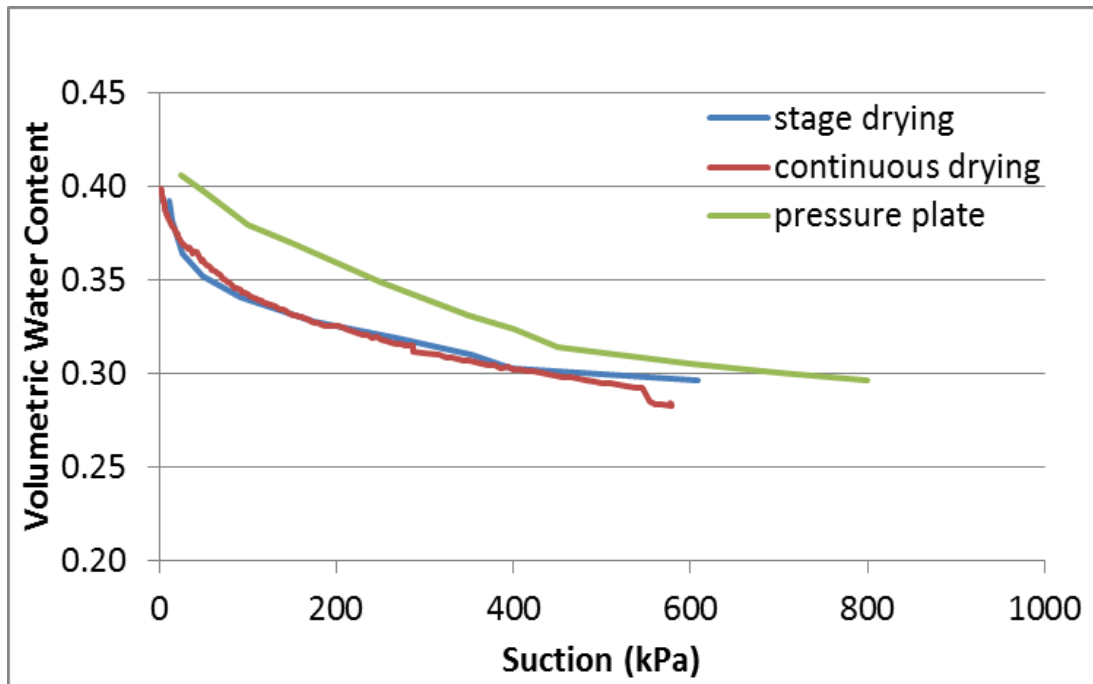
Figure 5.4 SWRC for different testing methods used, presented as volumetric water content against suction.

When calculating the volumetric water content, the changes in density of the sample is taken into account. From the graphs it can be noticed that the stage and continuous approach shows even better agreement, confirming the correctness of the results obtained. The third plot (Figure 5.5) presents the relationship between suction and degree of saturation (Sr).
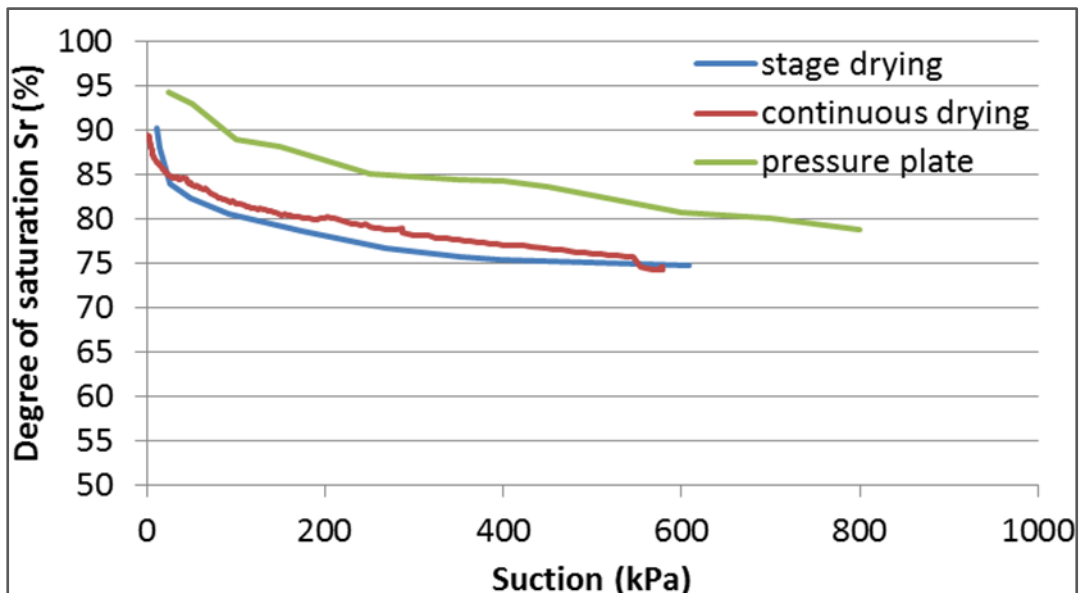

Figure 5.5 SWRC for different testing methods used, presented as degree of saturation against suction.

As for the previous figures there is again a quite good alignment for suction probe measurements (stage and continuous drying). However, it can be seen that the for pressure plate test specimen started from a higher initial degree of saturation (94% rather than 90%). There is one main conclusion deriving from those results. It is clear that the pressure plate results plot above the lines recorded for tensiometer readings. An explanation put forward by Toll et al. (2013) was that cavitation was prevented in the pressure plate tests (using axis translation) whereas cavitation could take place during natural drying. However, Toll et al. (2015) has shown that this discrepancy is due to different volumetric paths followed in each test. The next stage of the research was to investigate how the soil will respond when subjected to repeated continuous wetting and drying cycles (Figure 5.6). For that purpose the sample was prepared and subjected to drying as described earlier. When a certain value of suction was achieved then a continuous wetting path was commenced. The specimen was subjected to four hydraulic paths as presented on Figure 9. The graph shows that for each full cycle (drying and wetting) the hysteretic behaviour is quite different. For the first cycle the difference between the primary drying curve and the scanning (wetting) curve is much larger than for the second one. It shows that the three last paths lie very close to each other. Another practical observation was that the continuous approach was much less time consuming than the stage approach and the pressure plate method. A single path could be accomplished in 2 days whereas for pressure plate method it could be weeks.
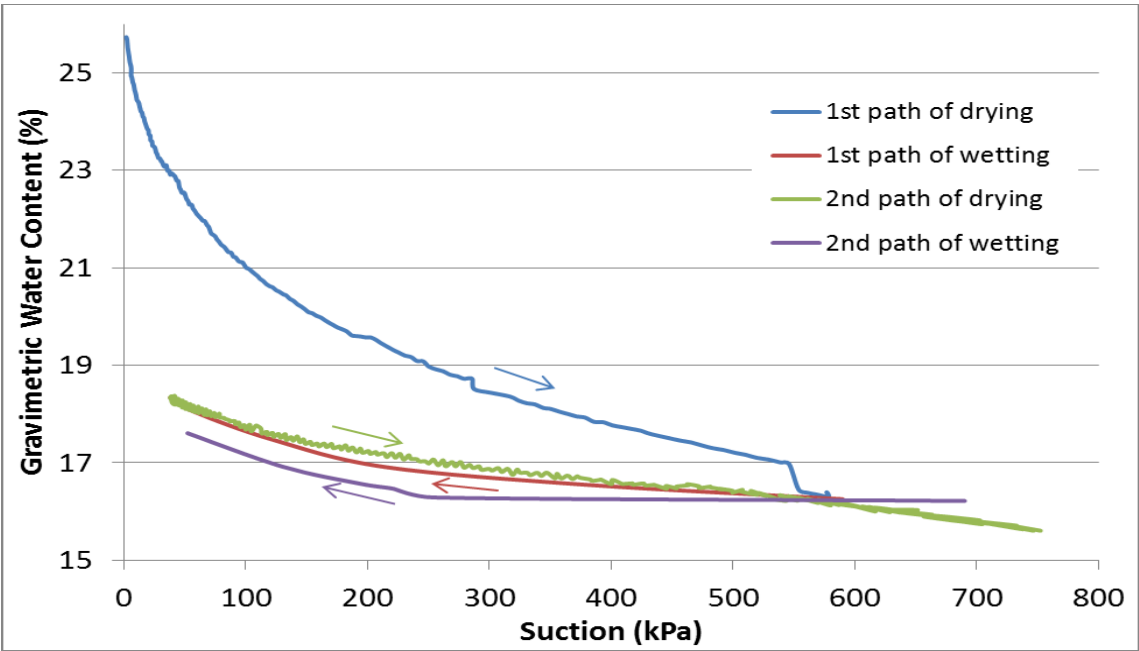

Figure 5.6 SWRCs for repeated drying and wetting cycles for sandy clay, using tensiometer measurements (continuous approach).

5.4. Comparison of multiple Soil Water Retention Curves sets for sandy clay

The results presented in the subchapter are the collection of the datasets performed by the researchers involved in the common project and those who performed their study on the same material using the laboratory facilities provided by Durham University. The results of SWRCs obtained by different researchers using different methods are presented on common graphs in Figures 5.7-5.9. The methodologies encompass pressure plate, stage drying, and continuous drying as per Lourenço (2008); pressure plate, stage drying, continuous drying, and filter paper according to Noguchi (2009); pressure plate, stage drying, and continuous drying assessments by Fraser (2014); continuous drying evaluations by Osinski (2016); continuous drying analyses by Asquith (unpublished); and dewpoint hygrometer examinations by Stirling and Hen-Jones (2015).
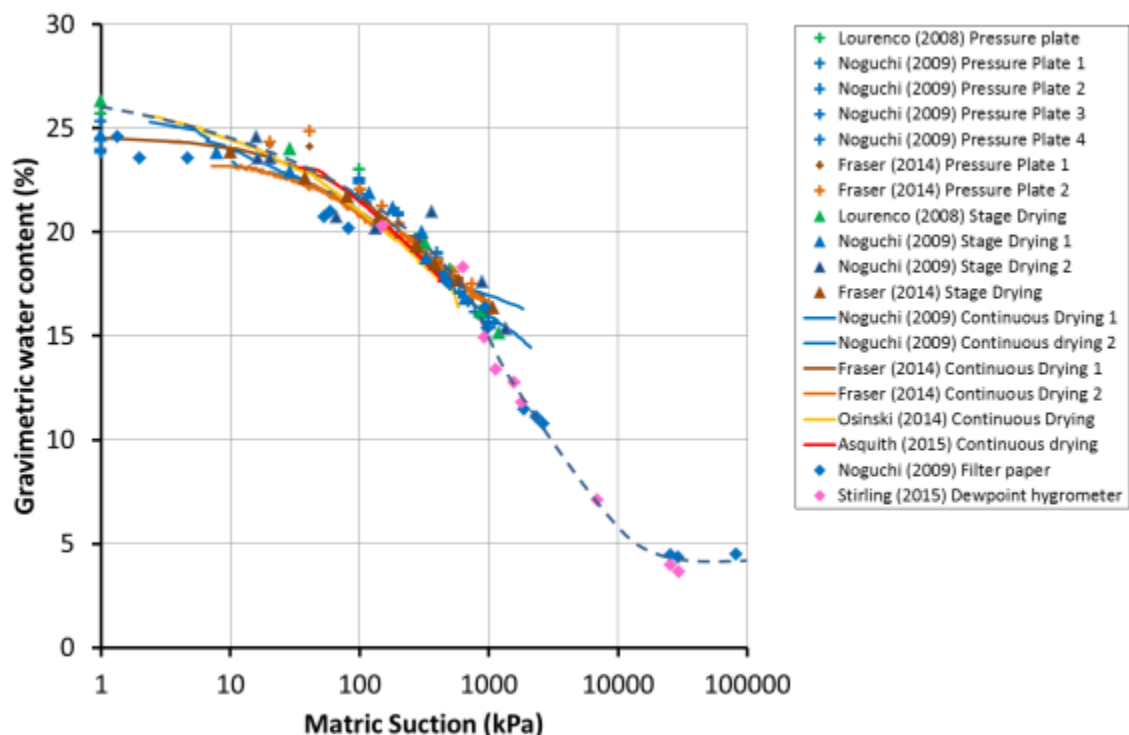

Figure 5.7 Soil water retention curves expressed in terms of gravimetric water content.

Figure 5.7 illustrates the data represented as gravimetric water content versus suction. Gravimetric water content is the metric typically employed by geotechnical engineers in practice. The data from the various approaches typically demonstrate substantial concordance. The ongoing drying experiments establish a rather narrow range of data. The filter paper tests and the dewpoint hygrometer tests exhibit substantial concordance in the elevated suction range (1,000-10,000 kPa). The dotted line in the figure likely represents the principal drying curve for this soil. Specimens prepared with a water content lower than the saturated level of

64

25% exhibit marginally flatter curves (analogous to scanning curves) that converge with the other data at elevated water concentrations. Figure 5.8 illustrates the lower suction range (up to 2000 kPa) on an extended scale. Figure 5.8 illustrates that the pressure plate data is positioned above the findings obtained from tensiometer measurements, especially within the range of 20-400 kPa. This aligns with the findings of Toll et al. (2013) that the axis translation tests indicate greater water contents than those determined by natural drying by tensiometer measurements. Toll et al. (2013) noted that cavitation was inhibited in the pressure plate testing (utilising axis translation), whereas it could occur during natural drying. Cavitation is not anticipated to occur at suctions below 100 kPa.
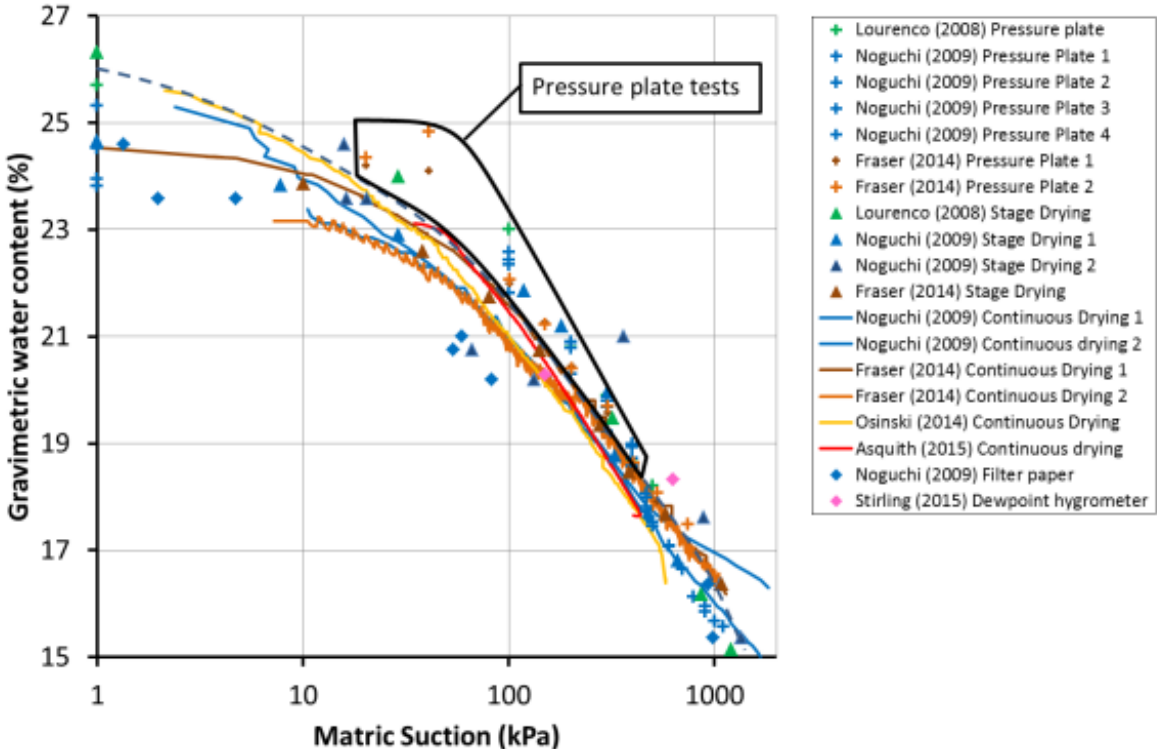

Figure 5.8 – Soil water retention curves expressed in terms of gravimetric water content (lower suction range).

The gravimetric water content plot suggests that the tensiometer tests are desaturating at lower suctions compared to the pressure plate testing, as seen by the reduced water contents. It is important to note that changes in gravimetric water content may result from both volume reduction (shrinkage) and desaturation. The data is consequently shown in terms of saturation degree in Figure 5.9. This indicates that the pressure plate tests desaturate at lower suctions compared to the tensiometer test. The pressure plate results trend (represented by the short-dotted line) signifies a divergence at approximately 80 kPa from the trajectories of the tensiometers (shown by the chain-dotted line). To comprehend these variations in saturation

levels, it is essential to examine the volume alterations occurring during the drying process. Figure 5.10 illustrates the data represented as traditional shrinkage curves, depicting void ratio vs gravimetric water content. The findings of three linear shrinkage tests conducted by Lourenço (2008) indicate a shrinkage limit of around 13-14%. Figure 5.10 illustrates that the tensiometer tests exhibit a comparable trajectory over the spectrum of water contents from 25% to 15%. They tend to track down close to the S =100% line, like the linear shrinkage tests. However, the pressure plate tests show a different shrinkage path, where they move away from the saturation line at water contents below 23%. They demonstrate less shrinkage than the other tests.
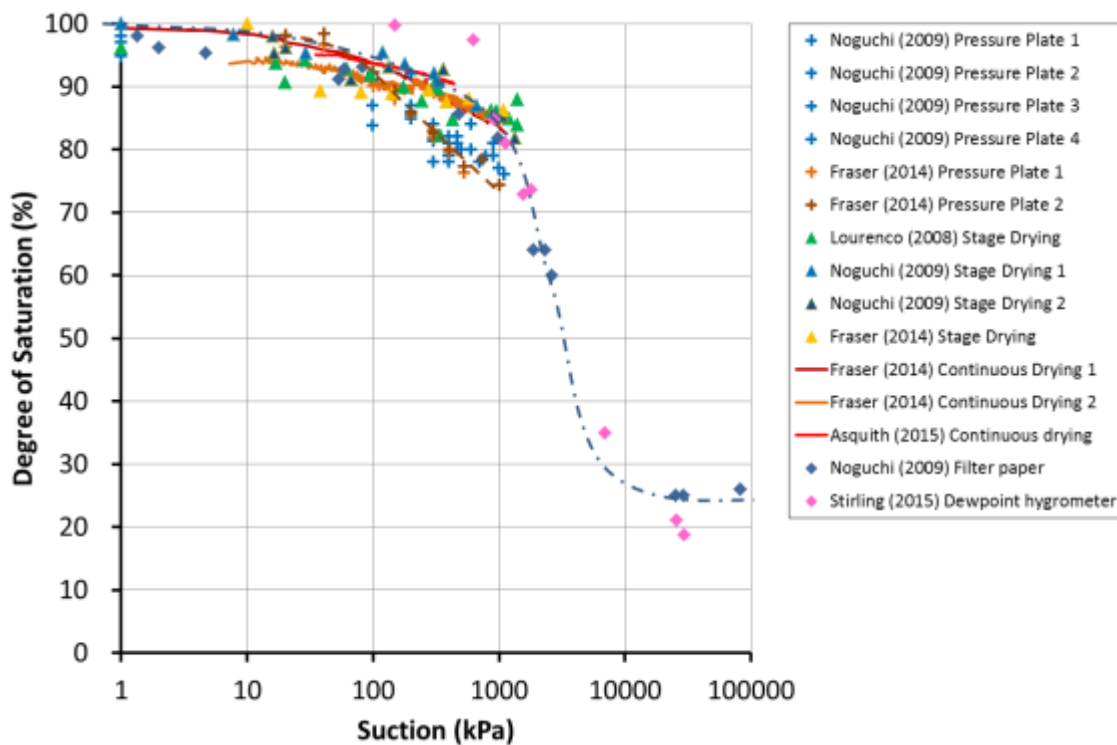

Figure 5.9 Soil water retention curves expressed in terms of degree of saturation.

It is also interesting to see that the filter paper tests and the dewpoint hygrometer tests, where drying was continued below 15%, show a similar pattern to the linear shrinkage tests, but reach different ultimate void ratios below the shrinkage limit. These results demonstrate the importance of obtaining volumetric measurements as part of the determination of the soil water retention curves. Having equipment that can provide continuous volume change readings is a therefore advantageous.
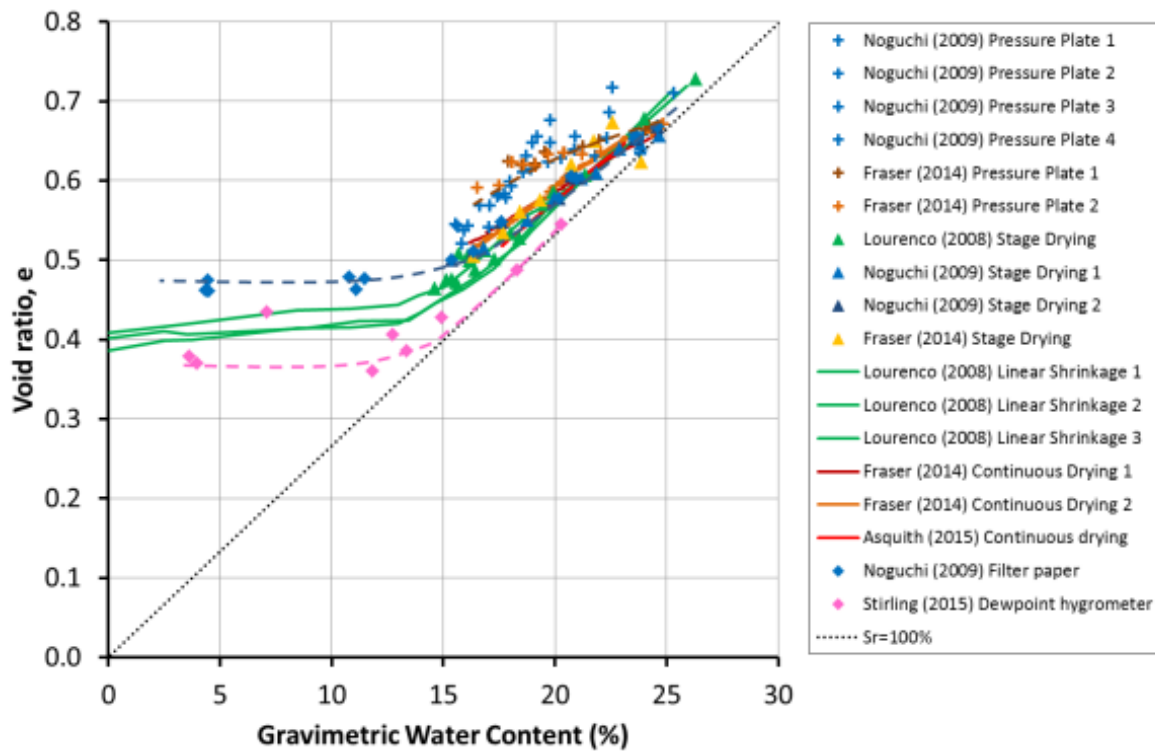
Figure 5.10 Shrinkage paths observed during SWRC testing.

5.5. Conclusions

New equipment has been developed for measurement of soil water retention curves, using a high capacity tensiometer. It provides continuous measurements of water content (from an electronic balance), suction (from a high suction tensiometer) and volume change (using LVDTs to measure changes in diameter and height). A large data set of soil water retention measurements have been made on a sandy clay fill material, the material used in the construction of an instrumented embankment to investigate climate impacts on infrastructure slopes. The results are compared with traditional pressure plate measurements, filter paper tests and chilled mirror hygrometer tests and high suction probe. It is confirmed that tensiometers measurements and pressure plate data give different results, as has been previously observed. The differences between the techniques can be explained by different volumetric responses. The pressure plate tests show different shrinkage paths, resulting in less volume change. This is reflected in significant differences in the degrees of saturation attained at the same suction. The pressure plate tests tend to show higher gravimetric water contents than the tensiometer measurements, but lower degrees of saturation. The results demonstrate the importance of obtaining volumetric measurements as part of the determination of the soil water retention curves. The research results were presented at ICTG, 2016 (Toll et al., 2016).

6. Soil Water Retention Curve determination for granular material

6.1. Methodology used for SWRC determination of tested sand samples

The samples of granular soil were analysed and the tests was performed at Nottingham University, as a part of MUMOLAD project. For the reconstituted specimen preparation fine sand of lowest available fraction was used. The soil material is classified as fine and uniform uncrushed silica sand. It is deposited in Bedfordshire county of east of England. Sand particles are subrounded and contain mainly quartz. The grain size ranges from 90 to 150 μm. The specific gravity of the sand is 2.65. The maximum and minimum void ratios are found to be 0.90 and 0.55, respectively. The coefficient of permeability is $1.44*10^{-4}$ m/s. All the main physical parameters are presented in table 3.2. The study has been already presented at MendelNet 2017 (Osinski et al, 2017). The presentation was awarded for the best scientific content.

The experimental setup used at this study is shown in Figure 6.1. It included an aluminium pedestal with a fitted miniature Pore Pressure Transducer (PPT) in the middle of its base for direct measurement of matric suction. PPT was supported on the pedestal using a cable gland at the bottom. Soil samples were prepared onto the pedestal due to the non–cohesive nature of the fine sand which makes challenging their transport from the preparation bench to the testing point. The soil specimens were prepared within a consolidation cutting ring with 75 mm diameter and 20 mm height which was placed on the pedestal. The desired density was achieved by compacting the soil using a tamper. The weight of the sample was determined by weighing the base pedestal and the ring before and after the soil compaction. Material was dried in the oven at 105 °C to determine the initial gravimetric moisture content. Finally, the entire system was placed on an electronic scale with a resolution of 0.001 g allowing continuous measurement of changes in the specimen's weight, due to evaporation.

The PPT was used for the direct measurement of matric suction in the specimen during drying and wetting processes. To make it working in desired manner the PPT had to be transformed into a tensiometer (Toll et al. 2013). This is a miniature size transducer (Druck PDCR81 Pore Pressure Transducer, König et al. 1994) with 12 mm length and 6 mm diameter (Figure 6.2). It consists of a diaphragm which deforms under the pressure of the pore water and produces an electrical signal. An extremely small water reservoir is located between the filter and the diaphragm.
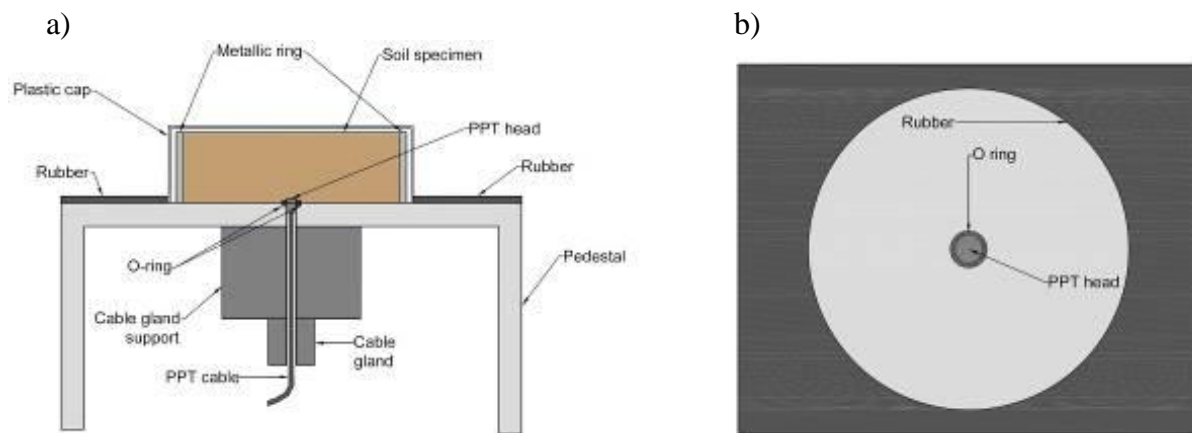
Figure 6.1 Experimental setup for tensiometer (modified PPT) method: (a) side view, (b) plan view.

The calibration took place in order to correlate the electrical signal produced by the sensor when subjected to pressure changes and the actual pressure. In order to accurately measure also negative pore pressure (i.e. suction), PPT was modified by fitting a high air entry porous disc in front of the diaphragm. The porous disc (filter) was saturated adequately, before testing, using the procedure described by Matziaris et al. (2015).

The elimination of air bubbles from the filter and the water reservoir ensured that pore water was in very good contact with the diaphragm and the suction readings were reliable. Several samples were formed by compaction of the material within the soil using tamping method. Same drop height, same mass of a hammer, same volume of soil was used in every test. To change the density of the sample the number of blows was limited to reach required value of the void ratio. When the sample was prepared the tensiometer (being fully saturated at all times) was carefully attached to the bottom of the pedestal on which the specimen was prepared. The tensiometer had to be placed being aware of potential cavitation process taking place in the meantime.

Figure 6.2 Pore Pressure Transducer (Druck PDCR81), fitted with a high air entry value porous disc.

6.2. Pre–testing of modified pore pressure transducer (tensiometer)

As mentioned before the tensiometer used in the study was modified to increase the suction measurement ability. To verify the accuracy and the response of the device the material used for pre–tests was clayey silty sand, which was much easier to prepare the sample from and gave more time for the tensiometer to respond to water content changes. For the pre–testing of tensiometer there were two approaches used in the study: stage drying and continues drying. For the first approach the suction was measured by drying tested samples to required water content value, outside the pedestal. When excepted gravimetric water content of each sample was achieved, the sample was placed in a sealed container and left to allow an even distribution of moisture within the specimen. After 24h the samples were placed on the pedestal and the suction was measured. There were 4 samples prepared at 14%, 15%, 18% and 20% (S1, S2, S3, S4 respectively). Set up for testing is presented on Fig. 6.3.

Figure 6.3 SWRC measurement set up using modified pore pressure transducer.

For the second approach there was sample prepared at 20% of gravimetric water content and left to dry on the pedestal left on the balance. The suction was measured simultaneously with a mass loss. The results obtained for both approaches are presented on Figure 6.4 and 6.5. They present measured suction over time, at different gravimetric water contents.

Figure 6.4 present rapid respond for the changing suction and different water contents. The equilibrium of recorded value of suction stabilizes after short time of about 400–700 sec. After the sample gets in contact with the tensiometer the reading of suction is very clear. However, more importantly when the sample is taken of the pedestal the value of suction is immediately reaching back the initial value of 0–1 kPa.
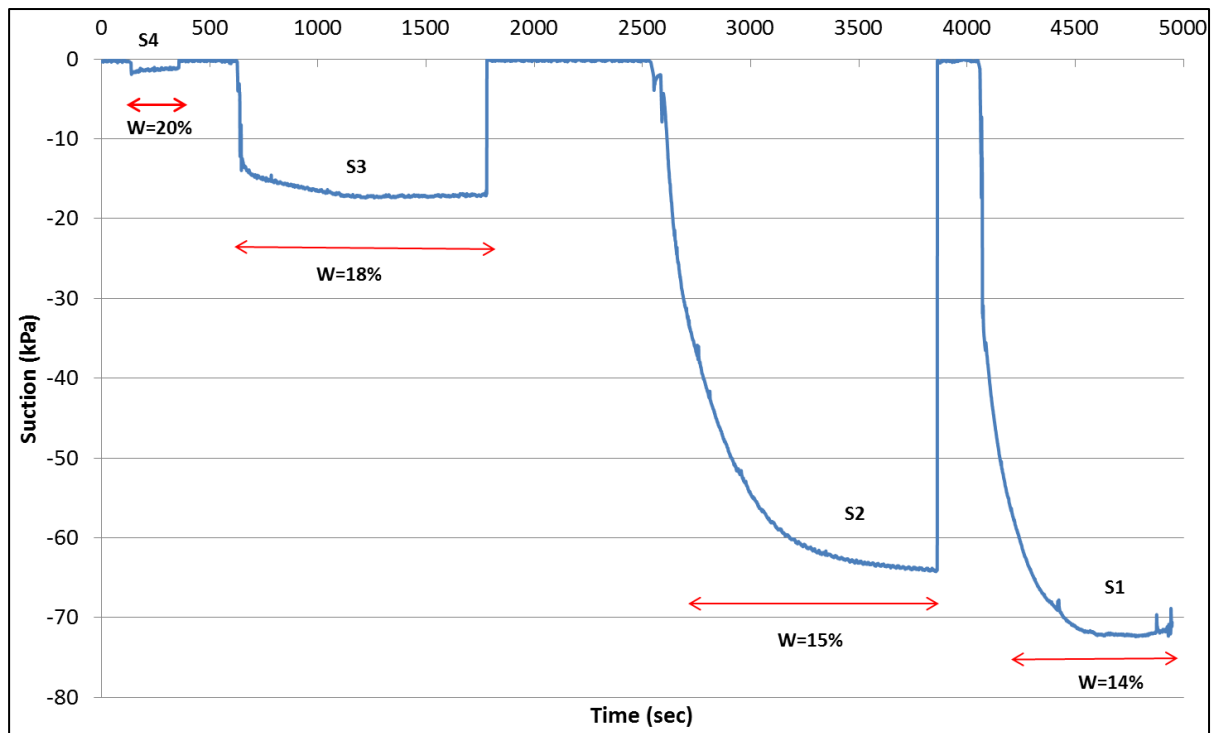
Figure 6.4 Suction measurements in drying stages for pre–test samples at certain water contents.

With lower water content the suction reading is increasing what was expected to happen, and proved the tensiometer to be working properly. The next approach of continuous drying allowed obtaining almost full SWRC using single sample. The sample was saturated up to 20% of water content and left for free evaporation. The whole set up was placed on the balance so the weight loss due to evaporating water could be precisely measured. The sample could be left over night as the all data (suction and weight) was collected using data acquisition system controlled by LabView. From Figure 6.5 it is quite clear how the suction is changing over time with water content decrease, caused by evaporation. However, more useful information from this plot is that cavitation point was captured at 125 kPa, what gave the real capability of measuring suction for this particular (modified) device. The differences in measured suction between the approaches are mainly due to different method of preparing the sample, using different compaction efforts.

6.3. SWRC results for fine sand samples

After confirming that the modified pore pressure transducer (tensiometer) was working properly the samples of fine sand were prepared and tested. The results are plotted on Figure 6.6. There were two samples tested on the research set up. The samples differ void ratio of e = 0.66 and 0.78. Due to difficulties when preparing the samples for similar water contents (looser

the sample lower the water content) for the same void ratio the initial moisture was 22% for denser specimen and 17% for the loose one. For verification of SWRC shape correctness, there were two more curves added to the plot. One was the referencing SWRC obtained coarser fraction (C), and second one was SWRC for the same material used in the study but obtained by using axis translation technique (Osinski et al. 2016; Toll et al. 2016).
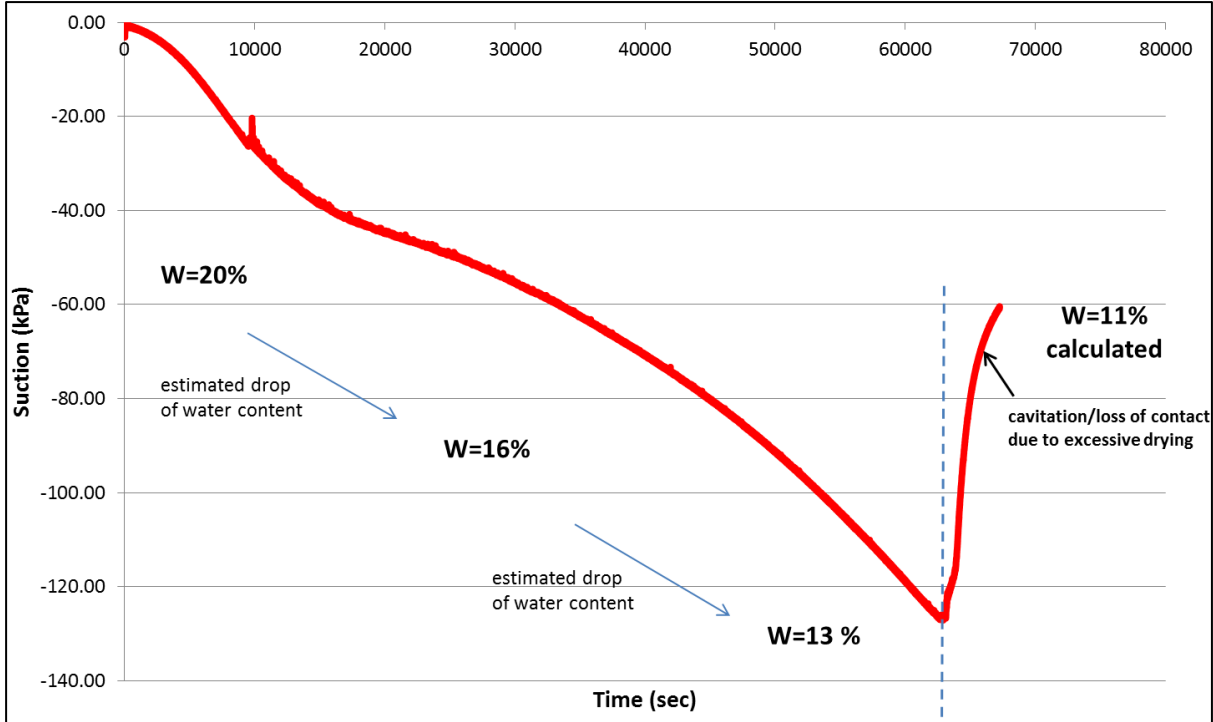

Figure 6.5 Suction measurement for continuous drying path (sample left open to the atmosphere over two days, starting from 20% of moisture content).

As seen from the graph (Figure 6.6) the reference curve for fraction C sand, the suction is lower for the same values of water content for fraction E. The behaviour is as expected, and is mainly caused by differences in fraction (the reference material was coarser). The other curve obtained by using axis translation method plots slightly above the curves of the fraction E sand, which is typical when applying this two different techniques. Plots of SWRC for fraction E sand (for tensiometer technique) allows clear identification of air entry value zone, transition and residual zone of saturation.

6.4. Conclusions

The aim of the study was to obtain and SWRC of fine sand and analyse the hydraulic behaviour by using modified pore pressure transducer. This was a part of the wider research aiming at determining changes of mechanical parameters of soil in different water content condition, at known values of suction. For such purpose the SWRCs had to be determined

before starting triaxial shearing tests. Using tensiometer technique is an efficient, very accurate and less time consuming method for measuring the suction, comparing to axis translation methods commonly used in triaxial cells. The most important conclusion is that the suction of tested material did not significantly respond to significant moisture content changes. The transitional zone fits within the range from 8 to 10 kPa, when the water content has changed from 20 to 3%. Such findings were very useful when preparing the samples at certain suction, for particular water content, for further tests on mechanical behaviour of unsaturated samples.
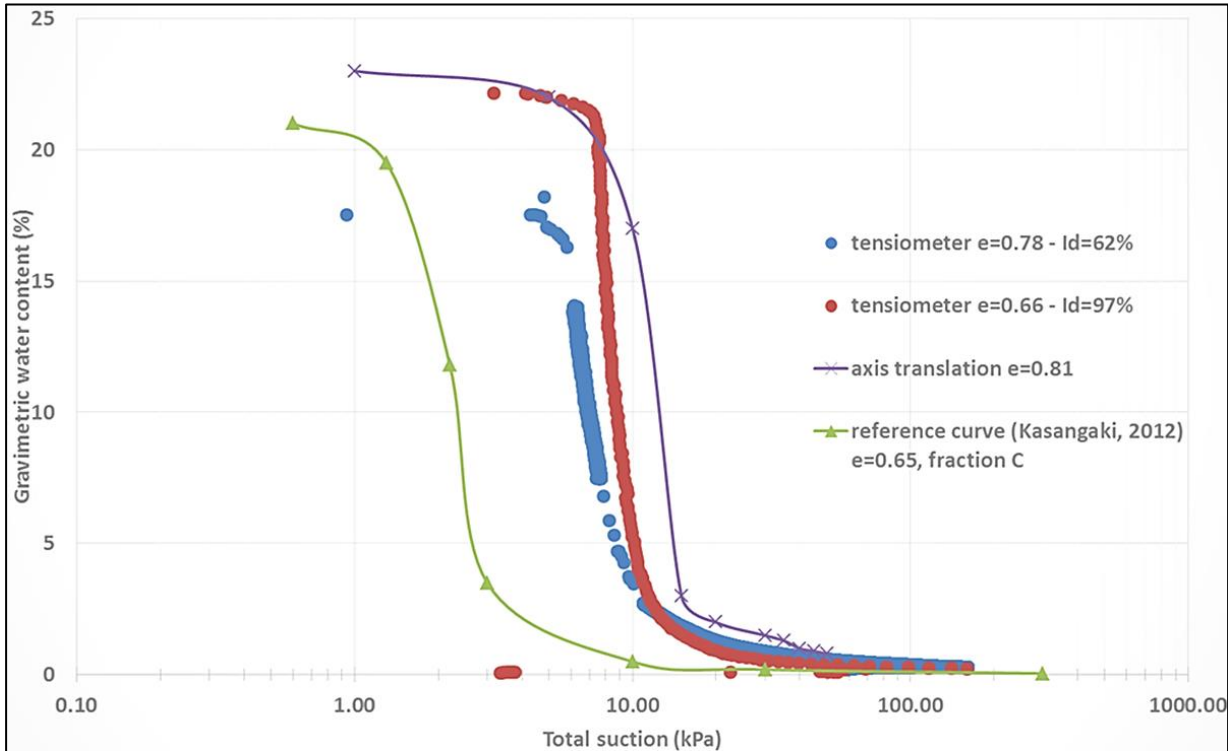

Figure 6.6 SWRCs for fine sand obtained by using modified pore pressure transducer (additional curves for results comparison).

7. Mechanical behaviour of the sandy clay soil

7.1. Introduction

A triaxial testing program was established to assess the mechanical behaviour of sandy clay material, with samples evaluated at a constant water content under unsaturated conditions. Given the limited permeability of the soil under examination, any potential trigger for the failure of an earth structure constructed with this material is anticipated to occur while sustaining a consistent water content. The pore water pressure was continually monitored using a high-capacity suction probe during the testing phase. Each test included a phase of constant water content compression (CWC), during which the sample experienced an increase in

confining pressure (net stress), followed by a period for pore water pressure to equilibrate. The specimen may have a change in volume during this phase due to the expulsion of air, but no water flow should take place. Subsequent to the continuous compression of water content, each specimen underwent a shearing phase, during which it was axially loaded to failure while sustaining a constant confining pressure. The triaxial testing program encompassed a series of saturated consolidated drained triaxial tests to establish a reference for the testing of unsaturated samples. The triaxial testing procedure was conducted on samples compacted at designated water contents of 15% (the optimum water content, W_{opt}), 20%, and 22%. Testing was confined to this range of water content due to the constraints of the high-capacity suction probe's suction range (2 MPa). To get insight into the behaviour of samples subjected to wetting and drying due to climatic variables, an additional series of samples was created at these water contents, which were subsequently wetted and dried after compaction. The wetting and drying processes were conducted outside to the triaxial cells, as detailed in Chapter 4, before being placed within double cell triaxial cells and subjected to CWC and subsequent shearing. The chapter commences with the presentation of the saturated test series, encompassing equipment, test techniques, and results, then followed by the unsaturated constant water test series in the same sequence.

7.2. Saturated triaxial tests

7.2.1. Triaxial testing apparatus

Conventional consolidated triaxial tests were conducted on fully saturated samples to establish a reference for the constant water triaxial testing of unsaturated samples. Samples were produced following the sample preparation process presented in previous chapter, and were saturated within the triaxial apparatus before consolidation and shearing. In this instance, owing to equipment availability, the samples examined were 38mm in diameter and 76mm in height, evaluated in typical triaxial cells utilising the setup depicted in Figure 7.1. The standard triaxial cells were appropriate for testing as the experiments were conducted under saturated circumstances, with volume recorded directly by water flow from the sample. The examination comprised three phases: saturation, consolidation, and shearing. Saturation was achieved by applying a heightened back pressure of 300 kPa to both the top and bottom of the sample to exclude any air present within it.
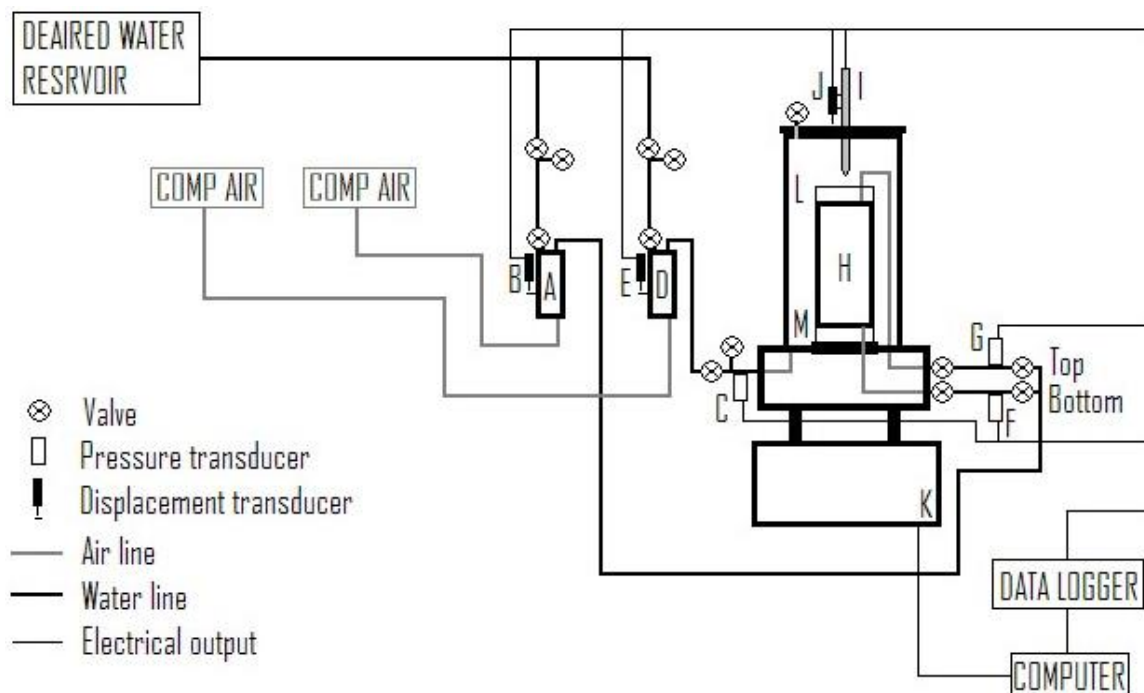
Figure 7.1 Triaxial testing apparatus for saturated samples.

By sustaining the cell pressure at 5 kPa above the back pressure, the effective stress was preserved near zero, at 5 kPa or lower. The B value was measured to track the course of saturation. The B value is the ratio of pore water pressure change to cell pressure change ($\Delta u/\Delta\sigma c$), where fully saturated samples should yield a B value of close to 1. During triaxial testing, it is standard procedure to saturate the sample until a B-value of 0.95 is attained, which corresponds to around 99.9% degree of saturation for soft clays (Black and Lee, 1973). To see the progression of the B value, the cell pressure was elevated by 100 kPa, and pore water pressure measurements were recorded from the pressure transducers linked to the top cap and base pedestal, while ensuring undrained conditions by sealing all drainage valves. Upon attaining a sufficient B-value ($\geq$0.95), the test proceeded to its second phase.

The sample was subsequently subjected to consolidation, during which the confining pressure was elevated to a specified value to establish a known effective stress, while consistently maintaining back pressure at 300 kPa. Consolidation persisted until no additional significant volume alteration was detected in the volume gauge, which was defined as a stable change rate of volume around 0.009 cm^3/hr. Upon completion of consolidation, drained shearing commenced at a rate of 0.005 mm/min. Table 7.1 presents the accuracy of each type of measuring equipment utilised throughout the saturation testing. The accuracy was assessed differently for various types of equipment:

either during experimental procedures or before to the experiments to monitor fluctuations in the recorded values. Accuracy values were acquired from trials conducted on the water-filled volume gauge, the displacement transducer positioned at mid-travel, and the load cell at rest. The precision of the pressure transducers was determined while the cell was subjected to a constant confinement pressure.

Table 7.1 Accuracy of the measuring equipment used in saturated triaxial testing.

Measuring equipment	Unit	Accuracy
Volume gauge	cm^3	±0.002
Displacement transducer	mm	±0.005
Pressure transducer	kPa	±0.2
5 KN load cell	N	±0.5

7.2.2. Triaxial testing program

The tests performed for the saturated triaxial testing program can be seen in Tables 7.2. The saturated tests (S) were identified in the form Sxx(yy) by the as-compacted water content (xx), and confining pressure applied during the triaxial testing (yy). Table 7.2 also presents the initial conditions of the samples.

Table 7.2 Triaxial testing program for the saturated test series, showing testing conditions.

Sample	Water content	Density Bulk	Density Dry	Void ratio	Degree of Saturation	Confining pressure
	w	ρ	ρ$_d$	e	Sr	
	%	Mg/m^3	Mg/m^3	-	%	kPa
S17(50)	16.82	2.17	1.79	0.42	94	50
S17(150)	16.55	2.18	1.90	0.42	94	150
S17(300)	16.75	2.15	1.85	0.44	93	300
S20(50)	19.54	2.00	1.71	0.57	92	50
S20(150)	19.73	2.02	1.73	0.57	91	150
S20(300)	19.69	2.02	1.69	0.62	94	300
S22(50)	21.85	2.04	1.65	0.62	95	50
S22(150)	21.76	2.02	1.68	0.61	92	150
S22(300)	21.78	2.03	1.69	0.62	96	300

7.2.3. Saturated tests results

The saturated tests were conducted utilising the configuration depicted in Figure 7.1. The samples utilised were smaller than those employed in the triaxial testing program for unsaturated samples due to equipment constraints. Nevertheless, sample preparation was same across all prepared samples; for the saturated testing, the specimens were extracted from a compacted sample, which was prepared identically to those utilised in the unsaturated constant water content tests. From each compacted sample, three specimens might be cored for the saturation test series. The tests were conducted on specimens derived from a singular compacted sample, resulting in identical beginning water contents for each group of subsamples in Table 7.2, except for S15(50), which was sourced from a different batch. The samples, when positioned within the cell, underwent saturation, achieving a saturation level of 100%. Table 7.3 delineates the criteria for the conclusion of the saturation and consolidation phases for each specimen evaluated.

Table 7.3 Conditions at the start and end of the consolidation stage for the saturated testing.

Test No.	Initial Water content %	Consolidation	Volume V cm³	Dry density ρ_d Mg/m³	Void ratio e	Degree of Saturation Sr %
S17(50)	16.82	Initial	90.2	1.65	0.54	100
		Final	88.2	1.72	0.53	
S17(150)	16.55	Initial	92.43	1.72	0.52	100
		Final	89.1	1.80	0.48	
S17(300)	16.75	Initial	92.1	1.77	0.52	100
		Final	86.8	1.86	0.40	
S20(50)	19.54	Initial	86.5	1.66	0.59	100
		Final	85.8	1.70	0.65	
S20(150)	19.73	Initial	87.6	1.65	0.61	100
		Final	85.7	1.73	0.54	
S20(300)	19.69	Initial	88.5	1.64	0.62	100
		Final	86.9	1.73	0.52	
S22(50)	21.85	Initial	83.0	1.67	0.66	100
		Final	82.1	1.72	0.62	
S22(150)	21.76	Initial	86.3	1.61	0.68	100
		Final	84.5	1.66	0.62	
S22(300)	21.78	Initial	87.6	1.60	0.66	100
		Final	85.1	1.67	0.64	100

As anticipated, samples exhibited an increase in volume at saturation, followed by a reduction in volume after consolidation, as illustrated in Figure 7.2. The variations in sample volume were ascertained by quantifying the alterations in fluid volume within the triaxial cell. This method is suboptimal, as the perspex cell may undergo volumetric alterations. Nevertheless, it offers an estimation of the variations in the sample's volume. The final stage of shearing commenced following consolidation.

The shearing phase was conducted under drained conditions, allowing water to flow in or out of the sample without a substantial increase in pore water pressure, with the largest observed variation being less than 3 kPa. The ultimate conditions of each studied sample are presented in Table 7.4. Figure 7.3 illustrates the relationship between deviatoric stress and axial strain for all saturation tests conducted at various confining pressures. Samples manufactured with 15% water content exhibited failure between 3% axial strain at 50 kPa confinement and 8% at 300 kPa confinement. The samples generated with elevated water content exhibited failure at increased axial strain values, ranging from 10% at 50 kPa of confinement to 17% at 300 kPa of confinement.

Figure 7.4 illustrates the correlation between axial and volumetric stresses generated during the shearing phase of each sample (compressive strains are indicated as positive). It is evident that the majority of the samples continue to exhibit volume changes at the end of each saturation test, particularly those prepared with 15% water content. Figures 7.5 to 7.7 illustrate the stress trajectories for each experiment.

Table 7.4 Saturated test series: sample characteristics at the end of each saturated test.

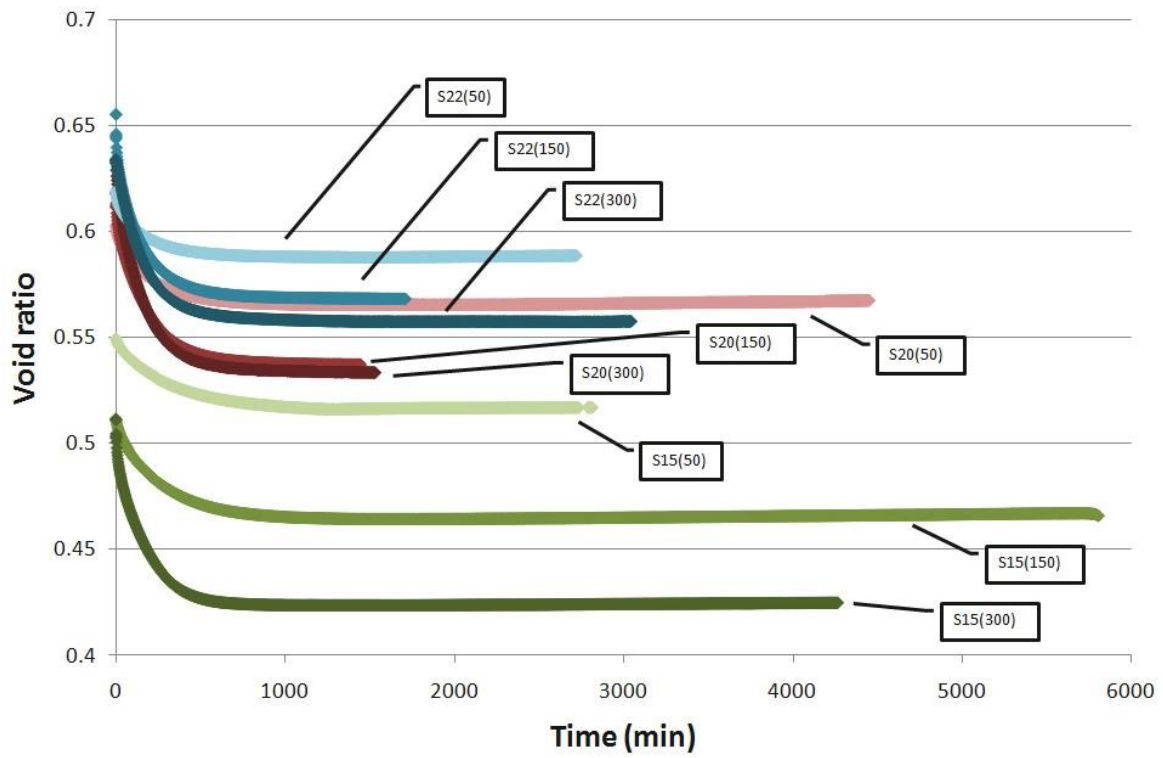| Test No.	Initial Water Content %	Final Water Content %	Sample weight g	Dry density ρ_d Mg/m^3	Void ratio e
S15(50)	16.82	21.78	192.9	1.69	0.56
S15(150)	16.55	18.62	196.8	1.73	0.57
S15(300)	16.75	17.79	193.1	1.79	0.49
S20(50)	19.54	21.78	176.5	1.69	0.59
S20(150)	19.73	19.36	175.9	1.75	0.55
S20(300)	19.69	18.48	176.0	1.82	0.49
S22(50)	21.85	22.30	169.7	1.71	0.58
S22(150)	21.76	21.39	170.1	1.77	0.49
S22(300)	21.78	21.79	165.2	1.79	0.53

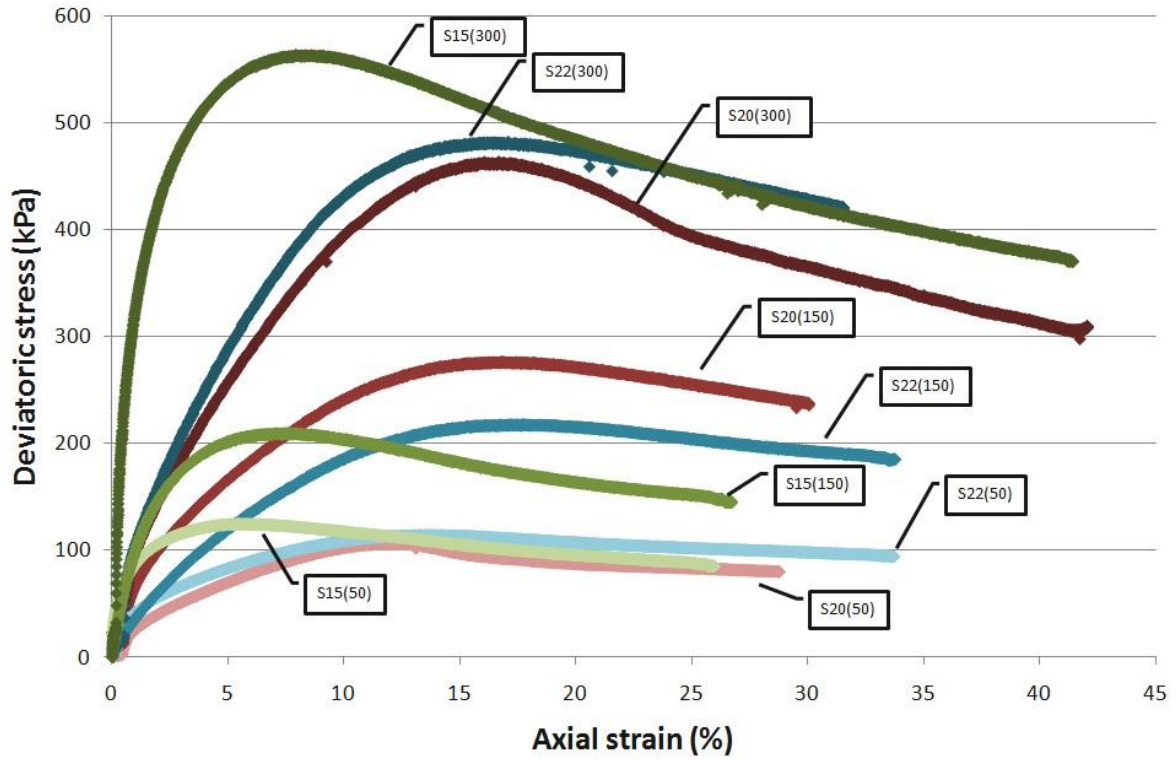**Figure 7.2** Consolidation stage for each sample.

Figure 7.3 Deviatoric stress-strain relationships for the saturated test series.
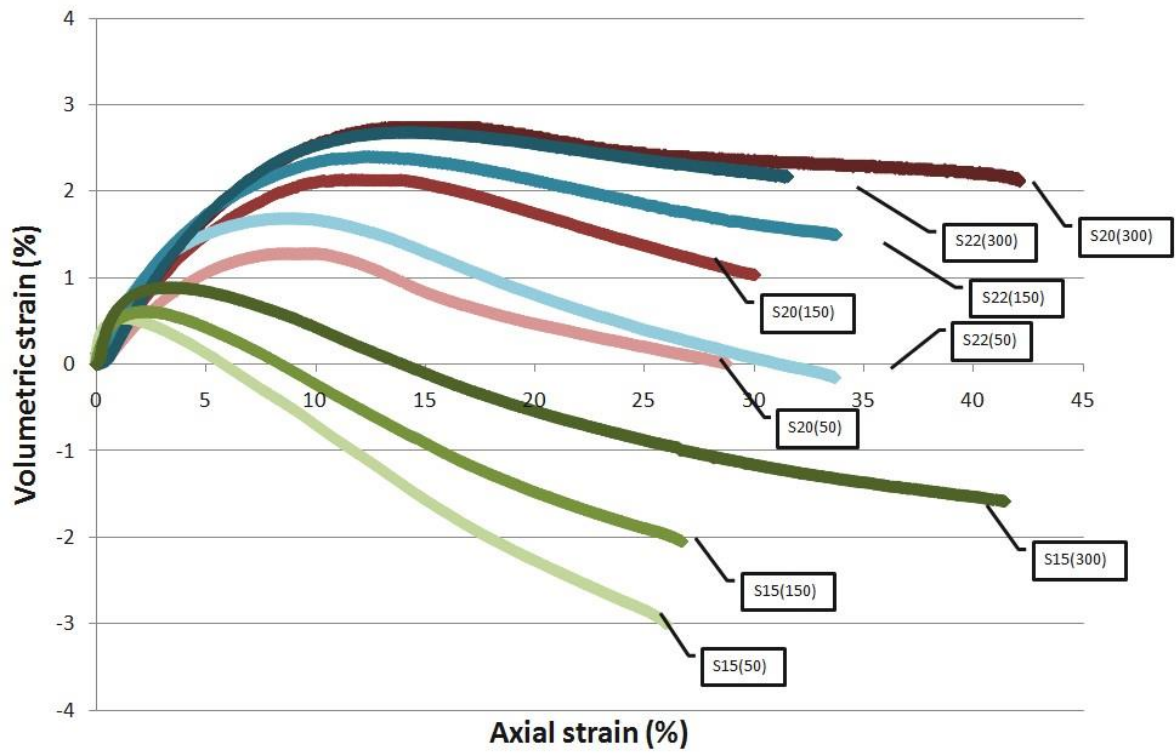
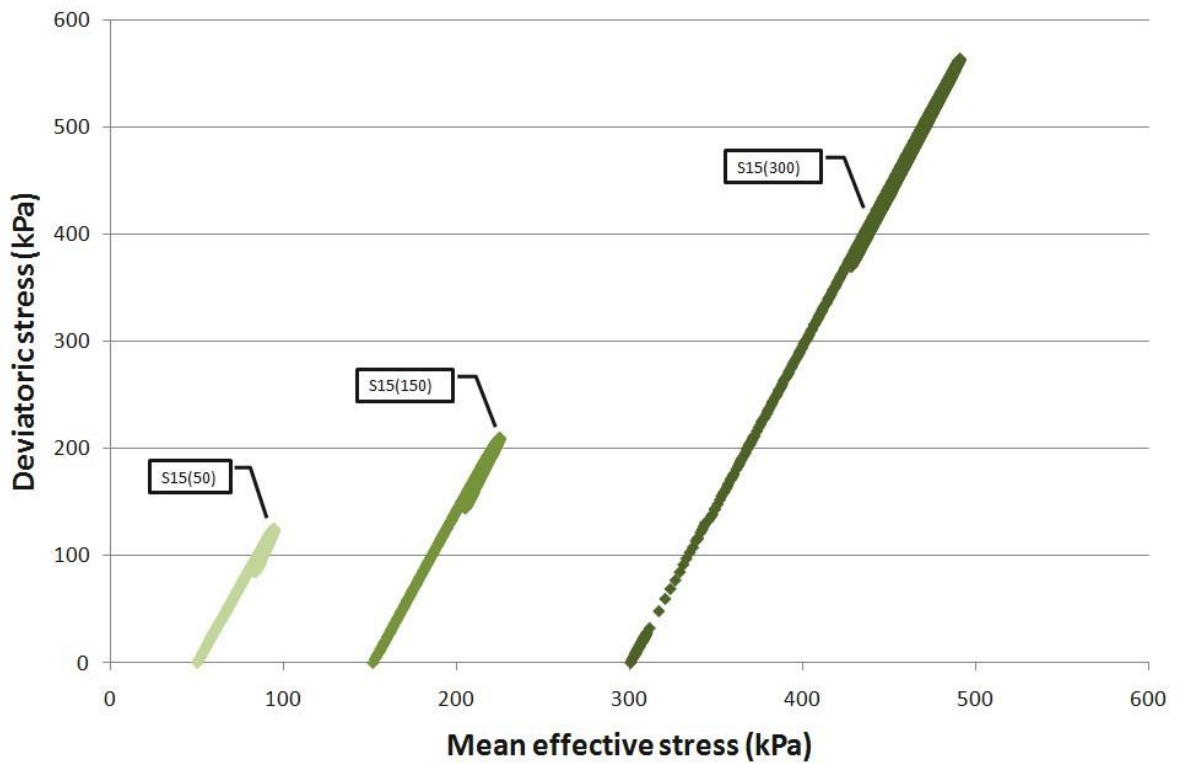**Figure 7.4** Volumetric-axial strain relationships for saturated samples.

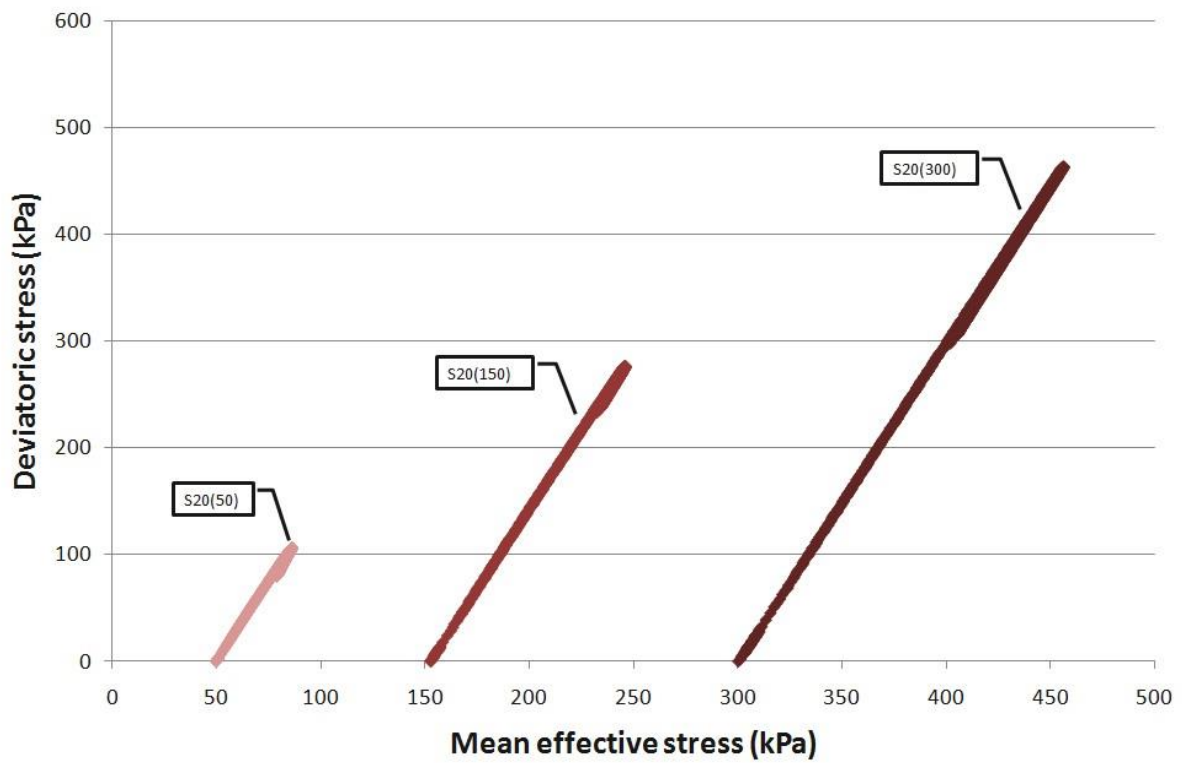**Figure 7.5** Stress paths for the saturated samples with as-compacted water content of 15%.

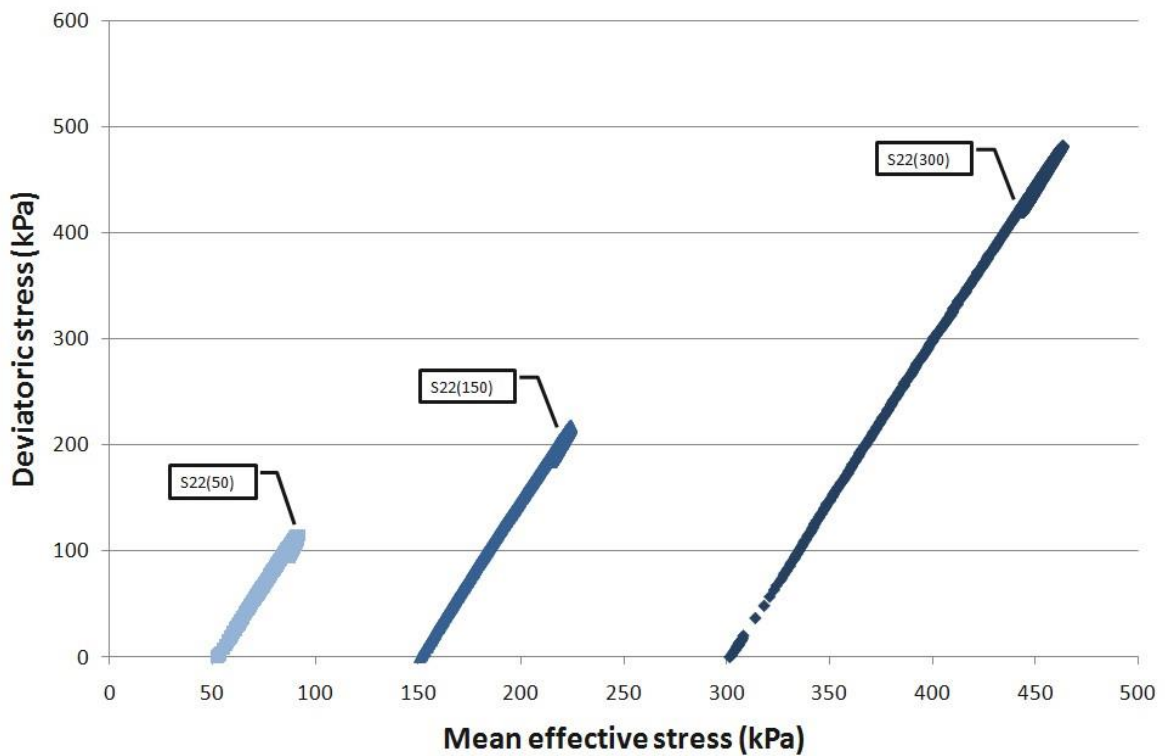**Figure 7.6** Stress paths for the saturated samples with as-compacted water content of 20%.

Figure 7.7 Stress paths for the saturated samples with as-compacted water content of 22%.

7.2.4. Critical state limit analysis for the saturated tests

The end points of the tests at which a state of plastic behaviour characterized by continuous deformation without any further increase in stress was observed and are presented in Table 7.5. These are assumed to be close to Critical State conditions, although with constrain, as it has been shown volumetric deformations were still occurring at the end of the tests, as can be seen in Figure 7.4.

Table 7.5 Critical state points of each saturated test.

Test	p'	q	ε_a	e	v	S_r
No.	kPa	kPa	(%)		1+e	(%)
S15(50)	82.0	79.8	25.42	0.57	1.55	100
S15(150)	211.2	161.2	24.43	0.53	1.52	100
S15(300)	440.0	400.2	37.83	0.50	1.46	100
S20(50)	80.0	84.1	28.26	0.61	1.60	100
S20(150)	240.7	255.7	28.34	0.49	1.49	100
S20(300)	417.7	345.1	39.58	0.45	1.45	100
S22(50)	87.8	96.8	34.33	0.63	1.61	100
S22(150)	237.2	252.5	35.11	0.56	1.51	100
S22(300)	455.1	451.2	30.08	0.49	1.49	100

As the table shows, the critical state points were achieved at high values of axial strain (ε_a), reaching values from 25% up to 40%. At such large axial strains, there can be concerns about non-uniformity of deformations and constraints due to boundary conditions. Nevertheless, it does seem that strains in excess of 25% are needed before the deviator stress and volumetric strains start to level off at constant values suggesting the critical state is being achieved. From equation 2.15 the critical state friction angle for the saturated tests was found to be 23° for samples saturated from 15% and 22% and to be 25° for samples saturated from 22%. Similar results were obtained for the samples that were saturated from 15% and 20%, suggesting a similar critical state limit, while for samples saturated from 22%, the critical state limit differed significantly. During the triaxial tests, the samples did not fully reach a critical state. The observed trends in Figure 7.3 suggest that the critical state would be reached at lower values of deviatoric stress, which would result in the slope of the critical state in the q-p' plane (M) being similar for all water contents. For the saturated tests M was found to be 0.93. The observed trends suggest that samples would continue to dilate, increasing in specific volume. On the critical state, this would suggest higher intercepts of the critical state line for each water content.

7.2.5. Constant water content test in triaxial cell

Constant water content tests (Fredlund and Rahardjo, 1993) were conducted to characterise the mechanical behaviour of the sandy clay soil. The constant water content triaxial testing comprised two phases:

- The specimen underwent continuous water content compression under isotropic conditions at a constant confining pressure σ_3 until the volume stabilised and the pore water pressure equilibrated.

- The specimen was subjected to shear under constant water content by incrementally increasing the deviatoric stress ($\sigma_1 - \sigma_3$). In each test, the shearing phase was maintained until a 20% strain was achieved, in an effort to observe ultimate conditions. Pore-water pressure variations during shear were quantified.

7.2.6. Wykenham Farrance double cell triaxial cell

The samples made with the sandy clay were unsaturated. The presence of air in unsaturated soil makes monitoring volume changes in a sample during consolidation, compression, or shearing tests difficult due to its compressibility. The conventional approach for assessing sample volume variation in triaxial testing of saturated soils, which involves measuring the pore fluid that exits or enters the sample, is inadequate as water volume and sample volume are not correlated in unsaturated soils. The most straightforward method to observe volume changes in unsaturated samples is to measure the volume of fluid (i.e., water) that exits or enters the cell (Bishop and Donald, 1961). The classic triaxial system, constructed from Perspex, exhibits unreliable fluid volume monitoring using the indirect technique due to the elastic behaviour of the Perspex under variable pressure and the occurrence of creep under constant tension. These alterations result from water absorption, heat expansion, and variations in cell volume corresponding to cell pressure (Wheeler, 1988). Despite their small size, these still exert considerable variances in the data acquired about measured volume. A double cell was favoured to address these challenges, namely the Wykeham Farrance (WF) double cell triaxial cell (Figure 7.10a). The cell volume resulting from variations in cell pressure is significantly diminished due to the presence of two cells, as the inner cell experiences equal pressures on both sides of its wall. The WF design resembles the Wheeler modified triaxial cell (Wheeler et al, 1995). The WF double cell system differs from the Wheeler cell by featuring an inside cell wall constructed of glass rather than Perspex, aimed at preventing water absorption by the inner cell wall. A significant characteristic of the WF

double cell triaxial cell is its dual-cell design, which ensures that the top cap of the inner cell experiences uniform pressures both internally and externally. This structure, by applying uniform cell pressure both inside and externally, eliminates cell expansion, hence preventing any volume change due to cell pressure. Figure 7.10b) and c) illustrate the components of the rig.

A significant shortcoming identified during testing with the WF double wall cell was the design of the top caps in both the inner and outer cells. A significant amount of air was consistently trapped at the top of both cells during the filling process. The presence of trapped air bubbles would significantly impact the findings of indirect volumetric measurement. However, when the cell is pressurised, the air bubbles are compressed and ultimately dissolve in the water. The influence of the air bubbles was noted during calibration. Nonetheless, if the pressure is maintained consistently throughout the test, the influence of initial air bubbles on the volumetric measurement can be disregarded (Mendes, 2011).
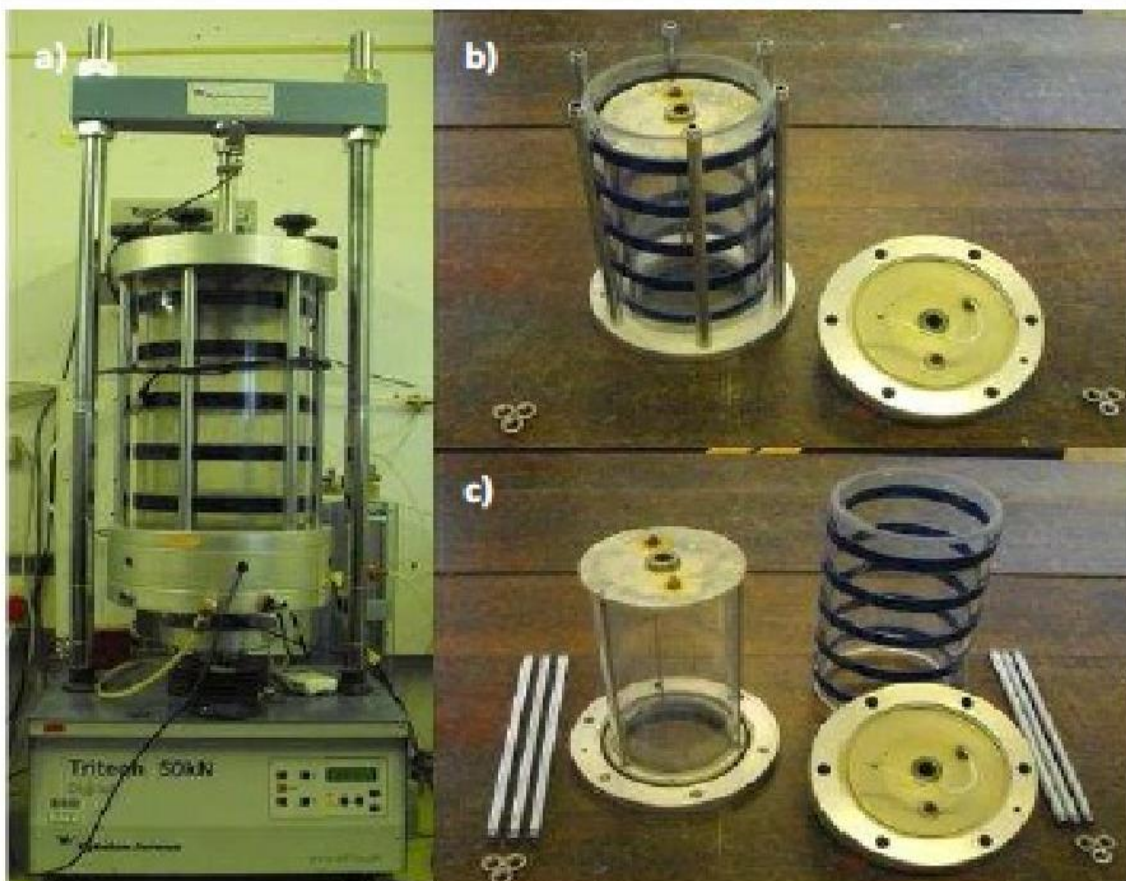
Figure 7.8 Wykeham Farrance double cell triaxial system; (a) fully assembled, (b) without outer cell top cap (c) view of the inner cell (after Mendes, 2011).

If air bubbles persist, fluctuations in pressure will influence the volumetric measurement due to the compressibility of air, thereby elucidating the erratic behaviour over the pressure cycles. The method involved pressurising the cell while keeping the sample's net stress near zero to prevent any deformation (consolidation) of the sample. A new phase, termed the equilibrium stage, was established in the constant water content test to accomplish it. During the equilibrium phase, in addition to elevating the pressure in both cells to the specified confining pressure, a positive air pressure of equivalent magnitude was applied within the sample, therefore ensuring that the net stress remained at zero. This phase persisted until consistent measurements were obtained on the volume gauge, indicating that all air in the inner cell had been crushed or dissolved. Following this phase, the constant water content compression stage was commenced.

It was originally planned to utilise a single hydraulic pump to pressurise the entire system (both the inner and outer cell). Nevertheless, a slight elevation in pressure within the outer cell was noted as the load cell was introduced into the inner cell. In this setup, the pressure was regulated solely by the pressure transducer that measured the pressure within the inner cell. The rise in pressure within the outer cell, while the pressure in the inner cell remained constant, compromised the integrity of the glass wall of the inner cell. To prevent the breakdown of the glass wall, the two cells were divided by a valve, and an additional pump was fitted, with each pump regulated independently by distinct pressure transducers, as illustrated in Figure 7.1. The source of the pressure increase in the outer cell was not completely determined. Nonetheless, it was believed to result from the adhesion of the volume gauge, which let a differential pressure to accumulate between the gauge's base (supplying the outside cell) and its top (supplying the inner cell).

7.2.7. Constant water content tests

The equipment arrangement presented in Figure 7.9 was employed to conduct constant water content (CWT) tests on unsaturated samples. The components utilised in the tests were:

- The confining pressure (σ_3) was applied in the inner cell using a hydraulic pump operated by a stepper motor manufactured by Wykeham Farrance. A 2000 kPa pressure transducer C was utilised to measure the water pressure in the line; a similar design was implemented to sustain a constant pressure in the outer cell, ensuring complete independence between both cells.

- A Wykenham Farrance loading frame H was employed to maintain a constant displacement rate of 0.025 mm/min, with displacement quantified by the vertical displacement transducer E. Axial stress (σ_1) measurements were obtained within the cell using a 10 kN capacity load cell D.

- The volumetric behaviour of the sample (ε_v) was assessed using the volume gauge A, constructed at the workshop of Durham University's School of Engineering. This is a rolling Bellofram device of the type invented at Imperial College. The observed volume variations on gauge A resulted from volumetric alterations in the sample, as indicated by the measurement of water flow within the inner cell, adhering to the principle of water's incompressibility. To obtain an accurate measurement, it was essential to entirely eradicate air bubbles to regard the water as incompressible.

- Vertical deflections (ε_a) were measured using an externally mounted axial displacement transducer with a 75 mm range, as well as sample-mounted mini linear variable differential transformers (mini LVDTs) that have a nominal range of 5 mm but can function across a 10 mm range.

- Pore water pressure (u_w) was assessed using a WF-DU high-capacity suction probe, also known in the literature as a high-capacity tensiometer, positioned at the bottom platen in direct contact with the sample.

- The lower platen had a flat surface with two air lines (refer to Figure 7.10). The objective of these tests was to conduct constant water content triaxial tests while monitoring the progression of suction utilising a suction probe. Direct measurement of pore water pressure utilising a high-capacity suction probe, without the application of axis translation, eliminated the necessity for installing a high air entry value stone in the platen.

- The air lines were employed to exert air pressure within the sample while the cell was equilibrating during the equilibrium stage. The administered air pressure was contingent upon the confining pressure, being 5 kPa less than the confining pressure to prevent the inflation of the rubber membrane encasing the sample.

Continuous water tests were conducted on compacted samples following the preparation process outlined in previous chapter, utilising the Double Cell Triaxial Cells (DCTCs).. Consistent with the saturated testing series, each test was designated in the format Cxx(yy),

where xx represents the as-compacted water content and yy denotes the confining pressure for materials evaluated in their as-compacted state. Dxx(yy) denotes samples dried from as-compacted conditions, while Wxx(yy) refers to other samples saturated from as-compacted conditions. The samples for triaxial test were 100x200 mm, in contrast to the saturated tests, which employed samples measuring 38 mm in diameter and 74 mm in height. This discrepancy influenced the test duration. The primary determinant of this duration was the water content of the tested samples. Various samples were assessed in as-compacted, wetted, or dried conditions. The tests with the longest durations involved samples that were wetted from an initial water content of 15% of the as-compacted state. Due to the time frame allowed for testing while visiting Durham University for STSM, the results of 15% water content samples were adopted from Mendes and Toll, 2016.

The initial conditions of the samples at the commencement of each constant water content test are presented in Tables 7.6, 7.7, and 7.8. The initial conditions denote the moment the samples were placed in the triaxial cell, with $w_{(ac)}$ indicating the water content acquired post-compaction and w_i signifying the original water content of the test. The starting suction, and other relevant details are also supplied.

Table 7.6 presents the tests specifications conducted on materials formed under the 15% as-compacted condition, encompassing a total of 10 CWT tests: Four samples were evaluated in their compacted state, four samples were saturated to 20%, and one sample was saturated to 22%. This table includes a sample that was wetted from 13% to 17%. The subsequent sample (test W13-17) was originally meant to be wetted from 15% to 22%; however, a misunderstanding regarding the first water content measurement led to differing conditions, this part of test was fully commenced by Mendes and Toll, 2016.

Table 7.7 pertains to the tests conducted on materials generated under the 20% as-compacted condition, encompassing a total of 10 CWT tests. Four samples were evaluated in their compacted state, three samples were dried to 15%, and the remaining three samples were saturated to 22% moisture content.
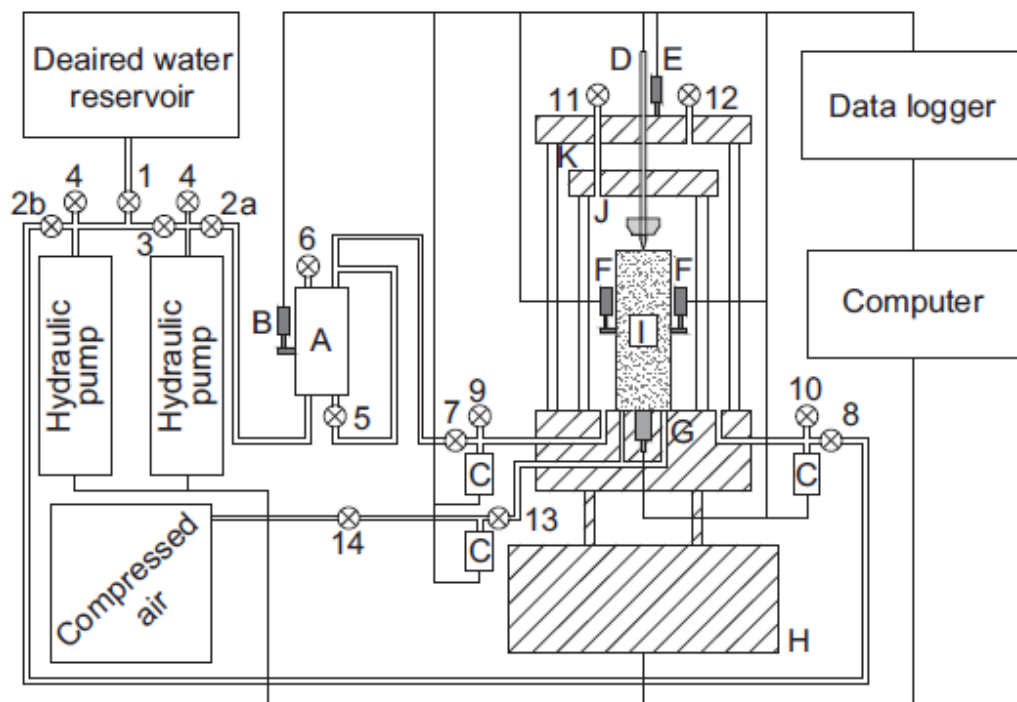
Legend:
A - Volume gauge
B - Volume change transducer
C - Pressure transducer
D - Load cell
E - Axial displacement transducer
F - Mini LVDT
G - High capacity tensiometer
H - Loading frame
I - Sample
J - Inner cell
K - Outer cell

Valves:
1 - Main deaired water supply
2a - Water supply/pressure line - inner cell
2b - Water supply/pressure line - outer cell
3 - Separator valve
4 - Bleeding valve - hydraulic pump
5 - Overlap - volume gauge
6 - Bleeding valve - volume gauge
7 - Main valve - inner cell
8 - Main valve - outer cell
9 - Drain valve - inner cell
10 - Drain valve - outer cell
11 - Bleeding valve - inner cell
12 - Bleeding valve - outer cell
13 - Compressed air supply - sample

Figure 7.9 Wykeham Farrance double cell triaxial system setup for constant water content testing (Mendes and Toll, 2016).

Table 7.8 presents the tests conditions conducted on materials prepared under the 22% as-compacted condition, encompassing a total of 10 CWT tests. Three samples were evaluated in their compacted state, three samples were dried to 15%, and the other four samples were dried to 22%[1].

All of the tables demonstrate that, despite minor variations in the suction values, the samples evaluated at the same water content (w_i) had comparable values for the majority of

the variables, including dry densities, void ratios, and saturation degrees. Tables 7.6, 7.7, and 7.8 made it evident that when the material was wetted or dried from its as-compacted state, the parameters changed as the water content increased.

As anticipated, specimen evaluated at w_i close to 15% often had increased dry density and suction. Suction should be maximum since it is the lowest water content, and higher dry density is expected because it corresponds with optimal water content. It is evident from all tables (Tables 7.6–7.8) that the sample volume varied according to the water content that was measured. The volume of samples that were dried reduced in comparison to those that were wetted from as compacted state.

With the exception of test D20-15(150), all tests showed a general tendency for the pore water pressure to drop throughout the continuous water compression stage. Since a smaller sample size indicates smaller voids, which are related to an increase in the degree of saturation under constant water conditions, it would be expected that the pore water pressure would increase during the compression stage with the size reduction of the samples.
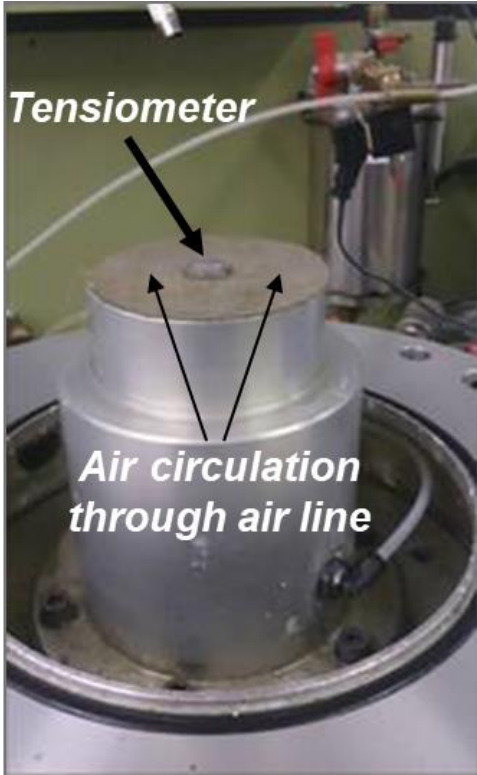
Figure 7.10 Pedestal configuration for unsaturated triaxial testing.

Table 7.6 Initial conditions at the start of the constant water tests for samples compacted at **15%** (after Mendes and Toll, 2016).

Test No.	Water content Wc_{ac} %	Water content Wc_i %	Dry density ρ_d Mg/m^3	Void ratio e	Degree of Saturation S_r %	Initial Suction s_i kPa
C15(50) 1	14.77	14.77	1.83	0.47	87.91	227
C15(50) 2	14.75	14.75	1.83	0.48	83.77	420
C15(150)	15.17	15.17	1.81	0.49	83.80	255
C15(300)	14.62	14.62	1.83	0.47	83.87	420
W15-19(150)	15.21	18.45	1.71	0.58	93.83	7
W15-19(300)	15.44	19.37	1.69	0.60	90.56	17
W15-20(50)	14.61	19.70	1.73	0.56	96.51	35
W15-20(150)	15.09	19.75	1.66	0.62	95.84	3
W15-22(50)	14.67	22.00	1.65	0.63	94.43	0.3
W13-17(300)	13.24	17.09	1.67	0.61	96.99	2

Table 7.7 Initial conditions at the start of the constant water tests for samples compacted at **20%.**

Test No.	Water content Wc_{ac} %	Water content Wc_i %	Dry density ρ_d Mg/m^3	Void ratio e	Degree of Saturation S_r %	Initial Suction s_i kPa
C20(50)	19.51	19.51	1.75	0.53	95.49	20
C20(150)	19.76	19.76	1.73	0.55	94.84	13
C20(300) 1	19.58	19.58	1.73	0.58	93.74	12
C20(300) 2	20.15	20.15	1.70	0.58	93.78	17
D20-15(50)	19.75	15.10	1.82	0.47	84.94	601
D20-15(150)	19.23	15.45	1.80	0.53	83.01	268
D20-15(300)	18.68	15.21	1.82	0.48	83.99	352
W20-20(150)	19.28	20.72	1.66	0.59	94.97	5
W20-22(50)	19.55	21.43	1.69	0.59	97.89	5
W20-22(300)	19.92	21.31	1.66	0.63	93.1	4

Table 7.8 – Initial conditions at the start of the constant water tests for samples compacted at **22%**.

Test No.	Water content Wc_{ac} %	Wc_i %	Dry density ρ_d Mg/m^3	Void ratio e	Degree of Saturation S_r %	Initial Suction s_i kPa
C22(50)	21.72	21.73	1.63	0.68	87.98	5
C22(150)	22.20	22.20	1.62	0.67	89.01	6
C22(300)	21.98	21.98	1.64	0.65	88.950	7
D22-20(50)	21.86	19.78	1.69	0.63	88.55	93
D22-20(150) 1	21.89	19.68	1.67	0.63	87.99	3
D22-20(150) 2	22.12	20.08	1.65	0.65	85.11	106
D22-19(150)	21.37	19.05	1.65	0.64	81.09	93
D22-16(50)	21.25	17.01	1.78	0.51	88.13	90
D22-16(300)	21.04	15.78	1.82	0.50	86.78	133
D22-14 (150)	22.01	13.89	1.83	0.50	79.12	239

In contrast, air pressure was applied to the samples during the equilibrium stage of these CWT tests prior to the compression step. The observed irregularity appears to be explained by a steady dissipation over time rather than an abrupt dissipation of air pressure as was initially thought. Because of this, even though the beginning values of the pore water pressure during the compression stage were impacted by the preceding equilibrium stage, by the time the compression stage ended, the air pressure had completely dissipated, which was made possible by the stage's extended duration. Samples tested with a W_{ci} of around 15% continued to have negative pore water pressure readings (suction) during the compression step in all tables (7.9 to 7.12).

At the end of the compression stage, at lower confinement values (50 and 150 kPa), tested samples with W_{ci} close to 20% only slightly exceeded negative values of pore water pressure. Regardless of the as-compacted water content, samples that were wetted from as-compacted circumstances consistently displayed positive values of pore water pressure throughout the constant water compression stage.

Table 7.9 – Sample conditions at the start and end of the constant water compression for samples compacted at Wc(ac) close to 15%.

	Test No.		Volume cm³	Dry density Mg/m³	Void ratio	Degree of saturation %	Pore water pressure kPa	Confining pressure kPa
Wc_i 15%	C15(50) 1	Initial	1660	1.840	0.47	87.94	-210.8	50
		Final	1653	1.848	0.46	89.20	-241.5	
	C15(50) 2	Initial	1687	1.834	0.47	84.12	-74.3	50
		Final	1679	1.843	0.47	85.42	-185.8	
	C15(150)	Initial	1683	1.816	0.49	83.96	-173.2	150
		Final	1681	1.818	0.49	84.22	-236.2	
	C15(300)	Initial	1676	1.847	0.46	85.35	-148.8	300
		Final	1664	1.860	0.45	87.28	-176.7	
Wc_i 20%	W15-19(300)	Initial	1788	1.702	0.59	88.97	283.2	300
		Final	1735	1.753	0.54	96.62	153.7	
	W15-19(150)	Initial	1812	1.737	0.56	89.71	136.3	150
		Final	1774	1.775	0.52	95.40	39.7	
	W15-20(50)	Initial	1789	1.737	0.56	95.73	4.5	50
		Final	1777	1.749	0.55	97.65	2.1	
	W15-20(150)	Initial	1827	1.699	0.59	90.37	99.4	150
		Final	1796	1.729	0.56	94.70	43.8	
Wc_i 22%	W15-22(50)	Initial	1821	1.669	0.62	92.64	24.9	50
		Final	1792	1.695	0.59	96.57	9.4	
	W13-17(300)	Initial	1819	1.746	0.55	84.27	294.7	300
		Final	1757	1.808	0.49	93.33	73.3	

The conditions at which the samples entered the shearing stage correspond to the final values on Tables 7.9, 7.10, and 7.11 since the shearing stage in this study begins when the continuous water compression stage ends. The results of the shearing step are presented in Figs 7.9, 7.12 and 7.15.

Table 7.10 Sample conditions at the start and end of the constant water compression for samples compacted at Wc(ac) close to 20%.

	Test No.		Volume cm³	Dry density Mg/m³	Void ratio	Degree of saturation %	Pore water pressure kPa	Confining pressure kPa
Wc_i 20%	C20(50)	Initial	1678	1.723	0.55	92.00	17.8	50
		Final	1668	1.733	0.52	93.56	-10.0	
	C20(150)	Initial	1624	1.745	0.55	95.15	76.5	150
		Final	1578	1.778	0.52	99.93	-1.1	
	C20(300) 1	Initial	1656	1.721	0.58	90.89	216.5	300
		Final	1637	1.732	0.54	92.34	205.9	
	C20(300) 2	Initial	1647	1.728	0.56	87.01	156.7	300
		Final	1608	1.769	0.52	92.00	98.2	
Wc_i 15%	D20-15(50)	Initial	1568	1.834	0.51	85.67	-695.1	50
		Final	1562	1.845	0.50	85.53	-681.7	
	D20-15(150)	Initial	1621	1.793	0.50	82.89	-246.1	150
		Final	1619	1.795	0.49	82.99	-261.3	
	D20-15(300)	Initial	1585	1.821	0.48	83.89	-22.2	300
		Final	1579	1.839	0.49	84.45	-354.1	
Wc_i 22%	W20-21(150)	Initial	1715	1.693	0.61	92.78	49.5	150
		Final	1671	1.741	0.57	99.98	26.7	
	W20-22(50)	Initial	1730	1.675	0.61	93.97	18.2	50
		Final	1711	1.683	0.59	96.89	12.6	
	W20-22(300)	Initial	1715	1.676	0.60	93.02	285.8	300
		Final	1706	1.681	0.59	94.56	275.3	

Constant water experiments conducted at the same $W_{c(ac)}$ were displayed using the same colour scheme to aid in the visualisation of the behaviour for the many variables provided. The colour graduation in each test set is the same across all graphs. The highest deviatoric stress for each test is shown in Tables 7.12, 7.13, and 7.14 for samples tested at $W_{c(ac)}$ close to 15%, 20%, and 22%, respectively.

Table 7.11 Sample conditions at the start and end of the constant water compression for samples compacted at Wc(ac) close to 22%.

	Test No.		Volume cm³	Dry density Mg/m³	Void ratio	Degree of saturation %	Pore water pressure kPa	Confining pressure kPa
Wc$_i$ 22%	C22(50)	Initial	1698	1.618	0.66	87.48	24.1	50
		Final	1669	1.638	0.64	90.29	9.7	
	C22(150)	Initial	1689	1.596	0.72	81.28	116.9	150
		Final	1701	1.580	0.69	84.34	76.5	
	C22(300)	Initial	1696	1.622	0.68	82.26	222.7	300
		Final	1657	1.658	0.64	86.97	148.5	
Wc$_i$ 20%	D22-20(50)	Initial	1593	1.747	0.55	94.68	-74.6	50
		Final	1601	1.739	0.54	95.20	-51.2	
	D22-20(150) 1	Initial	1626	1.669	0.61	86.78	33.1	150
		Final	1609	1.681	0.59	88.21	-0.4	
	D22-20(150) 2	Initial	1693	1.645	0.63	84.67	10.9	150
		Final	1686	1.660	0.62	86.45	-3.9	
	D22-19(150)	Initial	1675	1.675	0.61	85.53	- 28.7	150
		Final	1653	1.689	0.60	87.49	0.8	
Wc$_i$ 15%	D22-16(50)	Initial	1567	1.801	0.49	90.41	- 185.7	50
		Final	1541	1.799	0.49	91.51	-299.1	
	D22-16(300)	Initial	1538	1.822	0.50	87.72	- 76.9	300
		Final	1533	1.821	0.50	87.55	-131.3	
	D22-14(300)	Initial	1518	1.831	0.47	79.00	-40.0	150
		Final	1513	1.836	0.46	80.08	-179.1	
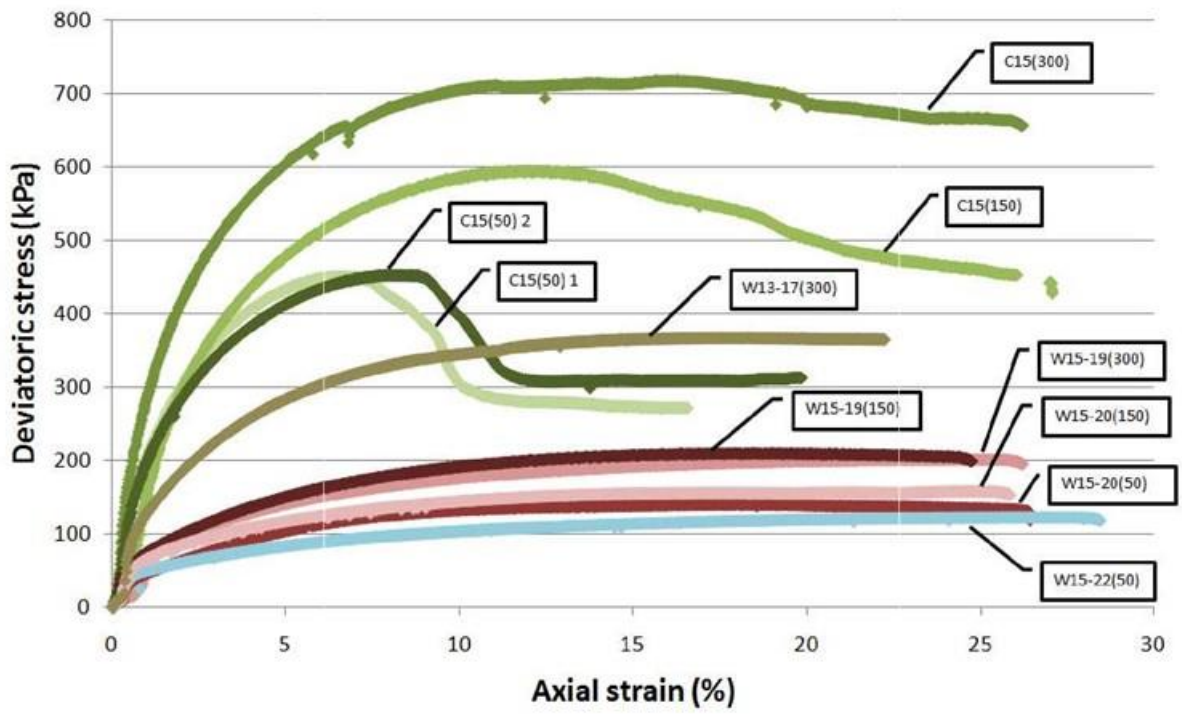
Figure 7.9 Samples deviatoric stress and axial strain at Wc(ac)= 15%.
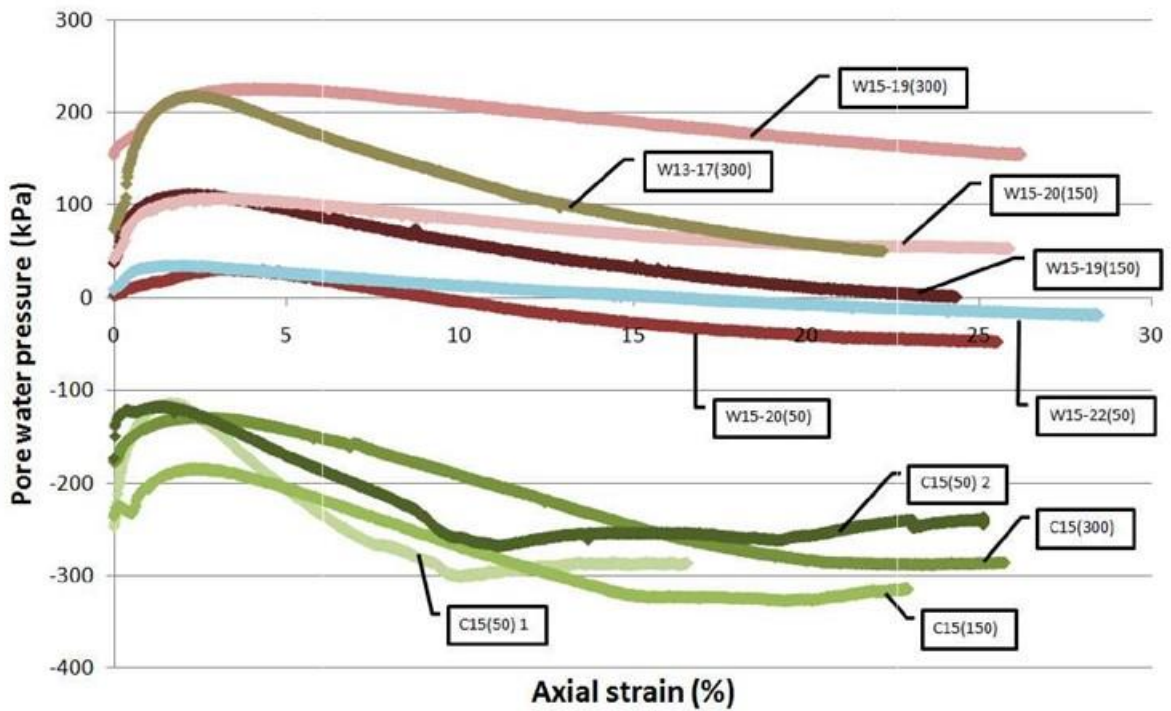
Figure 7.10 Samples pore water pressure and strain at Wc(ac) of 15%.
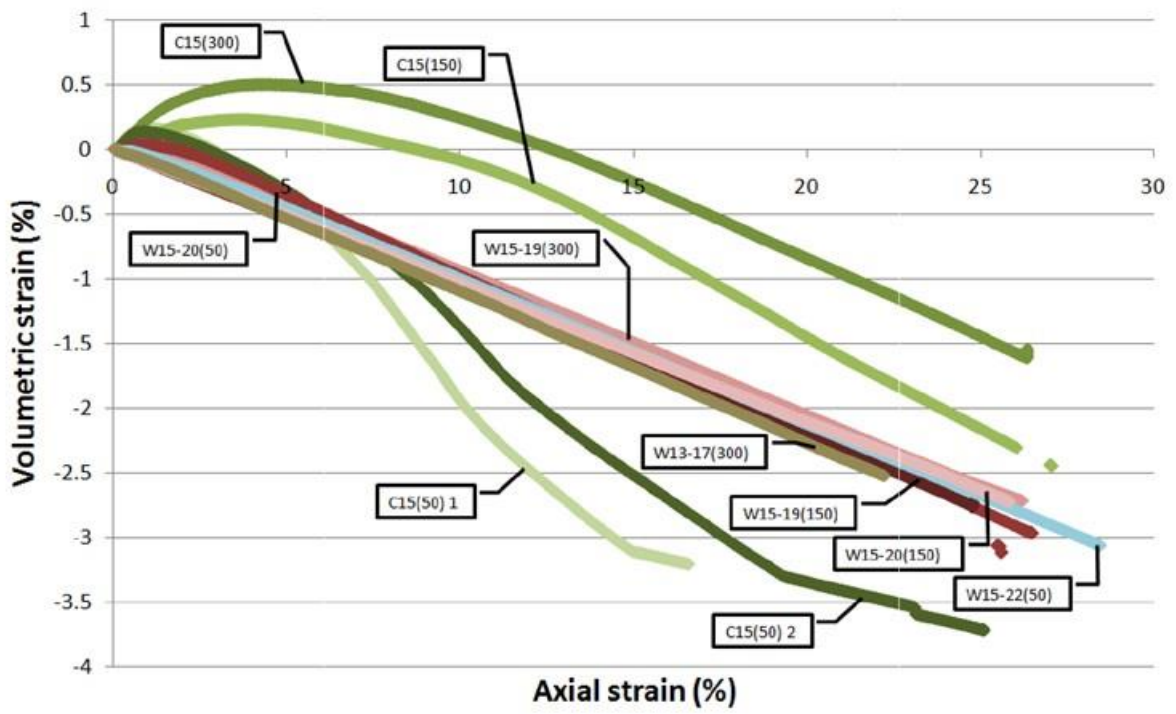
Figure 7.11 Samples volumetric and axial strain at Wc(ac) of 15%.
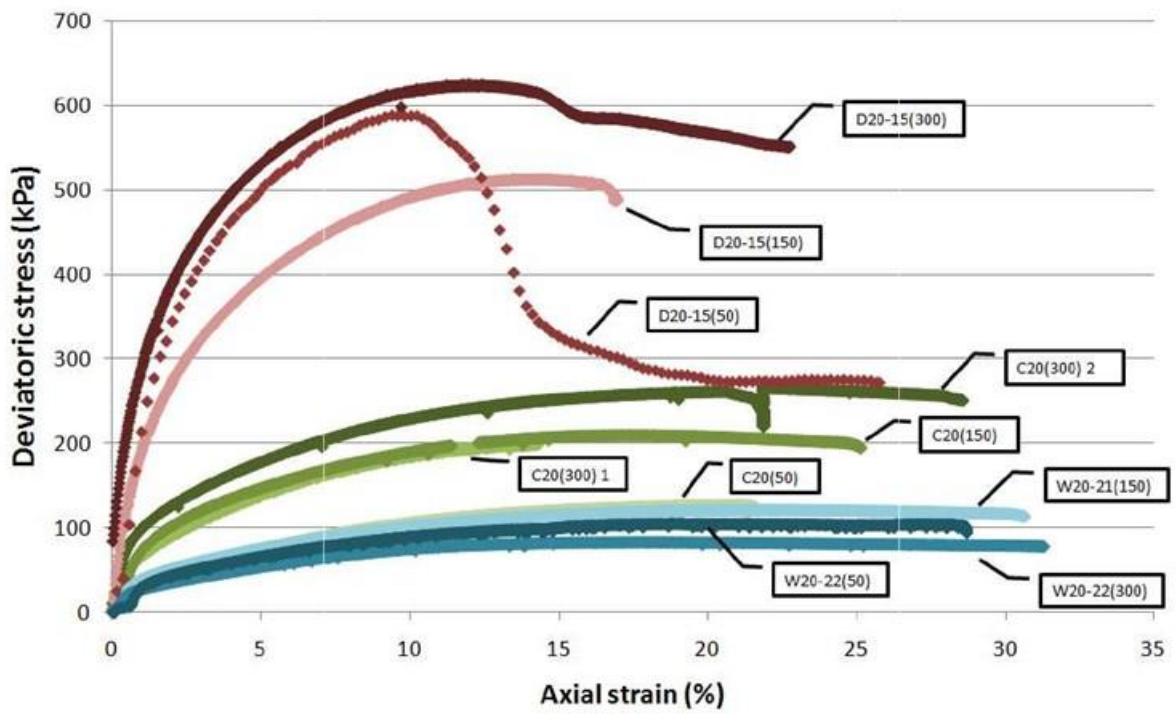
Figure 7.12 Samples deviatoric stress and axial strain at Wc(ac)= 20%.
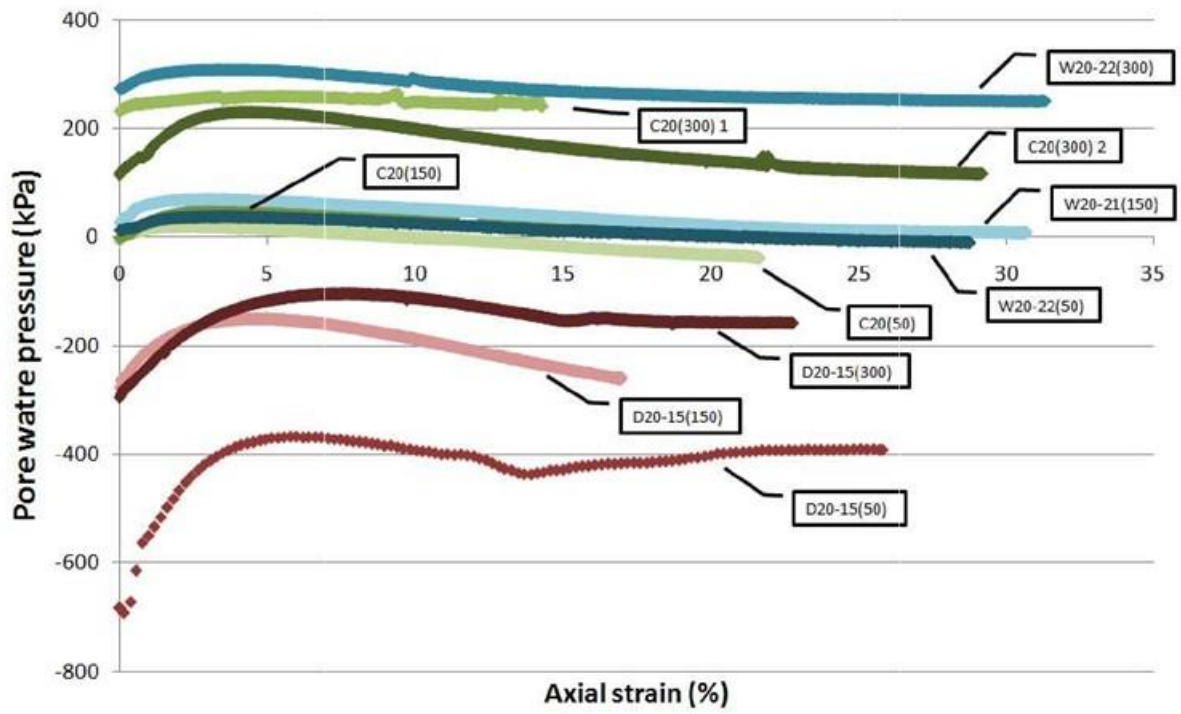
Figure 7.13 Samples pore water pressure and strain at Wc(ac) of 20%.
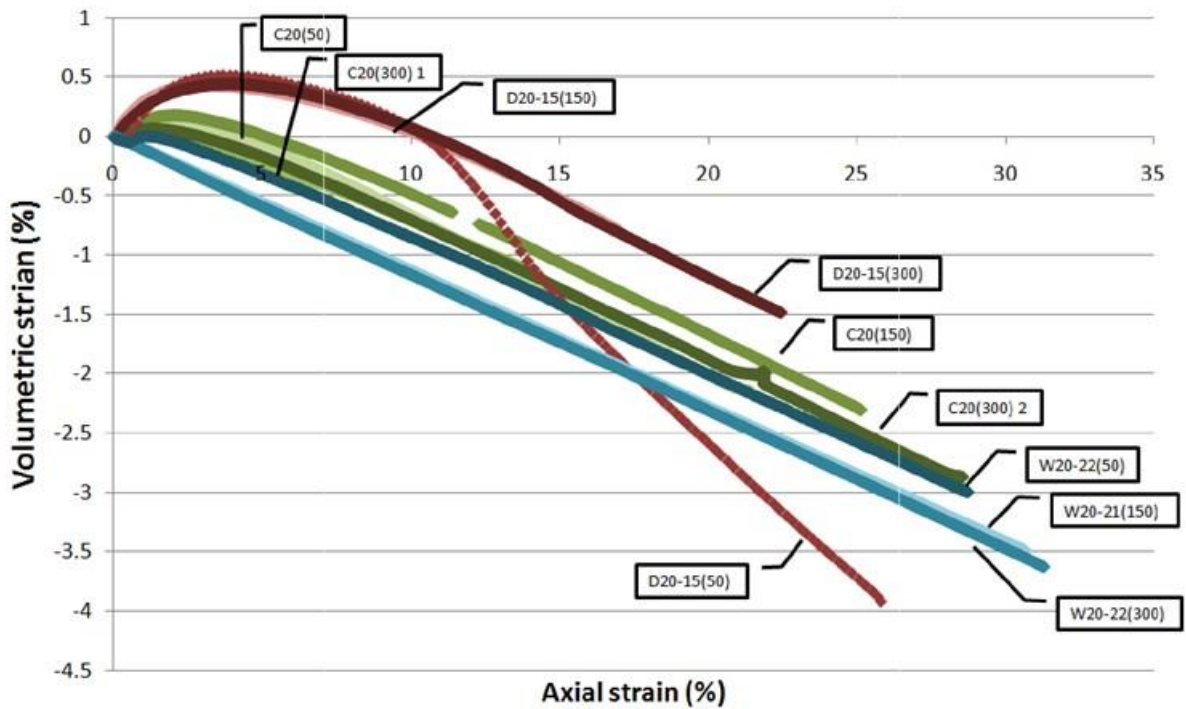
Figure 7.14 Samples volumetric and axial strain at Wc(ac) of 20%.
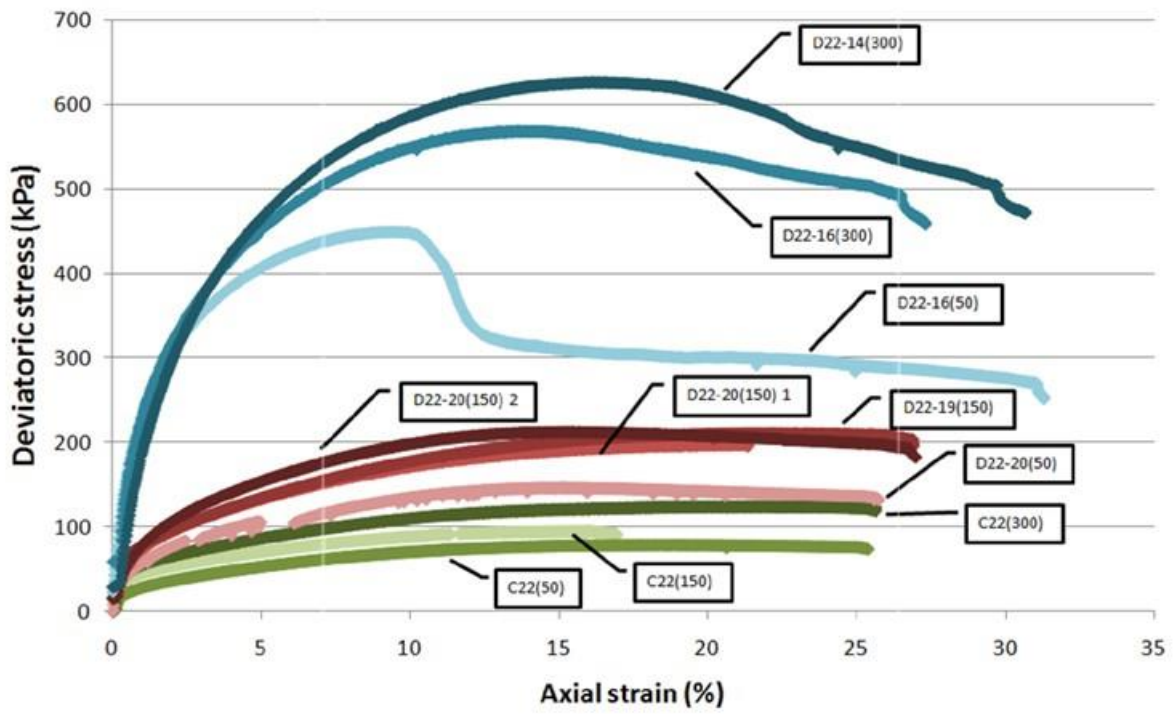
Figure 7.15 Samples deviatoric stress and axial strain at Wc(ac)= 22%.
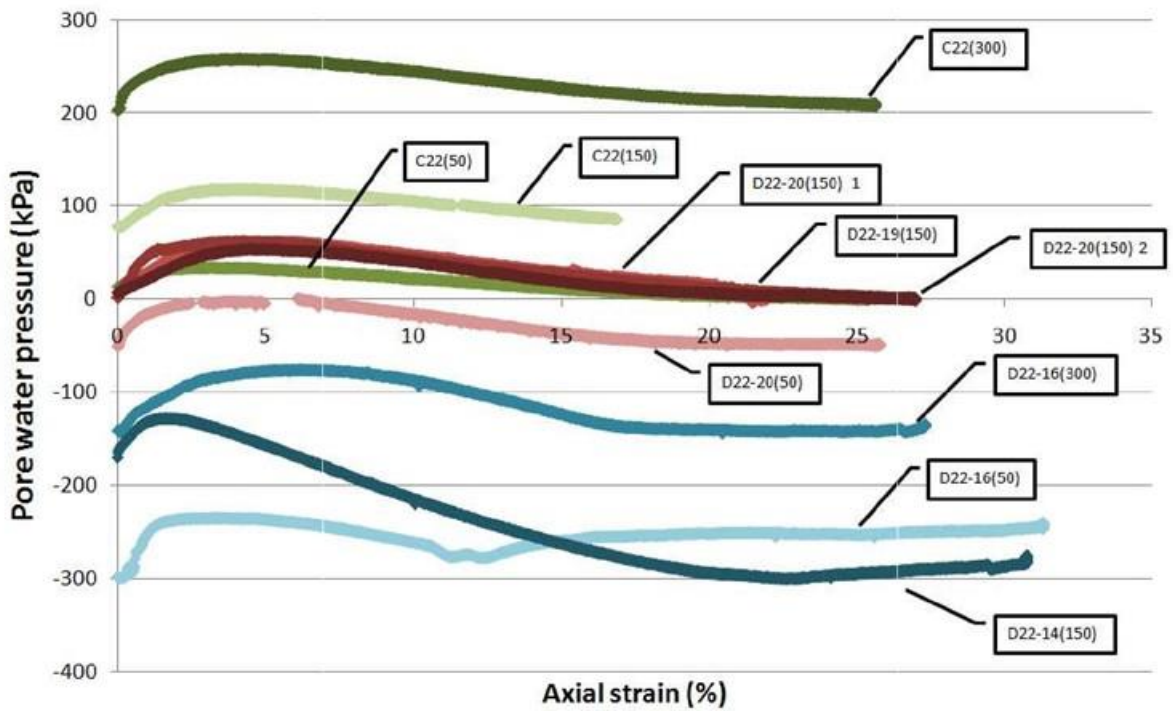
Figure 7.16 Samples pore water pressure and strain at Wc(ac) of 22%.
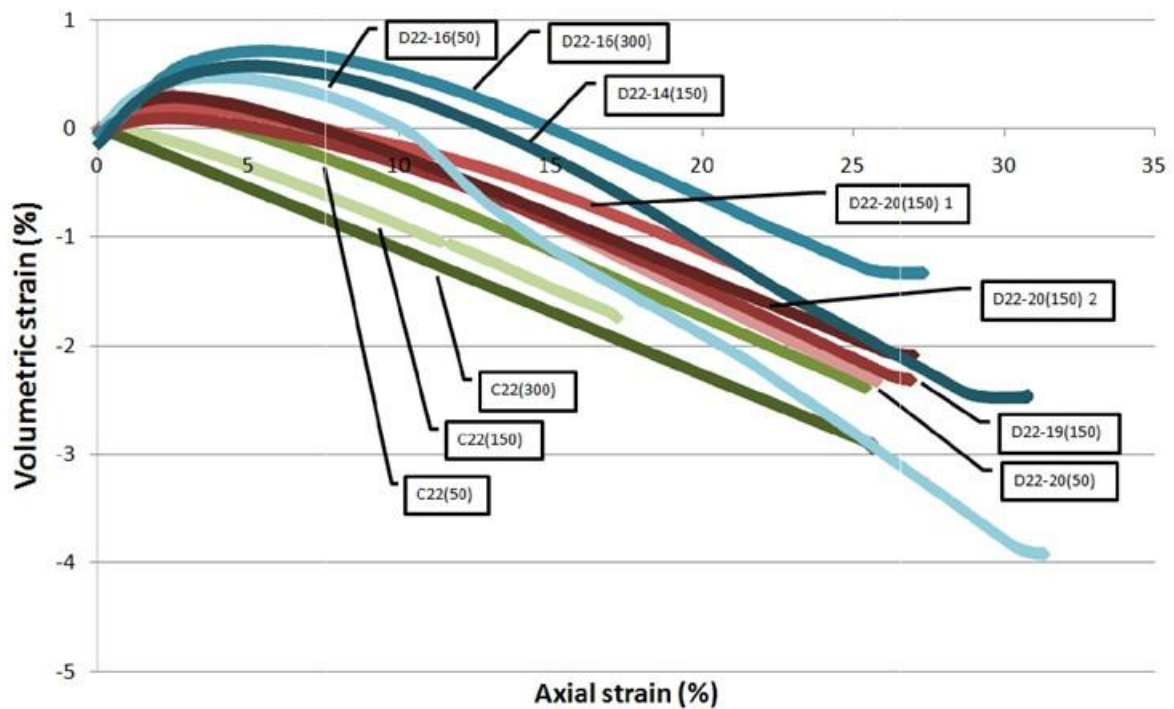
Figure 7.17 Samples volumetric and axial strain at Wc(ac) of 22%.

Table 7.12 Samples behaviour at maximum deviatoric stress at Wc(ac)= 15%.

	Test No.	Dry density Mg/m³	Void ratio	Degree of saturation %	Mean net stress kPa	Deviatoric stress kPa	Pore water pressure kPa	p-u_w kPa
	C15(50) 1	1.835	0.47	87.19	200.4	450.8	-242.8	443.2
	C15(50) 2	1.826	0.48	83.03	204.1	461.4	-210.2	414.4
Wc_i 15%	C15(150)	1.827	0.48	85.53	355.4	616.0	-292.3	647.7
	C15(300)	1.836	0.47	83.65	523.9	671.7	-287.8	811.7
	W15-19(150)	1.739	0.55	90.05	220.2	210.7	17.3	202.9
	W15-19(300)	1.710	0.58	90.17	367.3	201.9	160.2	207.1
Wc_i 20%	W15-20(50)	1.712	0.58	92.01	97.31	141.6	-35.4	132.7
	W15-20(150)	1.686	0.60	88.53	202.9	158.4	55.1	147.8
Wc_i 22%	W15-22(50)	1.646	0.64	89.39	91.3	123.3	-17.9	109.2
	W13-17(300)	1.773	0.52	88.06	423.2	368.9	71.2	352.0

As previously indicated, it was observed that conditions varied for various testing at this point. In the experiments conducted at values where W_{ci} was about 15%, the highest deviatoric stress value was obtained at negative pore water pressure values. This was also true in testing with confining pressures of 50 kPa and W_{ci} values of 20%, although with somewhat negative pore water pressure values in these cases. At positive pore water pressure values, the remaining tests were able to reach this stage.

Table 7.13 Samples behaviour at maximum deviatoric stress at Wc(ac)= 20%.

	Test No.	Dry density	Void ratio	Degree of saturation	Mean net stress	Deviatoric stress	Pore water pressure	p-u$_w$
		Mg/m³		%	kPa	kPa	kPa	kPa
Wc$_i$ 20%	C20(50)	1.730	0.55	88.15	92.9	127.8	-34.7	129.1
	C20(150)	1.749	0.56	95.91	221.5	210.1	13.8	205.6
	C20(300)	1.710	0.57	90.01	367.1	198.9	252.0	114.1
Wc$_i$ 15%	D20-15(50)	1.837	0.48	85.89	246.1	57.9	-386.9	634.1
	D20-15(150)	1.791	0.52	82.34	322.1	511.9	-223.9	546.5
	D20-15(300)	1.822	0.50	84.23	509.0	625.1	-126.9	634.9
Wc$_i$ 22%	W20-21(150)	1.711	0.61	93.53	191.0	120.9	17.9	171.9
	W20-22(50)	1.671	0.62	92.54	84.9	104.9	3.5	82.1
	W20-22(300)	1.643	0.65	90.02	328.1	84.3	264.8	65.5

Table 7.14 Samples behaviour at maximum deviatoric stress at Wc(ac)= 22%.

	Test No.	Dry density	Void ratio	Degree of saturation	Mean net stress	Deviatoric stress	Pore water pressure	p-u$_w$
		Mg/m³		%	kPa	kPa	kPa	kPa
Wc$_i$ 22%	C22(50)	1.621	0.70	86.78	76.6	78.4	5.5	72.1
	C22(150)	1.583	0.72	78.32	182.2	94.8	87.9	95.2
	C22(300)	1.615	0.69	81.76	340.9	123.9	213.1	127.9
Wc$_i$ 20%	D22-20(50)	1.734	0.56	92.67	99.3	145.9	-36.8	136.3
	D22-20(150) 1	1.671	0.59	85.86	215.9	197.9	-0.2	217.4
	D22-20(150) 2	1.652	0.61	84.62	222.0	213.1	16.9	203.9
	D22-19(150)	1.669	0.63	83.41	219.0	212.0	4.9	214.9
Wc$_i$ 15%	D22-16(50)	1.798	0.50	92.01	199.9	450.1	-259.1	459.1
	D22-16(300)	1.825	0.51	88.06	490.1	569.7	-113.1	603.1
	D22-14(150)	1.845	0.47	79.01	359.1	627.0	-271.2	630.1

When analyzing the axial strain at the maximum deviatoric stress it was found that for samples tested at W_{ci} close to 15%, the maximum deviatoric stress was reached at lower axial strain values: for confining pressures of 50 kPa, the axial strain ranged from 6-9% in Table 7.12, while values in Table 7.13 and Table 7.14 reached values between 17-21% and 18-27%, respectively. We also saw the same comparison for the remaining confining pressures. The samples with initial values of pore water pressure that were negative displayed the peaks in stress-strain behaviour during shearing on samples tested at a W_{ci} close to 15%. These samples included samples that were tested as-compacted at 15% of water content (tests C15(50) 1, C15(50) 2, C15(150), and C15(300), and samples compacted at water contents of 20% and 22% and dried to 15% (tests D20-15(50), D2015(150), and D20-15(300), as well as tests D22-16(50), D22-16(300), and D22-14(150). Considerable pore water pressure reduction which reached negative pore water pressure was the consequence of the drying, and it was maintained during shearing. In the remaining tests, that is, in tests where the W_{ci} was 20% or 22%, where the pore water pressure was primarily positive from the beginning, strength peaks were not visible. With the exception of the test that dried from 22% to 20% at 50 kPa of confinement, D22-20(50), even samples with low negative values of pore water pressure following the compression stage rose to positive values during shearing. The types of failure provide an explanation for the patterns of deviatoric stress with axial strain. The samples that were tested at a W_{ci} near 15% failed due to the shear surface forming, which is what caused the brittleness and strength peaks that are visible in the stress-strain relationships. Samples failed the CWT tests in aplastic behavior, resulting in bulging effect (please see Fig. 7.18). Since stresses and deformations can be taken to be rather homogeneous throughout the specimen, the variables based on principle stresses and strains were appropriate in defining the mechanical behaviour due to the systematic deformations. Concerns would arise that the deformations would become extremely non-uniform and that the overall stresses and strains would no longer accurately represent the specimen as a whole for the CWT tests in which the samples experienced shear surfaces.

Fig 7.18 Bulging effect on samples at Wc(ac)= 20% and 22% after shearing.

7.3. Conclusions

The chapter presents an attempt to characterise the mechanical behaviour of the sandy clay samples by performing triaxial tests in saturated conditions and unsaturated state by applying constant water content approach.

The experiments for constant water content were conducted in a double cell triaxial cell, whilst the saturation tests were carried out in traditional triaxial cells. When the sample voids are not saturated, the two-cell structure, in which the outer cell encircles the inner cell, allows for a more precise assessment of the volume change of samples. The DCTC is an appropriate piece of equipment to perform triaxial tests on unsaturated samples because of two features: first, the glass wall of the inner cell eliminates the water absorption issue found in cell walls made of Perspex, improving the accuracy of the cell volume changes; and second, a high capacity suction probe can be placed in the pedestal inside the inner cell to enable measurements of the pore water pressure directly in the sample, eliminating the need to use pore air pressures to simulate matric suction. Since the inner and outside cells' pressures are kept constant, the pressure surrounding the inner cell's wall will also be constant. This eliminates most wall deformations and lowers measurement error for volume changes inside the cell. Samples were subjected to constant water tests at predefined water contents of 15%, 20%, and 22%. Samples were examined under dried, wet, or as-compacted conditions based

102

on their initial water contents. At 50, 150, and 300 kPa confining pressures, tests were conducted. The samples tested at higher suction values (samples tested at water contents close to 15%) increased the failure and critical strength of the material, according to a comparison of the critical state parameters of the saturated test and the constant water content test. These samples also had lower degrees of saturation and void ratios, making them stiffer. It was discovered that the original, or as-compacted, conditions controlled the mechanical behaviour of the material. When the variations in the initial pore water pressure were considered, the testing procedure—whether it was wetting or drying—did not appear to have an impact on the behaviour. The findings and the actual hydro-mechanical behavior (SWRC and triaxial test results) were used in the slope stability modeling to asses the beahavior of slopes under different weather events.

8. Mechanical behaviour of fine sand used in the study

8.1. Introduction

The standard traixial test as describe in previous chapter is one of most commonly used geotechnical laboratory tests, widely applied to determinate strength, and deformation for variety of soils under drained and undrained conditions (Head, 1986). Triaxial test for analyses of granular material involves enclosing a cylindrical soil sample in a rubber membrane and placed inside a pressure chamber and subjecting radial stresses (confining pressure) and controlled increases in axial stresses or axial displacements just as for previously tested material (sandy clay). Depending on the type of triaxial apparatus the base pedestal can move vertically and by that movement vertical stress is applied to the specimen from the upper end.

The water pressure surrounding the sample in the pressure chamber controls confining pressure. Volume change of the sample can be measured in two ways: One technique is based on using controller volume change: for direct volume measurement, a water pressure/volume controller is to be filled with de-aired water and used to control the pore water pressure (back pressure) and to measure the pore water volume change going in and out from the sample. Second technique is based on cell volume change: the cell volume change can be measure and use to establish the total specimen volume change. This technique is not very satisfactory because the cell stiffness is not infinite and therefore specimen loading changes and cell pressure changes cause a volumetric change in the cell (these are the conditions that concerned samples teste in a double wall system referred in previous chapter).

In addition, the system needs excellent temperature stability especially when it comes to unsaturated test on granular samples where the suction values are not as high as for cohesive samples. Small changes in temperature can cause large changes in the volume of the cell water. Triaxial test data, in general, include evolution of axial and volumetric strain, deviatoric and isotropic stress, and pore pressure evolution.

8.2. Modified Bishop and Wesley triaxial cell for unsaturated soil samples

Triaxial testing system used to perform tests on granular material (as a part of MUMOLADE research project) is an Automated Stress Path type provided by GDS Instruments. The system is based on classic Bishop & Wesley- type stress path triaxial cell, and the GDS pressure/volume controller. It contains a number of components to enable the desired specimen stress state to be reached, and shear the specimen whilst recording the soil response. Figure 8.1 presents complete system diagram of equipment and arrangement of advanced pressure/volume controllers. Table 8.1 lists each primary component of a GDS triaxial system, along with its main function and parameter measured.
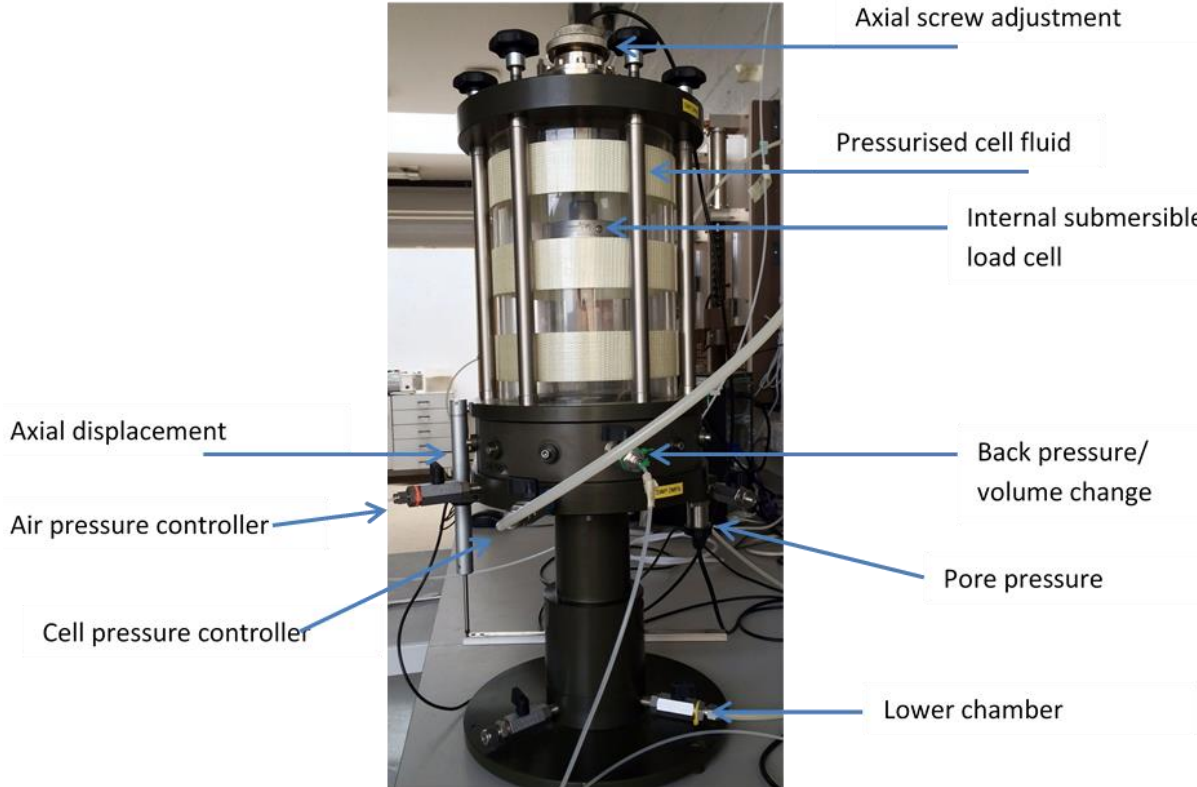
Figure 8.1 General set up of GDS triaxial Automated Stress Path equipment.

An unsaturated triaxial test works by applying a Back Pressure (u_w) and an Air Pressure (u_a) to a test specimen so that tests can be carried out on the sample in controlled unsaturated conditions in addition to fully saturated state. A Data Acquisition Interface may be used with the system to measure axial force, axial displacement, local axial and radial strain, pore pressure, differential pressure and atmospheric pressure. This uses a water pressure/volume controller to measure the after volume change and an air pressure/volume controller to measure the air volume change. By adding the two values the total volume change in the sample can be calculated.

Table 8.1 Critical state points of each test.

COMPONENT	MAIN FUNCTION	PARAMETER MEASURED
Triaxial cell	House the specimen and cell fluid	N/A
Pedestal and top-cap	Provide specimen seating and drainage ports	N/A
Rubber membrane, O-rings and porous discs	Seal the specimen from the cell fluid, allowing control over the effective stress and drainage	N/A
Cell pressure / volume controller	Apply confining stress to the specimen ($\sigma c = \sigma 3$) by pressurising the cell fluid	σ_3
Back pressure / volume controller	Apply back / pore pressure u to the specimen and measure volume change ΔV	ΔV
Velocity–controlled load frame	Shear the specimen through axial movement of a loading platen at a constant rate	N/A
Internal submersible load cell	Measure the change in axial load F applied to the specimen during shear	F (kN)
Pore water pressure (PWP) transducer	Measure the change in pore water pressure u within the specimen	u (kPa)
Axial displacement transducer	Measure the change in height (and hence axial strain εa) of the specimen	ΔH
Data acquisition unit	Convert analogue readings from the load cell, PWP and axial displacement transducers to digital data	N/A
GDSLab control & acquisition software	Control test hardware and record digital readings taken from the data acquisition unit	N/A

The main difficulty of an unsaturated triaxial test is to accurately measure the specimen volume change. For direct volume measurement, a water pressure/volume controller is filled with de-aired water and is used to control the pore water pressure (back pressure) and to measure the pore water volume change. An air pressure/volume controller is filled with air and is used to control the pore-air volume change. By calculation of the combined pore-air and pore-water volume changes the total volume change of the test specimen can be evaluated. The Advanced 2MPa/1000cc air pressure/volume controllers are similar mechanically to the Advanced,

2MPa/1000cc water pressure/volume controllers for de-aerated water. The control software or 'firmware' for the air controllers has been specially designed, however, for the much lower stiffness of air. The following points should be remembered when using air pressure controllers. The controllers can be run up from zero pressure provided there is sufficient volumetric capacity in the controller. The 1000cc version is essential here. Alternatively, the controller could be pre-pressurised at using a source of compressed air. This would 'save' volumetric capacity used up in pressurising itself. The controllers have not been designed for controlling water pressure. This is because the target pressure seek algorithms built into the programming of the controller (so-called 'firmware') is different for air (which is very comprssible) from the algorithm used for water (which is very much stiffer than air). The air pressure range is 2MPa with regulation to 1 kPa. The volumetric range is 1000cc with regulation to 1 cu.mm. (i.e 0.001 cc). When testing an unsaturated test specimen it is necessary to have more connections for transducers and air/hydraulic connectors than is normal for testing a totally saturated specimen. To accommodate this, the GDS cell for unsaturated testing has a modification which provides 12 access ports for the additional connections. This ring is known as an Access Ring. The direct volume measurement method for unsaturated testing uses a standard saturated testing system with the addition of the air pressure/volume controller and a modified base pedestal containing a high air entry porous disk. Air pressure is connected to the top of the test specimen as presented in Fig. 8.2. The air pressure and water pressures are maintained at different values to generate the 'matric suction' value present in unsaturated soils. By measuring both the air volume change and the water volume change the total volume change of the test specimen can be calculated.

Control/measure the air and water pressures and volume changes directly within the test specimen. This involves using a GDS pressure/volume controller to control the air pressure and air volume change in the test specimen. A second controller is used to control the pore water pressure and volume change.

The sum of the volume changes from these two controllers gives the total volume change in the test specimen. To perform such evaluation, the following parameters must be known: dry weight of material in the test specimen, specific gravity of the dry material, degree of saturation of the test specimen, volume of air in the controller. The volume of air in the controller may be calculated by completely filling the controller with de-aired water.
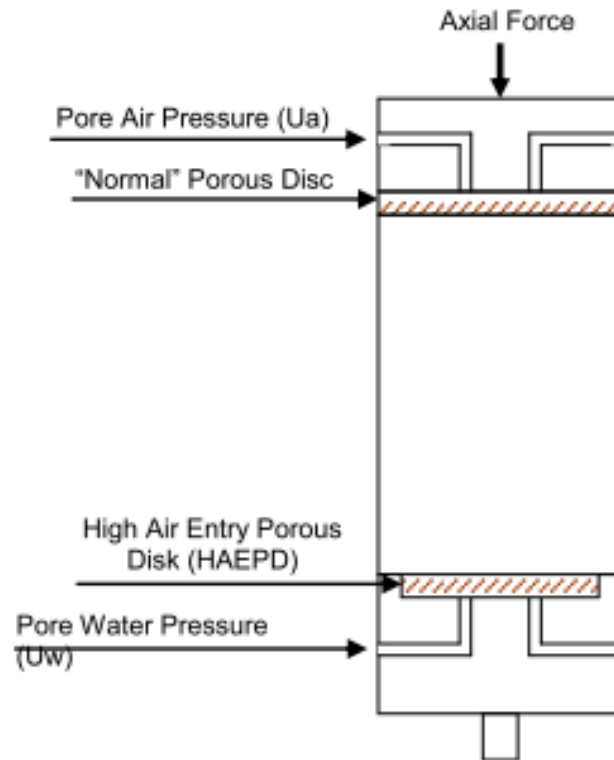
Figure 8.2 Schematic arrangement for soil sample placed on the pedestal.

The next step is to zero the volume change on the controller and then empty the controller. The controller should then be inverted so that the connector is the lowest point of the apparatus. Then the tube from the connector should be removed and a beaker of known mass beneath the connector should be placed, filling (with air) and empting the controller until no further water comes out is the next stage. The beaker should be weighted and from the weight of the water calculate the volume. This volume is the dead area of the controller. The controller should be run to the forward movement limit using the empty command. The operator should apply the fill command to run the controller to the back travel limit, the volume change displayed should be added to the dead volume. This figure is the total volume of the controller. Tests should always be started with the controller on the back travel limit. The entire set up of unsaturated triaxial test is presented in Fig. 8.3

8.3. Soil sample preparation method

There are several specimen preparation techniques, tamping and pluviation being the most common. The basic requirements for any of the method are an as uniform as possible distribution of void ratio to be obtained, and a wide range of densities is attainable by the same method. (Alshibli et al., 2000). It has been known that different methods of sample preparation

create different fabrics. Thereby, different responses are expected upon application of loading. The three most common methods used for sample preparation are: wet tamping, dry deposition, and water sedimentation. The water sedimentation and dry deposition methods can prepare very uniform specimen, but the voids of the specimen are not easy to control.
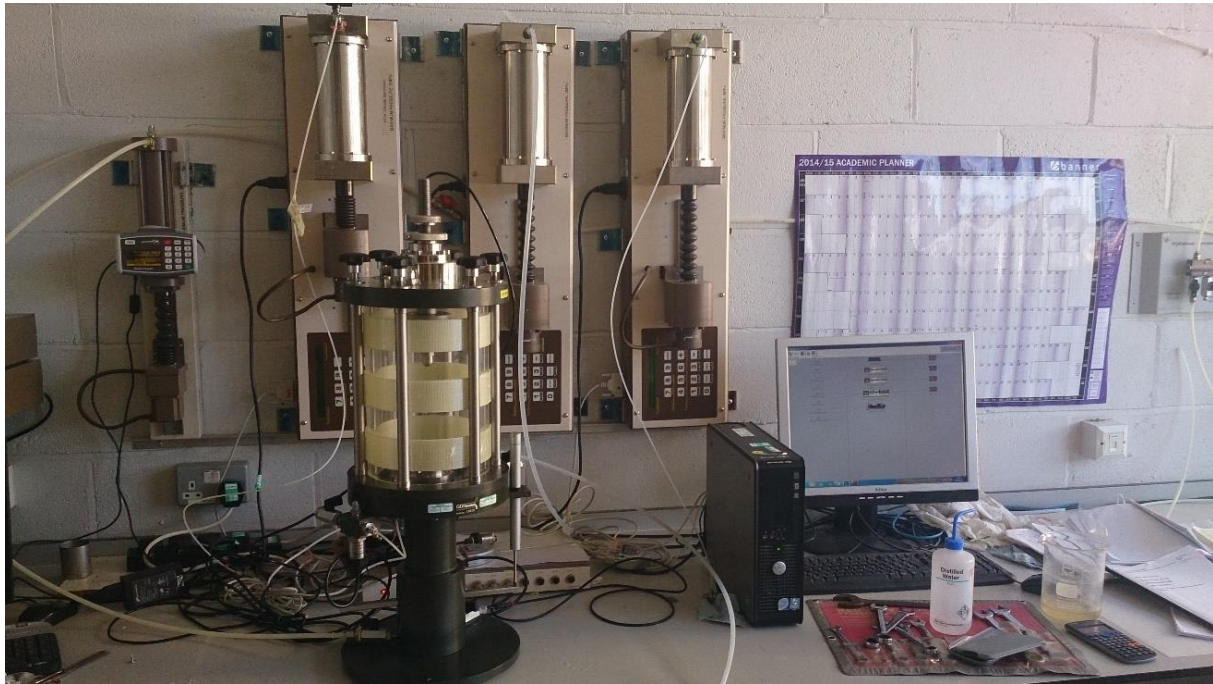
Figure 8.3 Triaxial research stage for unsaturated triaxial testing.

Using the moist tamping method very loose sample can be prepared due to the capillary effects between grains, it can be also used to prepare medium dense to dense sample. Besides, the void ratio is very easily controlled. The only thing is that specimen is less uniform than that prepared by the water sedimentation or dry deposition. Due to the need for medium dense sample, all samples were prepared dry tamping method in the study. The sample preparation procedure is described below. Sand material was gently spooned into the split mould on the pedestal in 5 layers. Each layer of the material was kneaded with steel rod with a 30mm diameter. The number of rodding for one layer was changed to achieve target density. When the mould was completely filled, porous disk was placed on the top of the sample followed by top cap, which was greased and attached to the latex membrane. The top end plate was attached with two o-rings. A vacuum is applied to the specimen through the drainage connection to help the specimen stay stable when the mould is removed.

The three- split mould was carefully split to prevent any disturbance to the specimen. The test cell was then sealed tightly and filled with de-aired water. By increasing pressure in lower chamber pressure with small increment, as slow as it is possible to position when sample is in

contact with loading ram. By that procedure we are sure sample is docked with loading ram. Cell pressure was maintained to 20kPa, to hold the specimen and then the vacuum in the specimen is removed, by opening drainage valve and closing it carefully. Then, 10kPa back pressure is applied to the sample in order to flushed water through the sample (no air bubble should be seen in the pipes). Approximate time for that procedure is about 30- 60min or until water starts to drain from open drainage valve. In order to keep back pressure value equal to pore reading.

Figure 8.4 Schematic arrangement for soil sample placed on the pedestal.

Calibration of the controller against pore pressure transducer should be checked before test. Both should be connected together, pressure target should be given (30kPa) on back pressure controller and pore pressure reading in the GDSLab software should be checked. That procedure should be repeated few times with different values of pressure.

8.4. Laboratory temperature conditions as factor influencing pore water pressure readings in unsaturated triaxial tests

Before commencing any laboratory tests, the researcher is obliged to make sure that the results of the measurements are not biased nor influenced by any external factors. For this reason, the author decided to perform a number of trail tests on the transducers and controllers, and their respond to changing laboratory environment conditions. The main considered factor was the laboratory room temperature. For the trial tests there were two approaches adopted. First, having the cell fully filled with water, without a soil specimen placed on the pedestal. The second approach aimed at recording the values of the pressure when the controller

connection and the transducer where left in the open water. The investigated devices were: pore pressure transducers (2 and 3 MPa), air pressure/volume controller, back pressure/volume controller, cell pressure/volume controller. The certified accuracy of the transducers used in the study are 0.15% of declared range, thus in this case they are 3 and 4.5 kPa respectively. The technical specifications of controllers used for tests are:

- accuracy of pressure measurement: <0.1% full range;

- pressure range: 2MPa,

- volume accuracy: volume = <0.25% for 1000cc (with +/-12 mm^3 backlash up to 16MPa and +/-5 mm^3 above 16 MPa),

- resolution of control (volume, pressure): 0.1 cm^3, 0.5 kPa,

- volume capacity: 1000cm^3

The devices used for recording the laboratory room conditions were sensitive electronic thermocouple and atmospheric pressure transducer. The entire measuring system was connected to common 8 channel serial pad and located next to each other, to give as much representative data as possible. There were two scenarios considered while performing the trial tests investigating the influence of the temperature on the readings. The first one allowed exposure of the entire measuring system to sunlight, and the temperature in the laboratory room was not anyhow controlled. However, for the second scenario, the air conditioning (AC) was set at maintaining constant room temperature during the entire test, and the system was protected from the sunlight influence. The main reason for performing the trial tests investigating the influence of the laboratory room temperature on pressure/volume change readings for unsaturated triaxal tests, were the fluctuations observed at the shearing stage of CU reference triaxial tests.

The example of plots presenting the unexpected backpressure records are provided on Figure 8.5. In the past there were number of researches performed on the influence of the temperature on the pore water pressures changes in soil, but there is a little knowledge of how precise and sensitive are the reading of devices used for such tests. The first research raising an awareness of the temperature influencing the pressure record for particular type of transducers were presented by Hall, et al. (1967). They proved the importance of having stable temperature conditions while performing the measurements, by obtaining sinusoidal fluctuations of the records. Sadrekarimi, 2016 also presented more recent investigations. The character of the consolidated undrained triaxial test is that the backpressure during the shearing stage is disconnected from the cell, so the pressure should stay constant.

a)
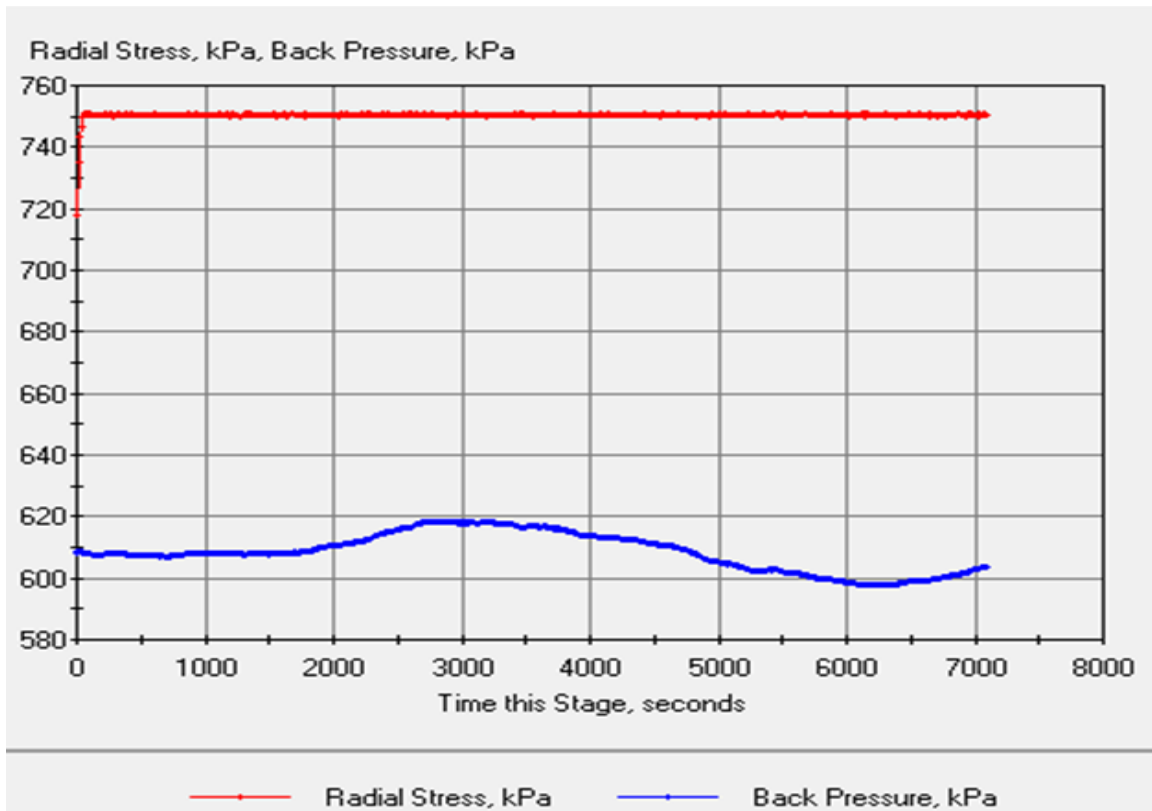
b)
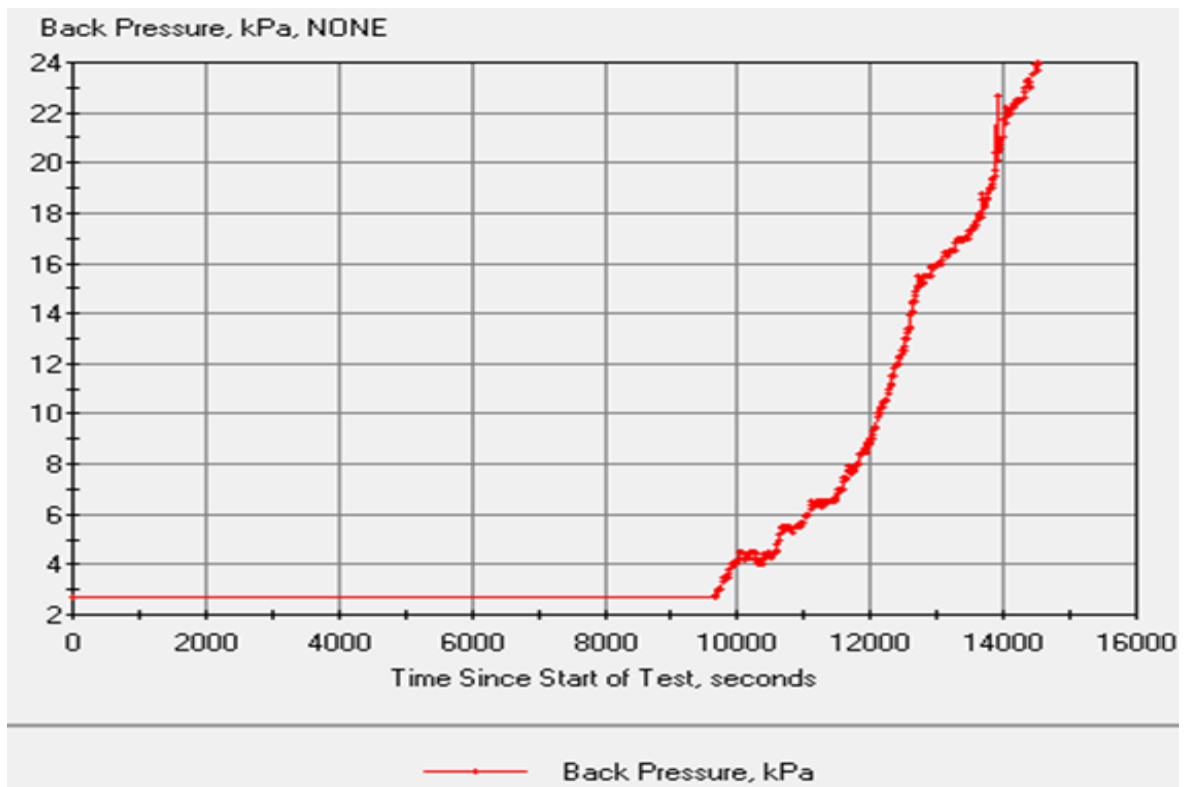
Figure 8.5 Fluctuations: (a) back pressure and steady radial stress (b) CU test at shearing stage.

Bearing in mind that the accuracy of the back pressure controller is more that 0.1% (what gives 2 kPa), the fluctuations shown on the graphs exceed 20kPa. That is 10 times the acceptable level, provided by the manufacturer. For the standard triaxial tests for high effective stress, this magnitude of error could be in some cases neglected. However, speaking of unsaturated soil, there is an air pressure/volume controller connected to the system, and both water and air pressure are used to maintained and control the suction. The Figure 8.6 presents the respond of the back pressure controller and 2MPa pore pressure transducer, connected to the cell fully filled with water and left over two days, in temperature uncontrolled room.

a)
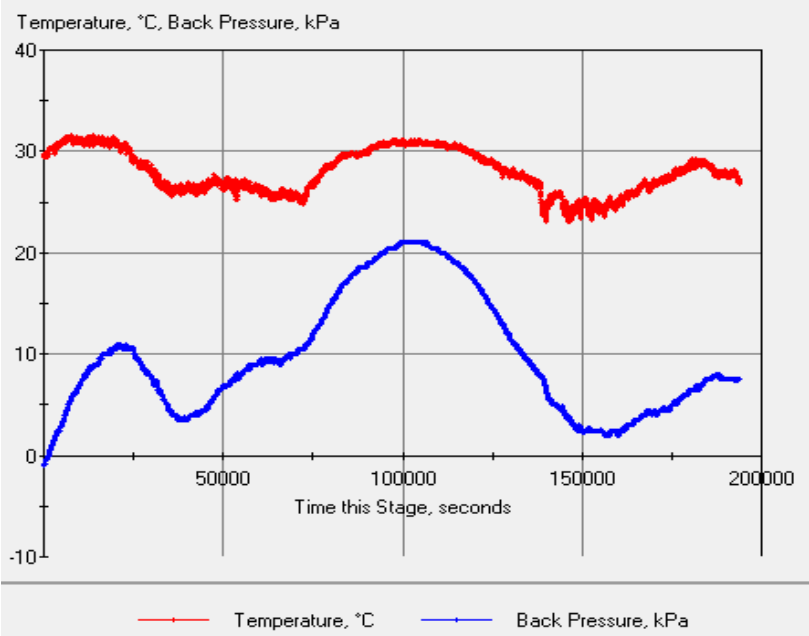
b)
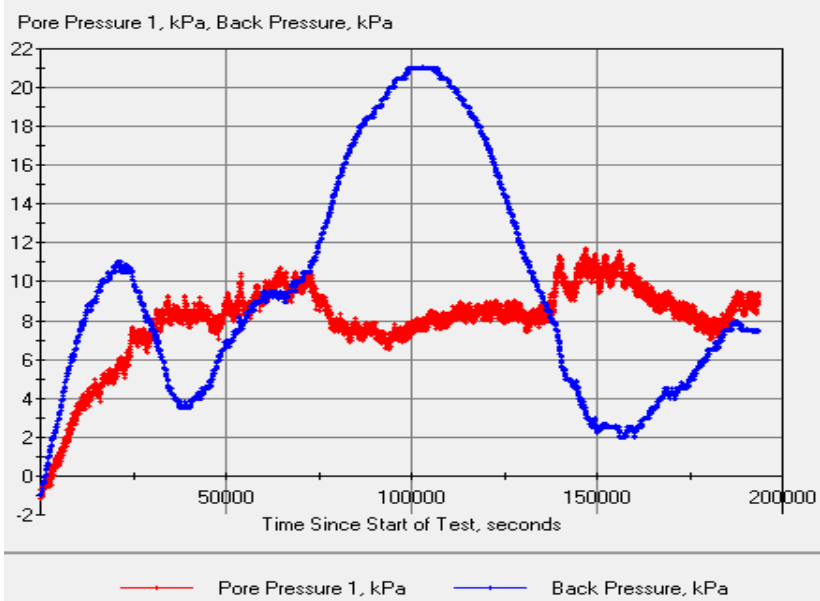
Figure 8.6 Fluctuations: (a) temperature and the back pressure increase (b) pore and back pressure.

Form the Figure 8.6a, it is clear that the backpressure readings are highly dependent on the temperature fluctuations. The following graph (Figure 8.6b), revealed that the pore pressure transducer is less sensitive to the temperature changes and seems to be rather stable (falls in an error range). The second set of tests presented on Figure 8.7, was performed using 3 MPa transducer, when the cell was partially filled with water, and sensors were submerged is shallow water. For these tests, the AC in the room was off, so the temperature was not controlled at all.

From the Figure 8.7 it could be seen that the change of the room temperature ranging from 22 to 30 °C (night and day time) significantly affects the pore pressure transducer records. According the manufacturer specifications the error of 3 MPa transducer should not exceed 4.5 kPa difference, but in fact it reaches almost 20 kPa starting from 0 kPa.

The final step of the tests was to investigate whether the fully controlled laboratory room temperature will result in more stable readings. For this purpose, the air condition was set to maintain the constant value (the room was isolated from air circulation). The results are presented on Figure 8.8. Plots indicate significant improvement of the readings, and the pressure records for controllers and transducer, fall in the acceptable error range, not exceeding 6 kPa in total. The experiment proves the importance of having the laboratory conditions fully controlled and monitored.

Thus, to conclude the triaxial shear test, commonly used in geotechnical engineering practice is crucial for determination of mechanical parameters of soil. This type of test is complex and consists of number of sensors that gives the readings, so the further calculations of shear strength can be performed.
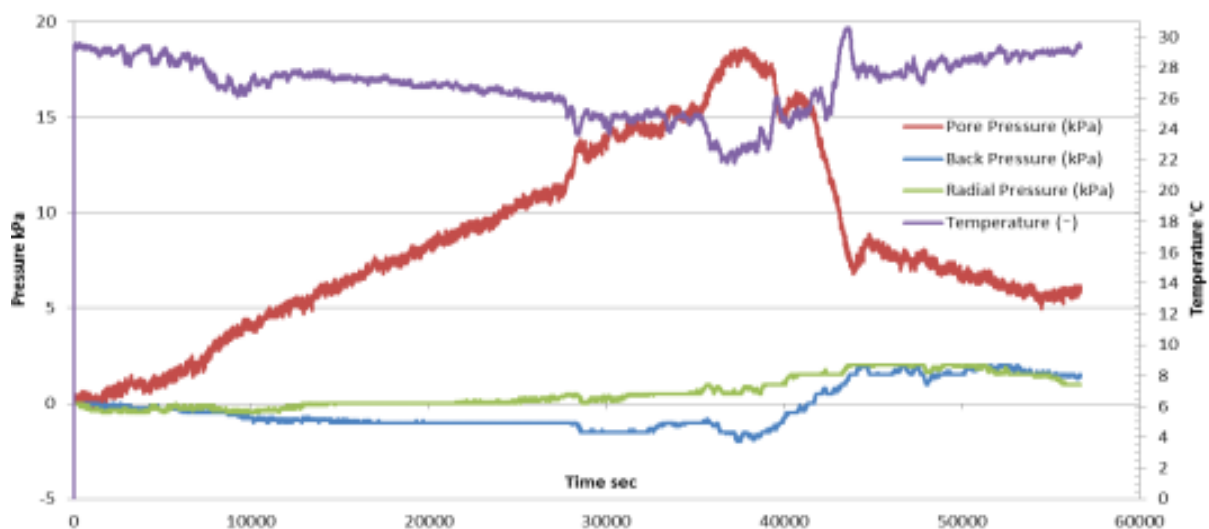
Figure 8.7 Relationship between the temperature and the back, radial and pore water pressure transducer readings, for uncontrolled room temperature.
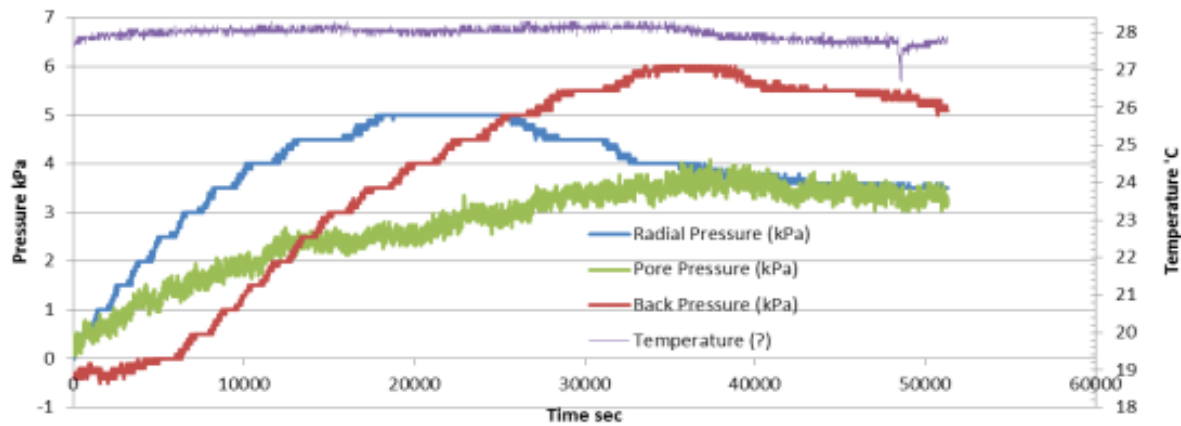
Figure 8.8 – Relationship between the temperature and the back, radial and pore water pressure transducer readings, at the constant laboratory room temperature.

When it comes to unsaturated soil mechanics, the triaxial rig needs to be additionally equipped with devices providing records, much more sensitive to the external sources of any potential disruption. This is why those tests need to be performed in perfectly stable laboratory environment. The present study was aiming at investigating how important for the precise measurement of parameters used for soil mechanical parameters determination, is the temperature and its changes during the testing. After performing a number of trail tests in temperature controlled room it was revealed that such change as of 7 °C, during 2 days lasting test, could cause obtaining the errors of pressure and volume readings exceeding the manufacturer's declared values by as much as 10 times. Such biased records in case of unsaturated soil mechanics, where highly compressible medium as air is considered, are not acceptable. Thus, before performing such sophisticated geotechnical test a laboratory researcher needs to make sure that the surrounding environment is stable and fully controlled at each stage of the test.

8.5. Experimental characterisation of shear behaviour of fine sand

8.5.1. Introduction

The present chapter aims at investigation of the mechanical behaviour of the granular materials both in saturated and unsaturated conditions. Investigating the unsaturated mechanical behaviour of granular soil using a suction-controlled triaxial device was one of the main goals of this research accomplished within a frame of Mumolade project at Unoversity of Nottingham. Thus, the experimental program was created to investigate the volumetric behaviour, shear strength, and stress-strain of compacted fine sand samples at various matric suction and net normal stress values. The axis translation approach was used

114

to manage the matric suction using Bishop-Wesley triaxial rig. Conventional triaxial compression tests were also performed on fully saturated and oven dry samples of the compacted test materials in order to determine the saturated and dry material behavior. The findings are used to numerically investigate the experimental slope filled with tested material and analyse the factor of safety results depending on assumed weather scenarios.

In total, 11 of the tests were completed successfully during the investigation. Prior to being sheared to around 21% axial strain in all tests, materials were isotropically compressed to various net normal stresses (or effective confining stress for saturated and dry testing). Three net normal stresses in total: 100, 150, and 200 kPa were considered. As a result, the data have been divided into three (3) categories based on the sample's compression to net normal stress. Out of the tests, one (1) tested saturated material and oven-dry material. Because of the high permeability of the test materials, both the saturated and dry tests were sheared drained with regard to pore air and pore water after isotropic compression. At matric suction values of 10, 50, and 100 kPa, the suction-controlled tests were carried out. These conclusions were drawn from the material's water retention properties, taking into account the likelihood of significant wetness in practical applications. As a result, the impact of suction on the material's isotropic compression and shear behaviour could be quantitatively evaluated in relation to the applied net normal stress level. All the test and their specifications are listed in Table 8.2. Tests are categorised based on the imposed net normal stress.

Table 8.2 Triaxial compression tests conditions.

Test no	e_0 (-)	w_0 (%)	S_{r0} (%)	$\sigma_3 - u_a$ (kPa)	$u_a - u_w$ (kPa)	Remarks
S1	0.55	0	0	100	-	T01-Dry test, T02-saturated test performed in conventional rig
S2					0	
S3		7	37	100	10	Unsaturated test; Bishop-Wesley cell with axis translation method was used
S4		2	6		50	
S5		7	37		100	
S6					50	
S7					50	
S8				150	10	
S9					50	
S10					100	
S11				200	50	
					100	

8.5.2. Isotropic compression behaviour

The tests were conducted to examine the behaviour of compacted fine sand during isotropic compression at various matric suctions. Samples from four experiments (S3, S5, S6, and S7) were prepared with the identical initial water content of 7% and compressed to the maximum net normal stress of 100 kPa at various forced matric suctions. A second test (S4) with a 2% water content was created to fall under this category of net normal stress. The maximum net normal stress of 150 kPa and 200 kPa, respectively, were applied to the remaining 3 tests (S8, S9, S10, and S11). Two tests were carried out in order to have a reference: test S2 was carried out using the well-known conventional triaxial compression test protocol, and test S1 was carried out on the dry sand.

It should be mentioned, though, that due to the labour-intensive nature of the later two tests of granular material samples (S1 and S2), the volumetric response of the samples was not recorded. Consequently, while calculating deviator stress, the original area was employed. To impose the desired matric suction the pore air pressure (u_a) and the pore water pressure (u_w) were simultaneously raised and then maintained at 20 kPa, in all suction controlled tests. The process of applying matric suction to the sample was carried out at a net normal stress of 20 kPa, which is equivalent to the confining stress used when back pressure in the traditional saturated triaxial tests on granular soils was applied (e.g. Head, 1986). This was achieved by increasing cell pressure, in proportion to the pore pressures. Volumetric strains were negligible since, at this point in the testing, the net normal stress was roughly comparable to the vacuum utilised to prepare the sample. After the matric suction of interest was induced, the sample was immediately examined for equilibrium in terms of both water content and volume change, and the net normal stress was increased to the desired value. Note that matric suction values of 10 kPa, 50 kPa, and 100 kPa were taken into consideration in the present analyses. Figure 8.9a illustrates how the applied pore pressures, or more accurately, the imposed matric suction and the applied net normal stress, caused the degree of saturation to begin to decrease. The degree of saturation decreased in test S5 from the as-compacted value of 37% to 7% at equilibrium, as seen in the figure 8.9. This reduction in saturation corresponded to a change in water content from 8.2% to 1.5%. But as soon as the load was applied, the degree of saturation tended to rise initially as a result of the sample volume being reduced without a corresponding drop in water content. The sample's matching volumetric response is displayed in Fig. 8.9b.

Depending on the applied suction, it took the sample anywhere from 8 to 14 days to reach equilibrium. Similar to axis translation testing, equilibrium was defined as the sample water content changing by no more than 0.2% over the course of a day. Samples with higher water content, smaller particle size, and lower suction values took longer to reach equilibrium. Sand samples with an initial 7% water content typically required 8 days for 100kPa suction, 11 days for 50kPa suction, and roughly 14 days for 10kPa. When the water content was reduced from 7% to 2%, the sample's equilibrium time at 50 kPa suction was reduced from 14 days to roughly 7 days.
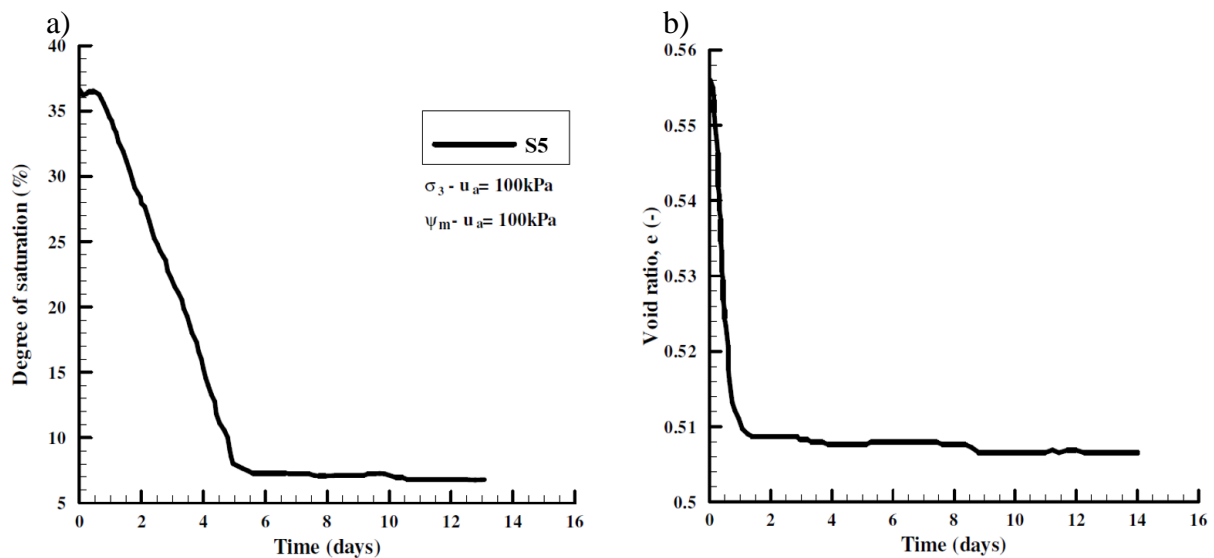
Figure 8.9 Equilibration time scale: a) for degree of saturation value, b) for void ratio.

Due to the fact that samples with varying suctions and initial water contents took variable amounts of time to reach equilibrium, a single equalisation time of 13 days was chosen.

As a result, any time-dependent impacts were minimised, and each sample was given enough time to follow the soil water retention curve (SWRC) on its own unique drying path. The examined sand samples was demonstrated to have a distinct drying path in the previous chapters, which allowed any wetter sample to swiftly follow its typical path after drying. Fig. 8.9 makes it clear that volumetric equilibrium was permitted and preceded the moisture equilibrium in every test at the end of the isotropic compression step. Its features have frequently been used in conjunction with the saturated parameters in the estimation of the more expensive unsaturated properties, such as transient flow (e.g. Barbour, 1998), permeability (e.g. Fredlund et al., 1994), and shear strength (e.g. Fredlund et al., 1996), to name a few. This is because measuring water retention is less demanding in terms of time and resources than directly measuring other unsaturated properties. One significant drawback to this method of

estimating other unsaturated properties from the features of the water retention curve and saturation parameters is that accurate estimations can only be achieved when the retention curve is applied under the same conditions that were used to measure it. This means that the sample condition needs to be tested for homogeneity before this sequence can be implemented.

The SWRC for sand samples is shown in Fig. 8.10. Using the triaxial cell and the axis translation approach, the test on wetting and drying paths was carried out. The triaxial samples were prepared with the same initial void ratio as the pressure plate samples, but as will be seen from the volumetric behaviour shown in the following paragraphs, their void ratio at equilibrium (and at peak deviator stress) was somewhat lower. Therefore, as shown in Fig. 8.10, it is widely accepted that the SWRCs can be used to constitutively estimate various unsaturated properties (Rassam & Cook, 2002).

Typically, scientists and engineers are aware of the expected volumetric response to an applied load of either dry or saturated cohesionless granular material. Due to its high permeability, air and/or water are virtually instantaneously released as the load is applied, indicating immediate compression and/or consolidation. Because of the limited permeability in clayey soils, these processes can take a long time. However, the presence of matric suction tends to complicate matters when it comes to unsaturated material. To the best of the author's knowledge, there is no information accessible on cohesionless granular materials, despite the fact that there is a wealth of experimental work on clayey soils in the literature. Thus, additional experimental data is still needed to address the topic of whether suction might have an impact on the volumetric behaviour of granular materials. For the tested fine sand, this is provided in the present section.

Fig. 8.11 shows the variations in the sample's total volumetric strain during isotropic compression at various net normal stresses and matric suction points. The samples' volume decreased after the net normal stress was applied, and the volume reduction increased with the applied confinement. Conversely, the findings seem to suggest that matric suction will not significantly affect the variations in volume of non-cohesive granular materials as a result of applied stress, if equilibrium is permitted. Bearing in mind that the temperature changes were kept at low level, usually within $\pm 1\,^{\circ}\text{C}$, the effect of temperature on the observations was minimized (potential temperature impact is discussed in details in previous chapter).

The results of the isotropic compression experiments at various matric suctions were further evaluated using the net normal stress and void ratio zone in order to determine the normal compression lines, if any. The outcomes are displayed in Figure 8.11b.

Overall, the findings indicate that the sample void ratio decreased as the net normal stress increased, and a normal compression line can be seen in the data scatter. Nevertheless, comparing the test results based on the imposed suction does not provide sufficient proof that the normal compression lines depend on the suction. Even though it will be demonstrated later that it had no effect on the shear behaviour, it is unclear whether the test on S4 sample's initial water content difference is to blame for its excessive outlying with respect to all other data points of its group despite the fact that distinct normal compression lines can be identified for each matric suction.

Worth noting is that S4 sample had an initial water content of 2%, compared to 7% for all the other test samples. The scope of the thesis did not allow to explain why the line for matric suction of 100kPa lies between the lines for 10kPa and 50kPa, even if it was claimed that the S4 results should be disregarded based on comparisons over a small range of void ratio and net normal stress. The findings in Fig. 8.11b further demonstrate that the tested sand samples do not exhibit the yield stress that is frequently seen in unsaturated clayey soils.

Whether this is due to the yield stress not existing in granular materials or the stresses taken into consideration in this study being significantly higher than the material's yield stress is not immediately apparent. To reach a conclusion, more experimental work in the lower range of net normal stress is required. There isn't any experimental data in the literature to support the existence or nonexistence of yield stress.
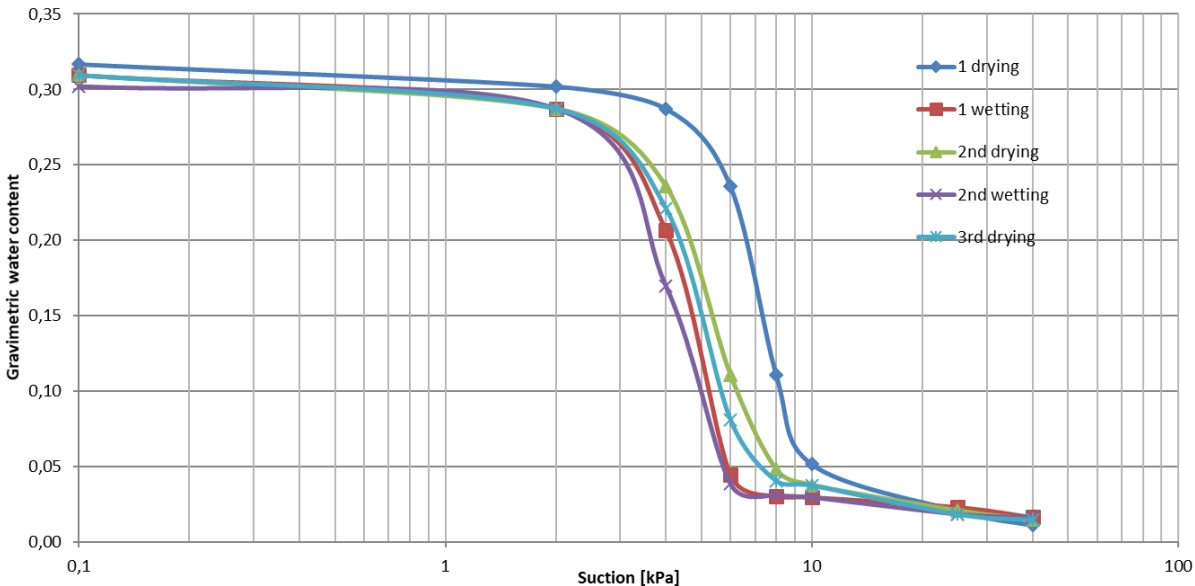
Figure 8.10 SWRC determination using multiplied cycles approach the triaxial cell applying axis translation method.
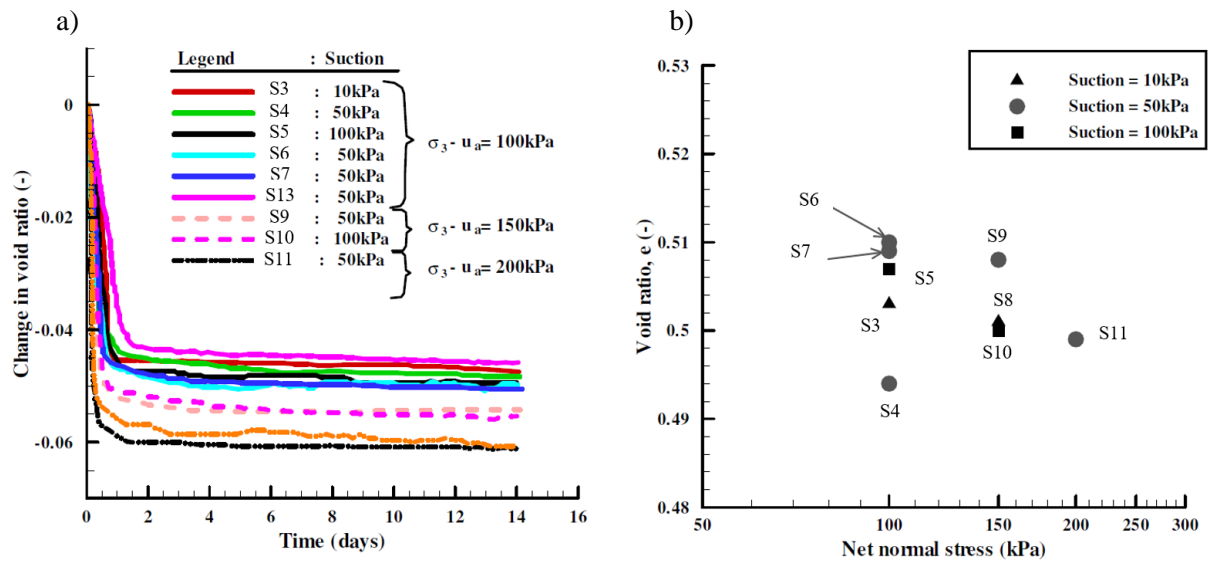
Figure 8.11 Volumetric behaviour at isotropic compression: a) void ratio based, b) net normal stress-void ratio based.

8.5.3. Shear behaviour

In order to evaluate their impact on the shear behaviour of the tested fine sand, samples were sheared at constant matric suction and net normal stress after isotropic compression in all the triaxial tests that were previously given and addressed in this section.

Using a global potentiometric displacement transducer, shearing was applied to an axial strain of roughly 21%. Figure 8.12a shows the stress-strain response of the tested fine sand in a q-ε_a zone, while Figure 8.12b displays the comparable volumetric response in a ε_v-ε_a zone. The graphic makes it quite clear that the tested fine sand's stiffness and peak deviator stress increased as a result of the matric suction action. In terms of volumetric change, the samples usually dilated into a barrel shape at the end of the test after first experiencing a minor constriction. Given that the stress-strain equations at different matric suctions tended to begin converging towards a common point, the effect of suction on the shear behaviour seemed to start diminishing beyond the axial strain of roughly 10%.

The failure mode was discovered to have an impact on the actual behaviour, even if this type of behaviour can be attributed to the dilation-induced disruption of water menisci. As a result, the measured shear quantifiers were impacted, and it was deemed inappropriate to investigate the essential state parameters. Numerous earlier researches have documented that the mechanical behaviour of particulate materials depends on various factors, including the circumstances of the sample and each test step.
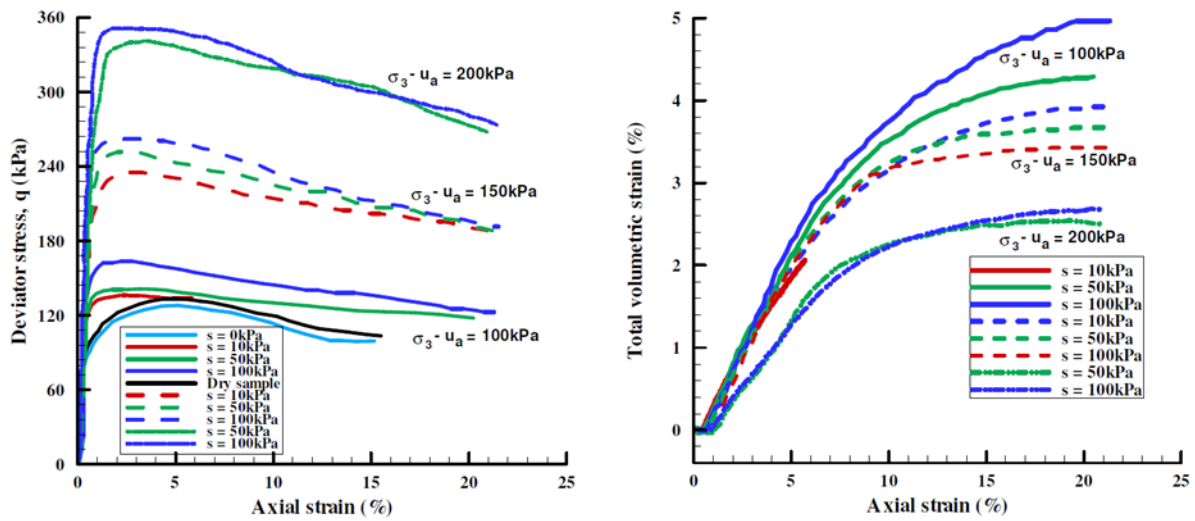
Figure 8.12 Suction controlled compression tests at the shearing stage a) q- ε_a at various suction   b) ε_v- ε_a at various suctions.

The quantity of water lenses or the wetted surface of the solid phase in the form of a degree of saturation or some function of a degree of saturation and modified suction to account for the sample's porosity are two examples of such conditions. In light of this, the sample's water content, saturation degree, and as-prepared and after isotropic compression void ratio were all recorded at different points during the test, as indicated in Table 8.3.

The table also includes the measured shear strength, the applied net normal stress, the imposed matric suction, and the axial strain that corresponds to the peak deviator stress. Additionally, samples with higher degrees of saturation tended to show stronger volumetric stability, as shown in Fig. 8.12b. To understand the impact of matric suction and net normal stress on shear strength, the findings are shown in Table 8.3 and in Figures 8.13a and 8.13b, respectively.

The results show that the material's shear strength inclined along with a rise in matric suction, as seen in Fig. 8.13a. The rise was nonlinear in that as suction increases, it seems that the rate at which shear strength build-up would slow down. In fact, it seems that the shear strength would eventually reach a maximum if suction was increased any further. In light of this reasoning, it is anticipated that as matric suction increases, the angle of friction should also decrease. It was discovered that there was just a slight variation in φ^b, or less than 1.0 degree. This implies that φ might reach a minimal value within the residual zone. Conversely, Fig. 8.13b demonstrates that the shear strength increased linearly with a rise in net normal stress. It was discovered that the angle of friction, which was independent of the matric suction that was applied, was 26° with regard to the net normal stress.

Table 8.3 Triaxial test results for fine sand at different stages.

Test no	Net normal stress $\sigma_3 - u_a$ (kPa)	Imposed Matric suction ψ_m (kPa)	Initial void ratio e_0 (-)	Initial degree of saturation S_{r0} (%)	Void ratio after isotropic compression e_{ic} (-)	Degree of saturation after isotropic compression S_{ric} (%)	Void ratio at peak deviator stress e_{peak} (-)	Degree of saturation at peak deviator stress S_{rpeak} (%)	Shear strength $\tau = q/2$ (kPa)	Axial strain at peak deviator stress (%)
1	100	-	0.55	0	0	0	0	0	67.2	4.2
2		0	0.55	0	-	100	-	100	63.9	4.1
3		10	0.54	36.12	0.50	15.57	0.54	14.50	68.1	2.1
4		50	0.55	9.31	0.48	5.62	0.54	5.25	72.0	1.4
5	100	100	0.55	35.89	0.51	6.82	0.56	6.20	80.1	1.1
6		50	0.55	35.89	0.50	6.91	0.56	6.33	69.8	1.1
7		50	0.54	35.89	0.50	7.41	0.56	6.81	72.0	1.4
8		10	0.55	36.98	0.51	11.00	0.53	10.48	120	2.4
9	150	50	0.54	36.01	0.51	7.55	0.54	7.00	124.5	2.1
10		100	0.56	36.29	0.49	7.21	0.55	6.52	130.5	1.3
11	200	50	0.56	36.02	0.50	7.32	0.56	6.68	171	3.1
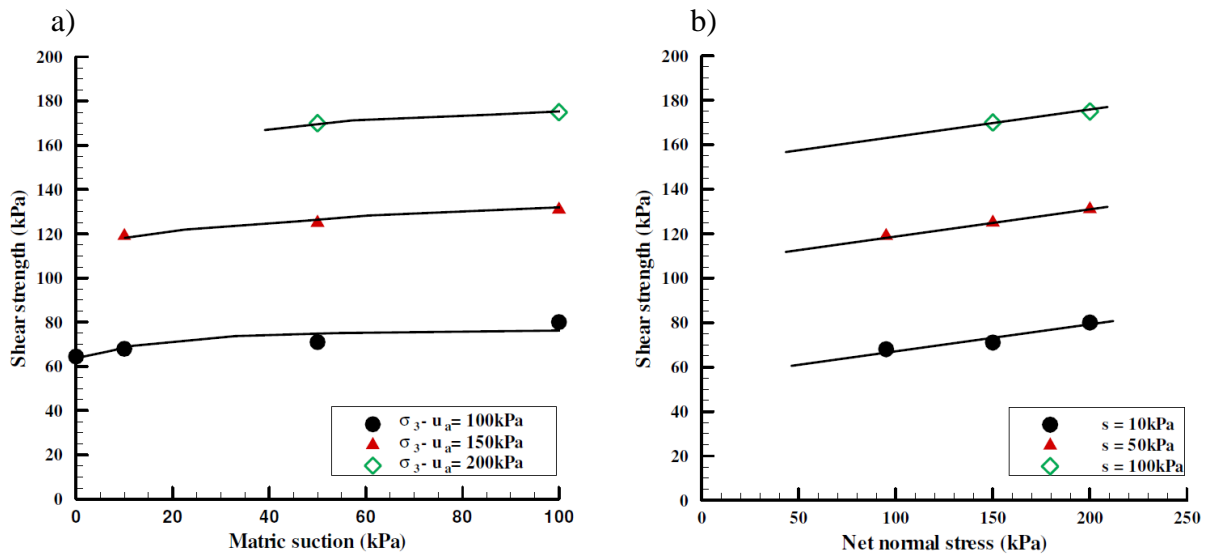
Figure 8.13 Results of variation in shear strength with: a) matric suction and b) net normal stress.

The extra inter-particle bonding force introduced through the liquid bridges maintained by the matric suction in the sample can account for the observed increases in stiffness and peak deviator stress, as well as the increases in shear strength and volumetric stability, with an increase in matric suction of the tested fine sand.

In contrast to these and numerous other investigations, the current study's findings indicate that the observed behaviour may be solely attributed to inter-particle bonding caused by the liquid bridging.

8.5.4. Initial water content effect on the shear behaviour in unsaturated conditions

Cohesive and noncohesive materials' mechanical behaviour is claimed to be greatly influenced by their structure. For example, aggregates of individual particles can form in clayey soils, leading to the formation of aggregated structures with inter-aggregate porosities.

Therefore, clayey soils may appear with varying mechanical behaviour depending on the degree of aggregation and the moisture condition. However, aggregation is not a major feature of soils that are primarily sandy. Rather, disparities in the orientation of the particles within the samples are attributed to distinct structures. Studies have indicated that the mechanical response of noncohesive granular materials might vary depending on the technique and water content employed to manufacture the samples (e.g. Yumamuro & Wood, 2004; Yumamuro et al., 2008). The question of whether inert spherical granular materials exhibit such a difference in behaviour remains unclear. This study looked into the matter, and the results are discussed in the present paragraph. Tests were performed on samples of fine sand compacted at varying water contents to evaluate the impact of structure, in terms of initial water content or degree of saturation, on the shear behaviour of cohesionless granular materials.

A comparison of the test S4 sample (made with 2% water content) and test S7 sample (of 7% water content) is shown in Fig. 8.14. The striking similarity of the data suggests that the sample structure caused by the initial water content had no impact on the tested sand's mechanical response. It follows that particle shape and/or other characteristics, rather than moisture-induced structure, are actually responsible for the behaviour differences that are frequently attributed to the initial water content in sands.
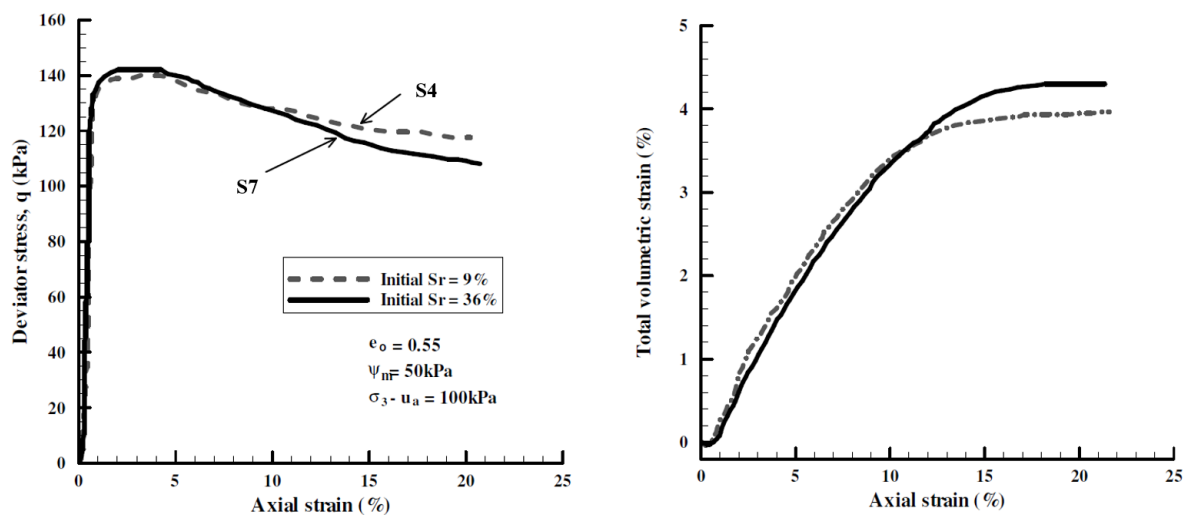
Figure 8.14 Result of shear behaviour of samples prepared with different water content.

8.6. Conclusions

The goal of the current study was to gain a better knowledge of how granular materials behave hydromechanically. Fine sand samples were subjected to triaxial unsrurated laboratory testing. Investigations were conducted into soil water retention and shear behaviour with a focus on how the bulk hydro-mechanical behaviour is affected by the particle-suction interaction via and how this influences the characteristics of soil. Both the tensiometer and axis translation methods were used to measure the water retention curves.

Conversely, the shear behaviour was examined through the use of both traditional and sophisticated unsaturated triaxial apparatuses with suction controlled by the axis translation technique. The following section outlines the main findings of the study in relation to the two main areas of investigation: shear and water retention behaviour. The major findings are that the shear strength rises with matric suction in a nonlinear fashion. The tested sand's shear strength rose at a decreasing pace with a propensity to attain a maximum value as matric suction was increased. This result shows that the observed rise in shear strength within the residual zone cannot be explained by matric suction alone. With a given net normal stress, shear strength grows linearly. Shear strength was observed to grow proportionately regardless of the imposed matric suction after an increase in the applied net normal stress, indicating that the internal angle of friction depends on suction. The shear behaviour of granular materials that are not cohesive is unaffected by the structure created by water flow. The tested sand's shear behaviour was unaffected by the preparation of samples with varying water contents, indicating that variables other than the structure created by the water bridge are in charge of the variance in shear behaviour that is frequently noted in soil samples prepared with varying water contents.

9. Numerical modelling of an experimental slope

9.1. Introduction

Rainfall is recognised as one of the most frequent triggers for slope failures. Rainfall infiltration causes a rise in pore-water pressure (or a decrease in matric suctions) within the slope, which has an impact on slope stability (Brand, 1981). The application of seepage analyses using rainfall as a surface boundary condition is crucial to evaluating this fluctuation

in pore-water pressure. The finite element approach (numerical modelling) can be used to analyse the seepage conditions of a tropical residual soils slope. Using this approach allows for the modelling of the rainwater infiltration process as well as the impact of soil parameters on variations in the water flow within the slope. Based on the findings of a seepage investigation, the slope's stability can subsequently be examined. It is imperative that soil properties, rather than just climate data, be taken into account when determining the stability evaluation for an unsaturated soil slope.

Thus, this chapter presents the numerical modelling of slope stability analysis by coupling the equations for the flow (hydrological) and deformation (mechanical) assessments. The analyses were carried out for two soils slopes; the first one filled with cohesive soil, namely sandy clay investigated in previously describe laboratory test in Chapter 7, and the slope filled with granular material analysed in chapter 8. It is usually reported that high precipitation, particularly heavy rainfalls, is the cause of slope failures. These events were noted to happen on both naturally occurring and artificially constructed slopes, with the latter showing a higher failure frequency (Liew, 2004). According to the majority of reports, the slopes held steady for a considerable amount of time before failing, either during or after protracted, intense downpours (Brand, 1984, Toll, 2001).

According to earlier research (Krahn et al., 1989, Day and Axten, 1989, Toll, 2001,), soil slope failures are often occure on shallow depth. This is because variations in pore water pressure are only caused by precipitation infiltration to a limited extent, close to the ground surface. This effect (caused by a wetting front moving forward) is typical; however, if the infiltrations are allowed to remain in a wet climate for an extended length of time, they will eventually move deeper and result in deep-seated instability (Macari et al., 1992, Fourie, 1996, Gasmo et al., 1999, Deutcher et al., 2000, Low et al., 2000, Dykes and Thornes, 2000). Moreover, exposure to specific rainfall patterns might result in a significant amount of slope failures in circumstances where the soil slopes have very permeable soil properties. In tropical climate locations, slope failures caused by rainfall are more frequent and occur more frequently, particularly during the monsoon seasons (Huat et al., 2012). Not only have some of these terrible events caused significant property damage, but they have also claimed lives. It is evident from the results reported in the literature that is under discussion that extended periods of strong or continuous rainfall, which are thought to be associated with climate change, are a major contributing factor to the occurrence of large slope collapse occurrences.

The significance of risk assessment in engineering design and the application of thorough numerical investigations to estimate and avert any kind of catastrophe to the finished works were also brought to light by those studies. This conclusion was proven based on the recorded rainfall data spanning over the period from before the incident till the end of the investigation. In addition, the needs of more research works and practical design approaches for slope design were also suggested in order to mitigate the risk of failure as minimal as possible. The forensic investigation consisted of detailed topography survey, subsurface investigation, laboratory testing, instrumentation scheme for slip surface detection, groundwater regime establishment and back-analyses using finite element method. Despite the many uncertainties in identifying and establishing the weak structure, subsoil variation and adverse groundwater level due to the natural heterogeneity of tropical residual soils, it was concluded that the major cause to slope failures are mainly related to prolonged and heavy rainfall. The geotechnical literature contains a wealth of research demonstrating the statistical relationship between rainfall and the slope stability of residual soils. Brand (1984) proposed that rainfall intensities of 70 mm/h and above can be utilised as a good indicator of the ability to trigger slope failures for residual soil slopes in Hong Kong. Premchitt et al. (1994) later demonstrated this empirical correlation by looking at a 20-year assessment of slope failures that happened in Hong Kong.

The impacts of antecedent rainfall, or the rainfall in the days preceding the occurrence, have also been documented to have a significant role in slope collapse (Rahardjo et al., 1998, Toll, 2001, Rahardjo et al., 2001). This factor, which is also known as the first state before the major rainfall event, basically helps to raise the moisture content of the slope, which in turn leads to the final precipitation event that triggers a failure. However, Brand (1984) has shown that, for slope failure instances in Hong Kong, the total 24-hour rainfall intensities and the peak hour rainfall typically determine the regulating parameters for rainfall-induced slope failures. As a result, it appears that the contribution of earlier rainfall was not as great. This is probably because many of the soils in Hong Kong are porous. Toll (2001) conducted an empirical study aimed at providing additional insight into the impact of rainfall on the slope stability of tropical residual soil slopes in South East Asia. Based on observations of previous small and severe slope collapses that happened in Singapore and were recorded by multiple researchers (Chatterjea, 1989, Wei et al., 1991, Li, 1995, Tan et al., 1988, Pitts, 1985, Yang and Tang, 1997), correlation was established in his study. The 5-day and 15-day quantified rainfall antecedent periods were compared to the data. For the latter, see Figure 9.1.
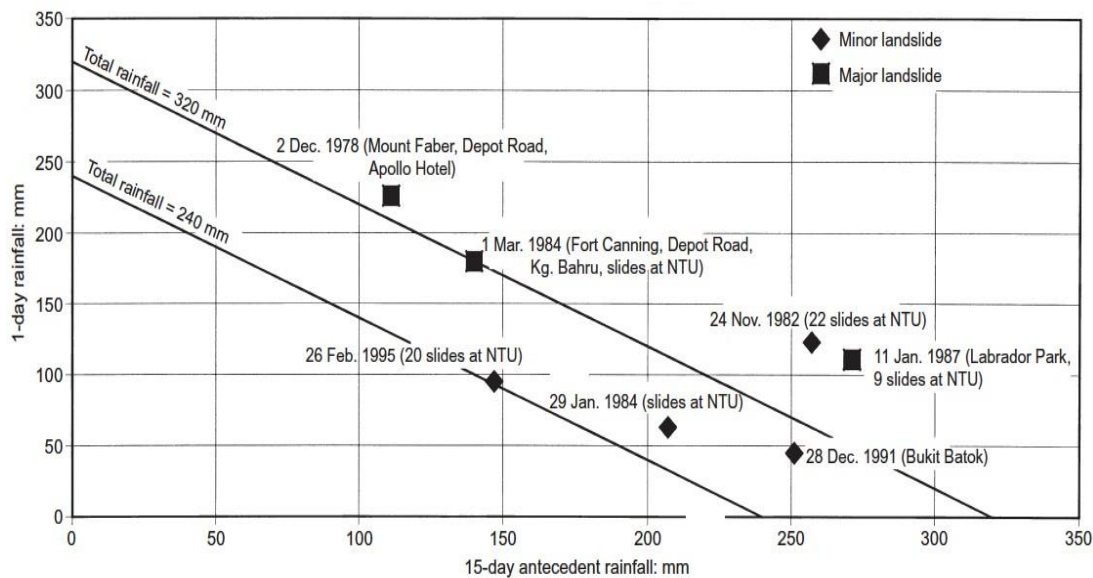
Figure 9.1 15-day antecedent rainfall for landslides in Singapore (after Toll, 2001).

Based on the plots, the author hypothesised that minor slope failures can be caused by a 100 mm total rainfall over the course of six days. Based on the results of the plots that show the occurrences of failures according to the daily and antecedent rainfall circumstances, the slope failures by total rainfall is indicated. Significant slope collapses could happen following a 24-hour rainfall of more than 110 mm, it was also mentioned.

The conditions for significant landslides are also stated in his study. however, the results were justified as being less certain because there was insufficient data available for rainfall that occurred 15 days in advance. However, it is thought that a line for 320 mm of total rainfall is crucial to serve as a lower bound for each significant case.

9.2. Numerical modelling of unsaturated soil slopes

9.2.1. Introduction

Because the finite element approach can represent the infiltration mechanism within slopes, its use for numerical modelling for slope assessments has gained importance (Tsaparas, 2002). This method allows for a good definition of the influence of soil parameters on variations of water flow within the slope. Its importance becomes even more apparent in situations with complicated slope issues that are outside the scope of standard methods. According to Md. Rahim and Toll (2014), it is typical for finite element analyses used for stability evaluations to compute the flow (hydrological) and deformation (mechanical) assessments in two distinct analyses. In order to demonstrate the impacts of rainfall infiltration

on pore-water pressure variations and the development of a perched water table, hydrological analyses, also known as seepage analyses, can be conducted under temporary circumstances (Leach and Herbert, 1982). To replicate the slope's real behaviour, various parameters including soil permeability, ground water table, rainfall intensities, and types of plants at the slope's surfaces must be taken into account throughout the studies. Next, the mechanical analyses, or stability assessments, could be carried out using these computed seepage conditions (Rahim, 2016).

9.2.2. Numerical modelling of the hydrological behaviour

Numerous published research detail the use of numerical modelling to investigate the infiltration process and how it affects an unsaturated slope's seepage conditions (Tsaparas, 2002). Hodge and Freeze (1977) were among the first to demonstrate this effect in a study that used a steady state analysis with a finite element model. Later research, however, revealed that seepage conditions within a slope can vary quickly during infiltration; for this reason, transient analysis is seen to be more pertinent (Leach and Herbert, 1982). In compared to the available field data, Leach and Herbert's (1982) early analysis using the finite difference model (FDM) revealed that the numerical model tended to overestimate the head at a given site. Moreover, it was shown that the outputs' magnitude of error decreased with depth. Because of this, it is advised to reduce the mesh diameters close to the ground, where quick variations in head occur. Because the modelling is so challenging, the incorporation of the evaporation and evapotranspiration impacts at the ground surface is frequently left out of analyses (Tsaparas, 2002). Actually, the kind of soil has a major influence on this intricate drying process, which is determined by the water content and negative pore-water pressure (Wilson et al., 1995). In their attempt to simulate evaporation, Gasmo et al. (2000) defined the surface boundary with a negative flux. In contrast to the available field data, it was discovered that the decrease of negative pore-water pressures at the ground surface occurred too quickly. Modelling the impacts of vegetation and surface desiccation is a crucial step in analysing the seepage status of a slope. According to Hodge and Freeze (1977), these effects are significant because they affect the distribution of pore-water pressure that develops close to the ground surface. In the event that grass covers a slope's ground surface, tiny passageways or fissures would form in the soil, producing a permeability value that is noticeably higher than at deeper depths (Anderson et al., 1996). Determining a representative layer close to the

ground surface with a high permeability value is therefore crucial (surface desiccated zone). According to Tsaparas and Toll (2002), field measurements of near surface permeability were two orders of magnitude lower than the values required in numerical models to accurately forecast infiltration rates. They included a 0.25 m thick soil layer that was defined at the ground's surface in their computer model assessments to account for this situation. In order to simulate seepage behaviour within a slope, researchers have also looked into the impact of the soil-water retention curve hysteresis. Vargas et al. (1990) have drawn attention to the challenges associated with simulating this criterion since soil water retention curves change from wet to dry at the conclusion of a rainfall event. Theoretically, the wetting process might still be going on at deeper depths, which could lead to numerical instability in the analyses. Because of this, in their numerical evaluations, the authors only used the wetting soil water retention curve. Tsaparas (2002) has found a similar problem resulting from attempts to include the draining mechanism in seepage calculations. The goal was to forecast a pore-water pressure drop that would be reasonable and consistent with field data during dry spells. Consequently, the adoption of the drying phase of the soil water characteristic curve was limited to times when the dry spell lasted more than twelve hours.

9.2.3. Numerical modeling of the mechanical behaviour

Slope stability analyses, which examine possible failure processes, are typically linked to the assessment of a slope's mechanical behaviour. This is because the linear elastic-perfectly plastic Mohr Coulomb constitutive model is typically used for slope stability assessment, and only ultimate limit states (failure circumstances) are typically of concern. Because of the loss of negative pore-water pressures brought on by infiltration, which lowers the soil's shear strength below the mobilised shear strength along the potential slip surface, the association between rainfall and slope failures can be explained (Brand, 1981). According to Vargas et al. (1990), a drop in suction would cause the soil's strength to decrease, which would lead to instability and shallow superficial slips. Positive pore-water pressures that have developed at the slope's toe may also be used to identify the instability. The application of unsaturated soil ideas is crucial in order to establish a link between the impact of infiltration and the stability of a tropical residual soil slope. The mobilised shear strength at the base of each slice in an analysis can be found using the conventional limit equilibrium approach with the Extended Mohr Coulomb concept incorporated (Figure 9.2).

$$\tau_m = \frac{b}{FOS}\left[c' + (\sigma - u_a)\tan\varnothing' + (u_a - u_w)\tan\varnothing^b\right]$$

(9.1)
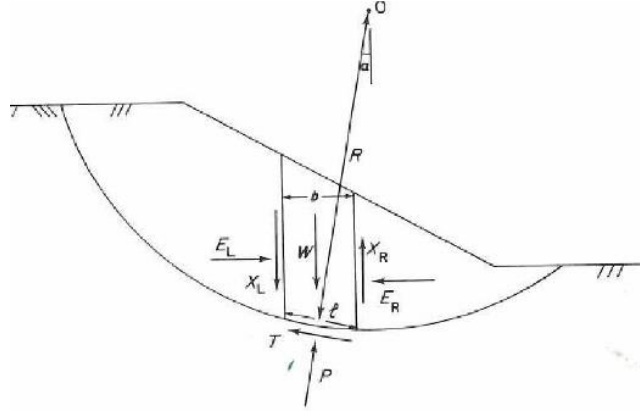
Figure 9.2 Interslice forces applied in limit equilibrium analysis (Tsaparas, 2002).

Barbour et al. (1992) expressed the moment equilibrium factor of safety (FOS)m and force equilibrium factor of safety (FOS)f as the following.

$$(FOS)_m = \frac{\sum\left[c'.b.R + \left(N - u_w.b\frac{\tan\varnothing^b}{\tan\varnothing}\right)R.\tan\varnothing'\right]}{\sum W.x - \sum N.f}$$

(9.2)

$$(FOS)_f = \frac{\sum\left[c'.b.\cos\alpha + \left(N - u_w.b\frac{\tan\varnothing^b}{\tan\varnothing'}\right)\tan\varnothing'\cos\alpha\right]}{\sum N.\sin\alpha}$$

(9.3)

where:
u_a - atmospheric pressure (0 kPa),

W - total weight of each slice,

α - the inclination of the base of the slice,

N - the normal force acting at the base of each slice,

R - the radius of the potential slip surface,

X - the horizontal distance from center of each slice to the center of moments,

f - the offset distance from the force to the center of moments.

Using the finite element method with the shear strength reduction concept (SSR) is another alternate method for calculating a slope's stability. According to Matsui and San (1988), the idea of SSR is to simultaneously reduce φ and c in little steps until a failure mechanism is established. Many finite element codes use this stability evaluation method, which yields the

concurrent reduction factor for the two shear strength parameters and expresses it as the slope's factor of safety in the end. The following is the formulation of deriving the factor of safety (FOS).

$$FOS = \frac{\tan \emptyset}{\tan \emptyset_r} = \frac{c}{c_r}$$

(9.4)

9.2.4. Fully coupled hydro-mechanical slope assessment

Geotechnical engineering practice is very interested in the relationship between the mechanical and hydraulic behaviour in unsaturated soils (Khalili et al., 2008). This is due to the fact that these two elements are really closely related, particularly during penetration. The primary parameters linked to the flux boundary condition at the soil-atmosphere interface are the features of water flow, variations in pore-water pressure, and soil shear strength (Hamdhan and Schweiger, 2011). In their 2011 study, Hamdhan and Schweiger evaluated the impact of rainfall and soil hydraulic properties (hydraulic conductivity and initial degree of saturation) on slope stability calculations performed with the finite element method. In order to complete the investigations, groundwater flow and deformation were simultaneously computed with time-dependent boundary conditions. This calculation is based on the idea presented by Bishop (1961), according to which the hydro-mechanical coupling effects are represented by the "effective" stress in unsaturated soils (Equation 9.1). Oberg and Sallfors (1997) and Vanapalli et al. (1996) proposed that the degree of saturation or the effective degree of saturation can roughly replace the component χ in order to support the idea. The amount of water in a soil's voids, or the degree of saturation, is observed to be closely correlated with the shear strength of unsaturated soils, as indicated by variations in the matric suction, the scientists report. Based on experimental data collected from multiple researchers, Figure 9.4 shows the link between the factor χ and degree of saturation (Vanapalli et al., 1996). To summarise, the integrated evaluations can demonstrate how precipitation affects the distribution of negative pore water pressures, or suction, and hence, slope stability. It may be inferred that a slope's stability declines with infiltration, lowering the slope's Factor of Safety (FOS) as a result (Figure 9.5). When comparing high permeability soil to low permeability soil, the reduction in FOS is considerably more pronounced. One of the major elements influencing the slope's FOS is the variation in soil water retention curves.

9.3. Coupled Hydro-Mechanical Analyses of an experimental slope subjected to rainfall events

9.3.1. Introduction

Numerical simulations using a variety of techniques, including the limit equilibrium method (LEM), the finite element method (FEM), the finite difference method (FDM), the boundary element method (BEM), neural networks, etc., were used to study the failure mechanism of slopes caused by rainwater infiltration. Although LEM is the most generally used method for slope stability analysis because it is simple and feasible, FEM and FDM provide more accurate findings because they handle stress distributions and slope displacement, which LEM does not permit. There are different software available allowing proper analyses of slope stability affected by rainfall. Very useful couple (hydro mechanical) tool could become a combination of SEEP/W and SLOPE/W. The packages of GeoStudio software can be used for seepage and slope stability analysis, respectively.

This is because the program's flexibility with regard to geometry makes it easier to continuously analyse the slope stability from soil in an unsaturated state to a saturated state through a transient rainfall infiltration analysis with a corresponding factor of safety evaluation. Rainfall extremes are shifting over time due to climate change, resulting in extended periods of severe rainfall that necessitate nonstationary approach-based research. These assessments are crucial because they can be used as a foundation for evaluating potentially unstable slopes that are vulnerable to failure as a result of a change in the surface flux boundary condition over time, hence reducing the danger of property damage and human casualties to some degree. As a result, this study takes into account the fluctuating weather extremes by examining the stability of the slope under both current and future scenarios, taking into account the maximum and 95 percentile rainfall intensities for various time periods. Seepage and slope stability are then examined using SEEP/W and SLOPE/W. Therefore, by examining the slope's stability under both present and future scenarios and taking into account the maximum and 95 percentile rainfall intensities, this study takes into account evolving extreme events. Thus the objective here is to analyze transient seepage into soil slopes consisting of different soil material (tested previously in laboratory) due to rainfall infiltration; to examine the stability of the slope in relation to temporary seepage brought on by infiltration of rainfall; to analyses the influence of changing weather events (rainfall) on slope stability.
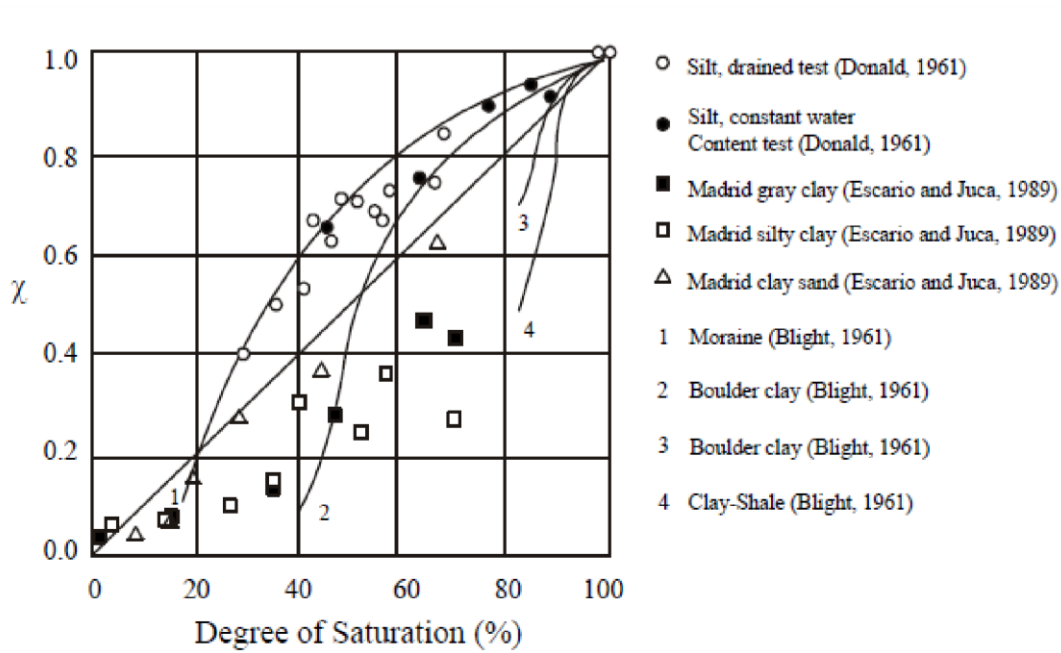
Figure 9.4 χ and Sr relationship (Vanapalli et. al., 1996).
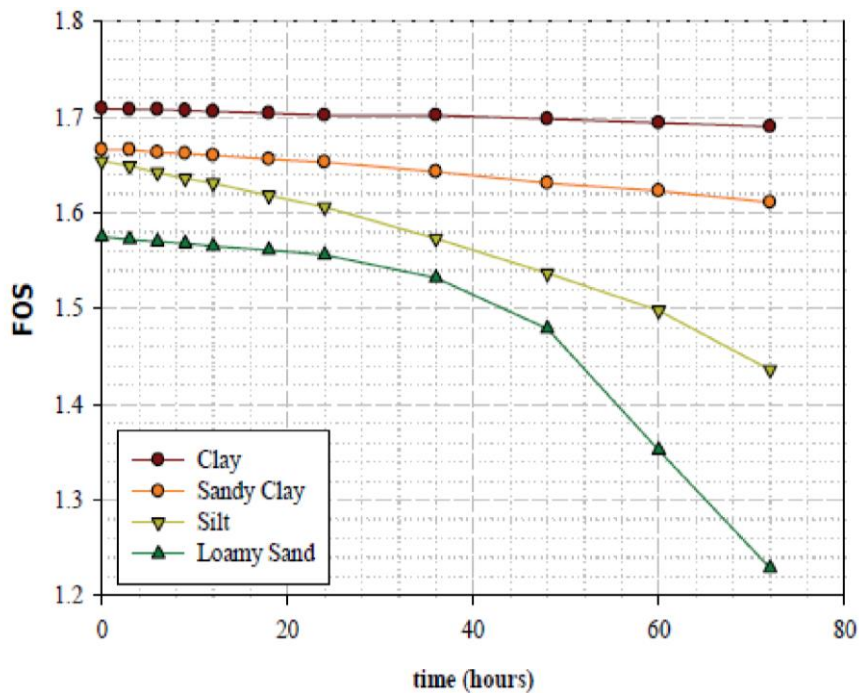
Figure 9.5 Change of FOS with time for unsaturated soil slope during a period of rainfall (after Hamdhan and Schweiger, 2011).

9.3.2. The approach used in the analyses

Seepage analyses

The investigation concerns an experimental embankment presented in figure 9.6 which is subjected to extreme weather event corresponding to hydraulic condition that the samples in laboratory where subjected to. The slope was filled independently with soil material as

tested and presented in previous chapters, adopting the hydro-mechanical parameters defined ich chapters 5, 6, 7 and 8. The adopted rainfall data is presented in table 9.1.

Table 9.1 Precipitation data adopted for modeling.

Scenario no	95 %rainfall intensity (mm/hr)	95 % rainfall intensity (m/s)	Maximum rainfall intensity (mm/hr)	Maximum rainfall intensity (m/s)
1	7.5	2.08×10^{-6}	50.5	1.420×10^{-5}
2	9.5	2.63×10^{-6}	60.00	1.667×10^{-5}
3	11.25	3.12×10^{-6}	70.5	1.95×10^{-5}
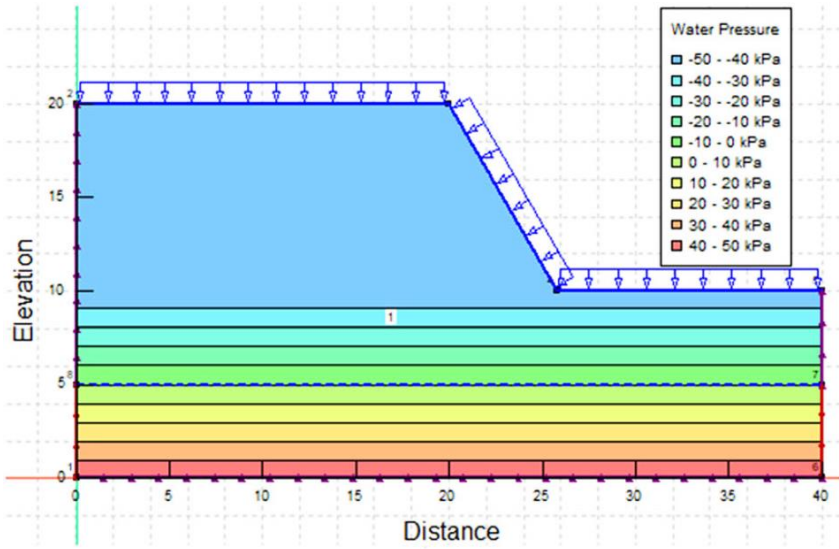
Figure 9.6 Experimental slope used in the seepage and slope stability analyses.

Using the SEEP/W computer program of the Geostudio software, an unsaturated/saturated transient seepage analysis were performed. In order to conduct the analysis in a more realistic manner, it is carried out over a period of five days, during which the first 24 hours of rainfall are recorded. The initial condition for the analysis is represented by the location of the initial ground water table with a maximum negative pore water pressure head assigned to it. The transient SEEP/W program is based on Darcy's law. With the exception of the fact that hydraulic conductivity varies with soil water content when the soil is unsaturated, this equation holds true in both saturated and unsaturated environments. The general governing differential equation for two-dimensional seepage is as follows:

$$\frac{\partial}{\partial x}\left(k_x \frac{\partial H}{\partial x}\right) + \frac{\partial}{\partial y}\left(k_y \frac{\partial H}{\partial y}\right) + Q = \frac{\partial \theta}{\partial t}$$

(9.5)

where H is the total head, k_x and k_y are hydraulic conductivity in x and y direction, Q is applied boundary flux, h is volumetric water content and t is time.

The pore air pressure is assumed to be constant at atmospheric pressure under transient conditions. So, pore water pressure (u_w) controls the change in volumetric water content. Therefore, the following form is a reduction of the equation utilised in the SEEP/W finite element computer program:

$$\frac{\partial}{\partial x}\left(k_x \frac{\partial H}{\partial x}\right) + \frac{\partial}{\partial y}\left(k_y \frac{\partial H}{\partial y}\right) + Q = m_w \gamma_w \frac{\partial H}{\partial t}$$

(9.6)

where m_w is the slope of storage curve.

Determining the characteristics of the material or soil and the boundary conditions is necessary before seepage analysis. The volumetric water content (VWC) function, also known as the soil water characteristic curve (SWC) and the hydraulic conductivity function (HCF), take into account the unsaturated/saturated material model to determine the attributes of the soil. The four built-in Geostudio software functions—VWC data point function, Sample functions, Van Genuchten function, and Fredlund-Xing function—can be used to build the volumetric water content function. However in this case the hydraulic characteristics were based on the laboratory analyses using different methods presented in previous chapters. The numerical analyses using SEEP/W requires applying boundary conditions that have to be specified. For this particular study the boundry conditions are: Rainfall intensity is applied as a flux boundary condition on the slope's surface; total head boundary condition is applied on the slope's sides below the ground water table; and nodal flux Q = 0 m^3/c, which represents no flow boundary condition, is applied on the slope's sides above the ground water table.

Slope stability analyses

The SLOPE/W computer program uses the seepage analysis results, which are produced as the distribution of pore water pressure. Utilising the Mohr-Coulomb failure model, the Geostudio SLOPE/W program yields the unsaturated shear strength. This model provides two methods for simulating the impact of matric suction on soil shear strength. To calculate the mobilised shear stress at the slice base, the first technique uses an angle to quantify the strength increase caused by matric suction. The following equation is employed by SLOPE/W when applying this approach:

$$\tau = c' + (\sigma_n - u_a)\tan\varphi' + (u_a - u_w)\tan\varphi^b$$

$$(9.7)$$

where c' is effective cohesion, σ_n is total normal stress, u_w is pore water pressure, u_a is pore air pressure, φ' is effective friction angle and φ^b is the angle defining increase in strength due to matric suction. All the parameters used in the computations derive from laboratory testing performed in Chapter 7 and 8. In the capillary saturated zone, where φ^b is equal to φ' (effective friction angle) and decreases as the soil becomes saturated, the value of φ^b is regarded constant in this equation, however it varies with the degree of saturation. Thus, it may be concluded that φ^b has to do with the SWRC, or volumetric water content function. Vanapalli et al. (1996) therefore provide an alternative approach that makes use of the relationship between φ^b and SWCC. Here is how the equation is expressed:

$$\tau = c' + (\sigma_n - u_a)\tan\varphi' + (u_a - u_w)\left[\left(\frac{\theta_w - \theta_r}{\theta_s - \theta_r}\right)\tan\varphi'\right]$$

$$(9.8)$$

The factor of safety can now be formulated as:

$$\text{FOS} = \frac{\sum \tau_r}{\sum \tau_m}$$

$$(9.9)$$

Where, τ_r stand for shear stresses resistance and τ_m is mobilized shear stresses.

There are four limit equilibrium methods in the SLOPE/W program that can be used to perform slope stability; these approaches differ in how they handle inter-slice forces. The force and moment equilibrium equations were both satisfied by the Morgenstern and Price technique, which also provides a relationship between the inter-slice forces. The premise of Janbu's simplified approach is that inter-slice forces are horizontal and only force equilibrium equations are satisfied. The Fellinius technique relies on the supposition that the moment equilibrium equation is the sole one satisfied and that there are no inter-slice forces. Bishop's reduced approach alone satisfied the moment equilibrium equation and also assumed horizontal inter-slice tensions.

9.3.3. Results and discussion

The findings are shown as changes in the distribution of pore water pressure within the soil over time, changes in FOS over time, and relative changes in FOS depending in applied rainfall intensity for slopes filled with different soil type. Based on these findings, a parametric

analysis is also carried out to clarify how variations in pore water pressure and the ensuing shift in the safety factor relate to the characteristics of the slope, the soil, and the intensity of the rainfall.

Time dependent PWP change

Plots of the PWP change over time for cohesive and granular soil are shown in Figs. 9.7 and 9.8. It is observed that for all three analysis periods at the 95 percentile and maximum rainfall intensity, respectively, the PWP at the soil surface for sandy soil slopes became zero after 7 hours and 1 hour of continuous rainfall. Both at the greatest intensity of rainfall and at 95%, the relative shift in PWP distribution is mild. For sandy clay soil, on the other hand, the PWP at the soil surface approaches zero (8.77 kPa) at the end of the rainy event (after 24 hours of rainfall) at 95% rainfall intensity and at the beginning of the rainfall event (after 2 hours) at maximum intensity. The quick loss of matric suction among soil particles is the cause of this early saturation of granular soil. For this soil, the relative variations in PWP are likewise negligible.
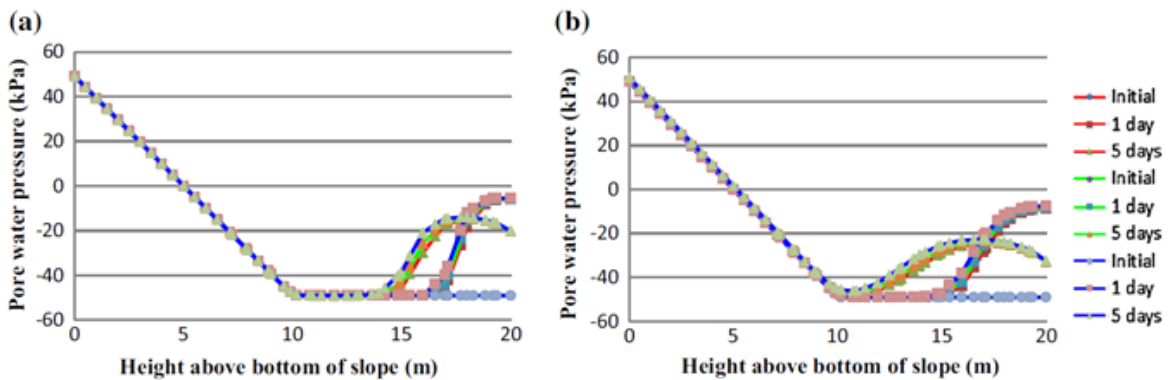
Figure 9.7 PWP distribution within the slope at 95% rainfall intensity a) for granular soil; b) for sandy clay.
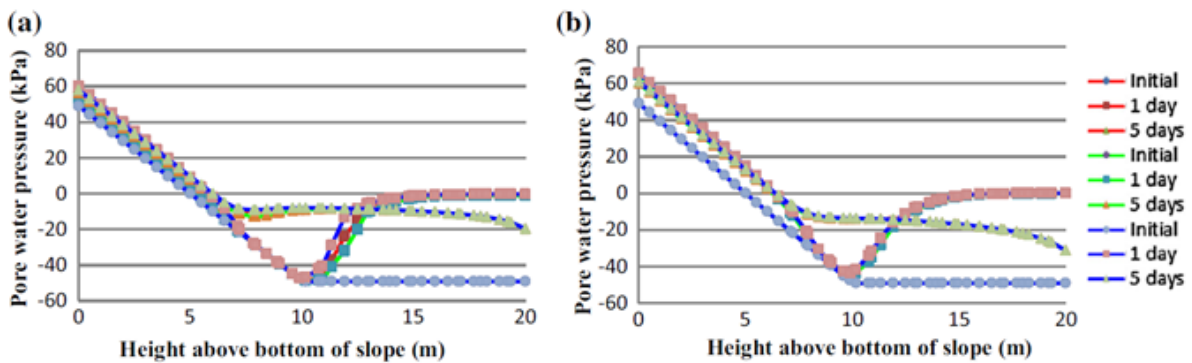
Figure 9.8 PWP distribution within the slope at maximum rainfall intensity a) for granular soil; b) for sandy clay.

FOS changes in time

Table 9.3 provides a comparison of FOS for the two types of soil. The percentage decrease in FOS for granular soil from its original value is found to be, for all scenario assessments, 1.98%, 2.2%, and 2.53% at 95% rainfall intensity and 20.59%, 20.15%, and 21.49% at maximum rainfall intensity. In comparison to the minimal FOS for the first scenario, the relative decrease in FOS for the second and third scenarios is 0.22% and 0.56% at 95% rainfall intensity and 2.13% and - 4.4% at maximum rainfall intensity. As opposed to this, for cohesive soil, the percentage drop in FOS from the starting value is, for each scenario, 5.01%, 5.63%, and 6.61% at 95% rainfall intensity and 33.62%, 33.44%, and 33.79% at maximum rainfall intensity. Furthermore, in comparison to the minimum FOS for the first scenario analysis, the relative change in FOS for the period of the second and third scenarios is 0.65% and 1.68%, respectively, at 95% rainfall intensity and -0.28% and 0.24%, respectively, at maximum rainfall intensity. It is evident that, in the scenario of the lowest intensity of precipitation, there is a negligible change in FOS for both types of soils at this area's maximum rainfall intensity (Figs. 9.9, 9.10).

Table 9.2 Factors of Safety of analyzed slope for different rainfall intensity and soil types.

Scenario no	Granular soil			Cohesive soil		
	Initial FOS	Min FOS		Initial FOS	Min FOS	
	95% and ax intensity	At 95% rainfall intensity	at maximum rainfall intensity	At 95% and maximum rainfall intensity	At 95% rainfall intensity	at maximum rainfall intensity
1	1.34	1.33	1.08	1.77	1.59	1.11
2	1.34	1.32	1.07	1.77	1.58	1.12
3	1.34	1.31	1.05	1.77	1.55	1.10
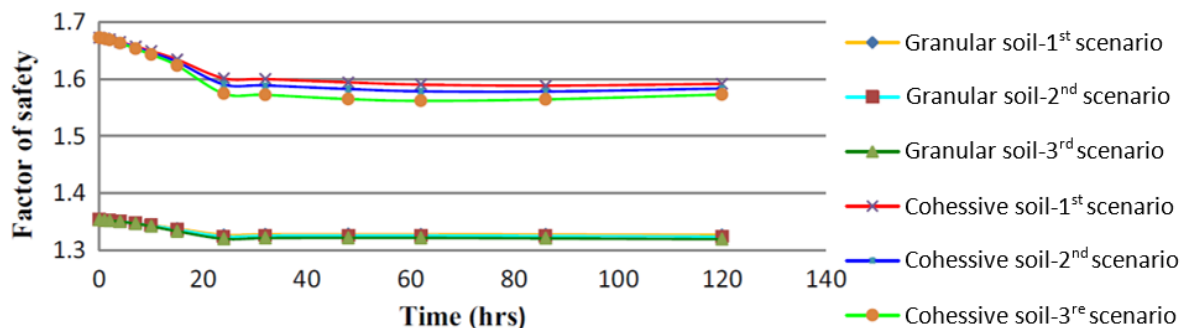
Figure 9.9 FOS results at 95% rainfall intensity for both types of soil.
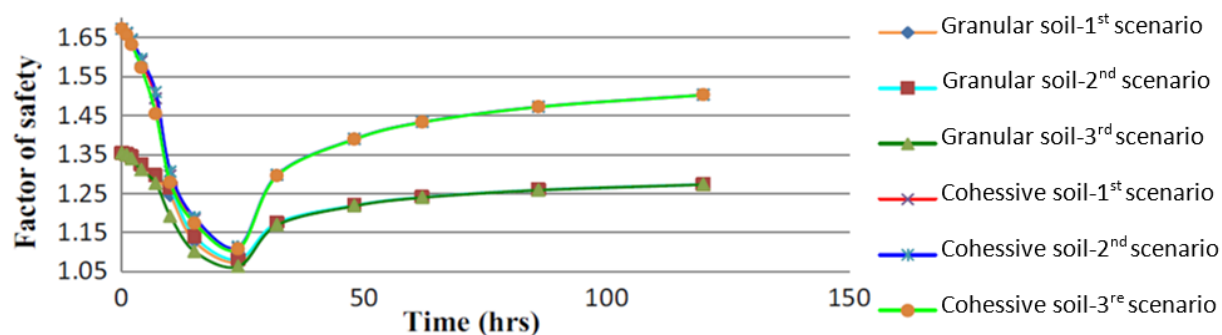
Figure 9.10 FOS results at maximum rainfall intensity for both types of soil.

Soil properties influence

The conducted analysis demonstrate how soil parameters affect the distribution of PWP and the FOS of soil slope. Two distinct soil types are analysed, with the assumption that the slope's properties remain constant. Given identical circumstances, granular soil slopes will see a greater infiltration of water than cohesive soil slopes, which will cause a greater decrease in FOS. The initial values of FOS for cohesive soil are 1.77 and granular soil are 1.34, according to the observations. The results show that the effects of soil properties are responsible for the observed behaviour. For sandy slopes, PWP at the soil surface reaches zero after seven hours of continuous rainfall, while for clayey soil slopes, PWP reaches a near-zero value even at the end of the rainfall event under 95 percentile rainfall intensity. For sandy soil slopes, the PWP at the soil surface reaches zero after one hour of continuous rainfall; however, for cohesive soils under maximum rainfall intensity, this number becomes zero after two hours of continuous rainfall. When the first analytical scenario is taken into account, the values of FOS for cohesive soil and granular soil under 95% rainfall intensity are 1.59 and 1.33, respectively. Additionally, for cohesive and granular soil, the value of FOS increases to 1.10 and 1.05 under maximum rainfall intensity, respectively.

10. Final conclusions and further research recommendation

10.1. Conclusions

Embankments and cut-offs constitute a significant portion of modern infrastructure, making it critical to understand how climate change will impact these structures. Equally important is the consideration of natural slopes in urbanized areas, as rapidly changing weather patterns in recent decades have led to severe human and economic losses.

The present research aims to anticipate and mitigate infrastructure failures associated with climate change. The thesis is divided into three major sections:

Hydraulic Behavior of Fill Materials: This section examines the hydraulic behavior of sandy clay and fine sand by analyzing soil water retention curves (SWRCs) using various laboratory methods. The study utilized modified pore water pressure (PWP) transducers and a continuous wetting-drying tensiometer stage—both developed by the author as part of an international research team working in a diverse academic environment through funded projects.

Mechanical Behavior of Soils: The second section investigates the mechanical behavior of two different soil types under varying water content. Soil suction was applied or controlled during triaxial tests conducted in a double-cell rig and a Bishop-Wesley chamber. The study explored how the mechanical properties of soils are influenced by their unsaturated conditions.

Slope Stability Analysis: The final section focuses on calculating the factor of safety and modeling pore water pressure (PWP) distributions in an experimentally modeled slope. Data from laboratory tests were integrated into the slope stability analysis. Throughout this section, the author aimed to demonstrate the hypothesis that soil properties, under various saturation states, play a critical role in selecting the appropriate geotechnical parameters for slope stability analysis. The thesis attempts to confirm that an interdisciplinary approach to stability analysis—one that accounts for the interactions between climate change, geotechnical parameters, and soil saturation—is essential for understanding slope behavior under different weather scenarios. To achieve the overarching goals of the thesis, several objectives were pursued, including:

- Assessing the effects of climate change on the stability of engineered earth structures.
- Investigating the hydro-mechanical behavior of fill materials, specifically sandy clay and fine sand, through unsaturated condition laboratory testing.
- Evaluating soil water retention characteristics (SWRCs) for cohesive and granular soils.
- Analyzing the impact of wetting-drying cycles on soil suction and mechanical strength, using newly developed instruments.
- Determining the mechanical behavior of soils under unsaturated conditions, examining how factors such as initial compaction, wetting-drying cycles, and water content influence shear strength and volumetric changes.
- Conducting numerical modeling of slope stability during simulated rainfall events, using laboratory data to predict changes in the factor of safety and pore water pressures.

Contributing to an interdisciplinary approach for predicting geotechnical failures by incorporating both hydrological and geotechnical insights to improve the long-term safety and cost-effectiveness of earth infrastructure under changing climatic conditions.

The current study focuses on understanding the hydro-mechanical behavior of fill materials used in construction under unsaturated conditions, with an emphasis on how changing atmospheric conditions, particularly precipitation affect the long-term serviceability and safety of earth structures. To answer nowadays geotechnical challenges such as slope stability analyses of slopes affected by changing weather events the author of the thesis conducted a research that allow formulating general conclusions.

The study highlight the importance of accurate mechanical and hydraulic parameters testing in understanding soil behavior under varying water content and suction conditions. For this purpose an innovative measurement system, employing high-capacity tensiometers and electronic balance equipped with LVDT transducers was employed. It offers determination of more comprehensive soil water retention curve (SWRC) data by continuously measuring water content, suction, and volume changes. This system enhances the accuracy of soil-water relationship assessments by integrating volumetric responses, which are often overlooked in traditional methods like pressure plate tests. The study confirms that results obtained from tensiometers and traditional pressure plate tests differ and divergence is attributed to varying volumetric responses during testing. The pressure plate method exhibits less volume change, leading to different degrees of saturation and gravimetric water content at the same suction levels compared to tensiometer results. The findings highlight the importance of incorporating volumetric measurements in SWRC assessments. In addition modified pore pressure transducers were used to analyze fine sand's hydraulic behavior, revealing that suction did not significantly change despite large variations in moisture content. The transitional zone between 8–10 kPa of suction, corresponding to a decrease in water content from 20% to 3%, plays a crucial role in sample preparation for subsequent mechanical tests. This finding aids in understanding soil behavior under unsaturated conditions.

Triaxial tests performed under both saturated and unsaturated conditions (using constant water content for sandy clay) revealed that samples with lower water content and higher suction exhibited increased stiffness and shear strength. The initial compaction conditions, rather than the wetting or drying path, primarily controlled the mechanical response of the material. Samples with lower water contents displayed higher failure and critical strength due to lower degrees of saturation and void ratios.

When performing unsaturated triaxial tests in modified Bishop-Wiseley cell it was observed that the shear strength of the tested fine sand increased with matric suction in a nonlinear manner, with diminishing returns as suction increased. This suggests that matric suction alone

cannot fully explain the rise in shear strength, particularly in the residual zone. Shear strength also increased linearly with net normal stress, indicating that suction affects the internal friction angle. The shear behavior of non-cohesive granular materials was found to be independent of the water flow-induced structure. The preparation of samples with varying water contents did not significantly affect their shear behavior, pointing to other factors beyond the water bridge effect influencing the variance in shear strength across different water content conditions.

The combination of SWRC and triaxial test results provided valuable insights for modeling slope stability under varying weather conditions. This data is critical in predicting the performance of infrastructure slopes under different climatic impacts, emphasizing the importance of hydromechanical characterization for engineering applications.

Further analyses concerned computation of slope stability analyses subjected to different rainfall scenarios. The modeled slopes were filled with the soil material investigated in the first part of the thesis.

In summary, the analyses proved that soil type and rainfall intensity significantly affect the pore water pressure distribution and slope stability, with granular soils being more susceptible to early instability due to faster infiltration and saturation, while cohesive soils retain stability longer under moderate conditions but still face critical failure risks under extreme rainfall.

Granular soils slope experienced a rapid reduction in matric suction due to higher water infiltration rates, resulting in early saturation. Specifically, PWP at the soil surface drops to zero after 7 hours of continuous rainfall, whereas for maximum rainfall intensity the drop down is reached 1 hour. Cohesive soils (sandy clay) demonstrate a slower reduction in PWP, with near-zero PWP occurring at the surface only after 24 hours of rainfall at 95% intensity. However, at maximum rainfall intensity, the PWP reaches near-zero after just 2 hours. While both soil types show similar trends of decreasing FOS with increasing rainfall intensity, granular soils exhibit smaller percentage decreases in FOS at lower rainfall intensities (around 2-3%) compared to cohesive soils, which show slightly higher reductions (5-6%). Cohesive soils start with higher initial FOS values (1.77) compared to granular soils (1.34), indicating inherently better slope stability under dry conditions. However, as rainfall progresses, granular soils experience a more significant reduction in FOS. At maximum rainfall intensity, the FOS for cohesive and granular soils converges to similarly low values (1.10 for cohesive soil and 1.05 for granular soil), indicating that both soil types face significant risk of slope failure under extreme rainfall conditions. For both soil types, the relative changes in FOS are more significant under higher rainfall intensities. At 95% rainfall intensity, the FOS changes for cohesive and

granular soils remain relatively minor, indicating better stability under moderate conditions. However, at maximum rainfall intensity, the relative change in FOS increases significantly for both soils. The parametric analysis reveals that while both cohesive and granular soils are susceptible to slope instability, granular soils are more vulnerable to rapid pore water pressure increases and FOS reductions under heavy rainfall. However, under extreme conditions, both soil types are at risk of failure, emphasizing the importance of understanding soil properties and rainfall intensity in slope stability assessments.

10.2. Further research recommendations

Although the thesis successfully achieved its planned objectives, further insight into the modeling aspect is still needed. Future research should focus on developing models capable of predicting the time scale and likelihood of failures caused by rapidly changing climatic conditions. This may require testing on a real-scale slope where a landslide has already occurred or on an experimental embankment driven to failure. In such cases, more sophisticated fully coupled models or even new models would be needed. Another key milestone would be validating the thesis's proposed laboratory testing approach in real-world scenarios. This validation would help confirm the accuracy of the research methodology, which aims to develop early warning systems for natural disasters, an initiative the author is currently involved in. Further research in unsaturated soil mechanics and slope stability analyses should focus on several key areas to address current challenges and improve predictive capabilities for slope failure under various conditions. When it comes to laboratory testing and analyses the focus should be placed on capturing nonlinear soil behavior under transient conditions where soil properties may change dynamically. Another aspect is integration of thermo chemical, and biological processes. Unsaturated soil behavior is influenced by thermal changes, chemical reactions, and biological factors (e.g., root reinforcement). Further research should incorporate these multi-physics processes into slope stability analyses, particularly for regions where temperature fluctuations or chemical weathering play a critical role in slope instability. The approach investigating multiscale influences (macro and micro) is also one of the nowadays field of interests. Linking micro-scale soil particle interactions with macro-scale slope stability can deepen our understanding of how changes at the microscopic level influence overall slope behavior. By addressing these research areas, the field of unsaturated soil mechanics and slope stability analyses can advance toward more accurate and sustainable solutions for mitigating slope failure risks, especially in the context of changing environmental conditions.

References

Al-Khafaf, S. and Hanks, R. J., (1974) Evaluation of the Filter Paper Method for Estimating Soil Water Potential, Soil Science, Vol. 117, No. 4, pp. 194–199.

Al Mukhtar, M., Robinet, J. C. and Liu, C. W. (1993). Hydro-mechanical behaviour of partially saturated low porosity clays. Engineering fills (eds. B.G. Clarke, C.J.F.P. Jones, and A.I.B. Moffat) Thomas Telford, London, 87-98

Alonso E. E., Gens A. and Josa A. (1990). A constitutive model for partially saturated soils. Geotechnique 40, No. 3, 405-430.

Anderson, M. G., & Kemp, M. J. (1991). Towards an improved specification of slope hydrology in the analysis of slope instability problems in the tropics. Progress in Physical Geography, 15(1), 29-52.

Barbour, S. L. (1998). Nineteenth Canadian Geotechnical Colloquium: the soil–water characteristic curve, a historical perspective. Can. Geotech. J. 35, No. 5, 873–894.

Barbour, S. L., Fredlund, D. G., & Pufahl, D. E. (1992). The osmotic role in the behavior of swelling clay soils. In Mechanics of swelling: From clays to living cells and tissues (pp. 97-139). Springer Berlin Heidelberg.

Bishop, A. W. and Donald, I. B. (1961). The experimental study of partly saturated soils in the triaxial apparatus. Proc. 5th Int. Conf. Soil Mech. Found. Engng, Paris 1, 13–21.

Black D. K. and Lee K. L. (1973), Saturating Laboratory Samples by Back Pressure, ASCE Journal Soil Mech. Found. Eng. Div., Vol. 99, SM1, pp. 75-95.

Blatz, J. A. and Graham, J. (2003). Elastic-plastic modelling of unsaturated soil using results from a new triaxial test with controlled suction. Geotechnique 53, No. 1, 113-122

Blight, G. E. (1967). Effective stress evaluation for unsaturated soils. ASCE Journal of Soil Mechanics and Foundations Engineering Division, vol. 93, SM2, 25-148.

Brackley, G. K. (1987). SCS inventory and classification procedures. In Proceedings— pinyon–juniper conference. General Technical Report INT-215. USDA Forest Service, Ogden, Utah, USA (pp. 231-235).

Brand, E. W. 1981. Some Thoughts on Rainfall-Induced Slope Failures. Proceedings of the 10th International Conference on Soil Mechanics and Foundation Engineering,

Stockholm, 3, 373-376.

British Standard Institute (1990), BS 1377-4: Methods of test for Soils of civil engineering purposes Part 4: Compaction-related tests, BSI, Milton Keynes.

Briggs, K., Smethurst, J., Powrie, W. & O ' Brien, T. 2016. Interpreting the influence of tree root water uptake on the long term hydrology of a clay fill railway embankment. Transportation Geotechnics, 9, 31 – 48.

British Standards Institution, British Standard Methods of Test for Soils for Civil Engineering Purposes: Part 1, General requirements and sample preparation. British Standards Institution, London (BS1377), (1990

Brocca, L., Ponziani, F., Moramarco, T., Melone, F., Berni, N., & Wagner, W. (2012). Improving landslide forecasting using ASCAT-derived soil moisture data: A case study of the Torgiovannetto landslide in central Italy. Remote sensing, 4(5), 1232-1244.

Bulut, R., Leong, E. C. (2008). Indirect measurement of suction. Geotech. Geol. Eng. Vol.26, N. 6, pp. 633-644.

Bulut, R., Lytton R. and Wray W. (2001) Suction measurements by filter paper method. American Society of Civil Engineers Geotechnical Special Publication No.115 pp 243-261.

Burland, J.B., (1965a). The yielding and dilation of clay. Correspondence. Geotechnique, 15, 211-214.

Cavarretta, I. (2009). The influence of particle characteristics on the engineering behaviour of granular materials (Doctoral dissertation, Imperial College London (University of London)).

Chandler, R. J., Crilly, M. S., and Montgomery-Smith, G., (1992). A Low Cost Method of Assessing Clay Desiccation for Low- Rise Buildings, Proceedings of the Institution of Civil Engineers, Vol. 92, No. 2, pp. 82–89

Chandler, R. J. and Gutierrez, C. I. (1986). The filter paper method of suction measurement. Geotechnique, vol. 36, n.2, 265-268

Chatterjea, K. (1990). Observations on the fluvial and slope processes in Singapore and their impact on the urban environment. PhD thesis, Hong Kong.

Chatterjea, K (1994) Dynamics of Fluvial and Slope Processes in the Changing Geomorphic Environment of Singapore, Earth Surface Processes and Landforms, Vol. 19, pp. 585-607

Colmenares-Montanez, J.E., (2002). Suction and volume changes of compacted sandbentonite mixtures. PhD thesis, University of London (Imperial College), London, UK.

Croney, D. (1958). The movement and distribution of water in soils. Geotechnique, 3(1):1–16.

Cunningham, M. R. (2000). The mechanical behaviour of a reconstituted, unsaturated soil. Ph.D. thesis, Imperial College of Science, Technology and Medicine, University of London.

Cui Y. J. and Delage P. (1996). Yielding and plastic behaviour of an unsaturated compacted silt. Geotechnique 46, 291-311.

Cui, Y.J., Tang, A.M., Mantho, A.T. and De Laure, E. (2008). Monitoring field soil suction using a miniature tensiometer. Geotechnical Testing Journal 31 (1), 95–100.

Cunningham, M. R., Ridley, A. M., Dineen, K. and Burland, J. J. (2003). The mechanical behaviour of a reconstituted unsaturated silty clay. Geotechnique 53, No. 2, 183–194

Dahigamuwa, T., Gunaratne, M., & Li, M. (2018). An Improved Data-Driven Approach for the Prediction of Rainfall-Triggered Soil Slides Using Downscaled Remotely Sensed Soil Moisture. Geosciences, 8(9), 326.

Day, R. W., & Axten, G. W. (1989). Surficial stability of compacted clay slopes. Journal of Geotechnical Engineering, 115(4), 577-580.

Delage P., Romero E.E., Tarantino A. (2008) Recent developments in the techniques of controlling and measuring suction in unsaturated soils 1st European Conference on Unsaturated Soils, Durham, UK, 33-52

Deutscher, M. S., Gasmo, J. M., Rahardjo, H., Leong, E. C., & Tang, S. K. (2020). Field measurements of pore-water pressure profiles in residual soil slopes of the Bukit Timah Granite Formation, Singapore. In Unsaturated Soils for Asia (pp. 777-782). CRC Press.

Dijkstra, T. & Dixon, N. 2010. Climate change and slope stability in the UK: challenges and approaches. Quarterly Journal of Engineering Geology and Hydrogeology, 43, 371 – 385,

Dineen K. (1997). The influence of suction on compressibility and swelling. Ph.D. thesis,

Imperial College of Science, Technology and Medicine, University of London.

Dineen, K. and Burland, J.B. (1995), A new approach to osmotically controlled oedometer testing, Unsaturated Soils, Alonso and Delage (eds), 2, 459-465

Donoghue, A.M. (2006). The performance effects of suction probe saturation in laboratory testing applications, MEng. Report, Durham University.

Dykes, A. P., & Thornes, J. B. (2000). Hillslope hydrology in tropical rainforest steeplands in Brunei. Hydrological Processes, 14(2), 215-235.

EEA 2012. Climate change, impacts and vulnerability in Europe 2012. An indicator-based report. EEA Report, 12/2012. European Environment Agency, Copenhagen.

EEA 2015a. The European environment – state and outlook 2015: synthesis report. European Environment Agency, Copenhagen.

EEA 2015b. Climate change impacts and adaptation. http://www.eea.europa.eu/ soer-2015/europe/climate-change-impacts-and-adaptation [last accessed 1 April 2017].

Fawcett, R.G. and Collis-George, N. (1967). A filter paper method for determining the moisture characteristics of soil. Australian Journal of Experimental Agriculture and Animal Husbandry, n.7, 162-167.

Fourie, A. B. (1996). Predicting rainfall-induced slope instability. Proceedings of the Institution of Civil Engineers-Geotechnical Engineering, 119(4), 211-218.

Fraser, A. (2014). Water retention behaviour of soils, MEng Fi-nal Year Project Report, Durham University.

Fredlund D. G. and Morgenstern N. R. (1977). Stress state variables for unsaturated soils. J. Geotech. Eng. Div., ASCE 103, GT5, 447-466

Fredlund, D. G. and Rahardjo, H. (1993). Soil mechanics for unsaturated soils. New York: Wiley.

Futai, M. M. and Almeida, M. S. S. (2005), An experimental investigation of the mechanical behaviour of an unsaturated gneiss residual soil, Geotechnique 55, No. 3, 201-213

Gallipoli, D., Gens, A., Sharma, R. and Vaunat, J. (2003a). An elasto-plastic model for unsaturated soil incorporating the effects of suction and degree of saturation on mechanical behaviour, Geotechnique 53, No. 1, 123–135

Gallipoli, D., Wheeler, S. J. and Karstunen, M. (2003b). Modelling the variation of degree of saturation in a deformable unsaturated soil. Geotechnique 53, No. 2. 105-112

Gardner, R. (1937). A method of measuring the capillary tension of soil moisture over a wide moisture range. Soil Science, vol. 43, 277-283.

Gasmo, J M (1997) Stability of Unsaturated Residual Soil Slopes as Affected by Rainfall, MEng Thesis, School of Civil and Structural Engineering, Nanyang Technological University.

Gasmo, J., Hritzuk, K. J., Rahardjo, H., & Leong, E. C. (1999). Instrumentation of an unsaturated residual soil slope. Geotechnical Testing Journal, 22(2), 134-143.

Glendinning, S., Hughes, P.N. et al. 2014. Construction, management and maintenance of embankments used for road and rail infrastructure: implications of weather induced pore water pressures. Acta Geotechnica, 9, 799 – 816.

Glendinning, S., Helm, P.R. et al. 2015. Research-informed design, management and maintenance of infrastructure slopes: development of a multi-scalar approach. In: IOP Conference Series, Earth and Environmental Science (EES),26, 012005.

GDS Ltd. 2018. Advanced Triaxial Testing: Part 2. [Online]. Accessible at: www.gdsinstruments.com [12.09.2018].

Hall, W. B., Jackson, J. D., & Watson, A. (1967, September). Paper 3: A review of forced convection heat transfer to fluids at supercritical pressures. In Proceedings of the institution of mechanical engineers, conference proceedings (Vol. 182, No. 9, pp. 10-22). Sage UK: London, England: SAGE Publications.

Hamblin, A.P. (1981). Filter paper method for routine measurements of field water potencial. Journal of Hydrology, 53, 355-360

Hamdhan, I. N., & Schweiger, H. (2011). Slope stability analysis of unsaturated soil with fully coupled-deformation analysis. In Annual Conference of the International Association for Mathematical Geosciences (pp. 1-18). IAMG.

Harrison, B. A. and Blight, G. E., (1998) The Effect of Filter Paper and Psychrometer Calibration Techniques on Soil Suction Measurements, Proceedings of the Second International Conference on Unsaturated Soils, Vol. 1, International Academic Publishers, Beijing, China, pp. 362–367.

Head, K. H. (2006). Manual of soil laboratory testing.

HIGHWAYS AGENCY (1998). Specification for Highway Works. The Stationary Office, London.

Hilf, J. W. (1956). An investigation of pore-water pressure in compacted cohesive soils. Technical Memorandum 654. Denver: US Bureau of Reclamation.

Hodge, R. A. L. & Freeze, A. R. (1977). Groundwater Flow Systems and Slope Stability. Canadian Geotechnical Journal, 14, 466-476.

Hong, Y., Adler, R., and Huffman, G. (2006). Evaluation of the potential of NASA multi-satellite precipitation analysis in global landslide hazard assessment. Geophysical Research Letters, 33

Huat, L. T., Ali, F., & Ibrahim, A. S. (2012). An investigation on one of the rainfall-induced landslides in Malaysia. Electronic Journal of Geotechnical Engineering, 17, 435-449.

Hughes, P. (2005) personal communication.

Hughes, P., Glendinning, S. and Mendes, J. (2007). Construction Testing and Instrumentation of an infrastructure testing embankment, Proc. Expert Symposium on Climate Change: Modelling, Impacts and Adaptations, Singapore, pp. 159-166.

Hughes, P.N., Glendinning, S., Mendes, J., Parkin, G., Toll, D.G., Gallipoli, D., Miller, P. (2009). Full-scale testing to assess climate effects on embankments. Special Issue of Engineering Sustainability, Institution of Civil Engineers, 162, No. ES2, pp. 67-79.

Hughes, P.N., Glendinning, S, Toll, D.G.(2005) REPORT ON THE DESIGN AND CONSTRUCTION OF THE BIONICS EMBANKMENT

Hulme, M., Jenkins, G. J., Lu, X., Turnpenny, J. R., Mitchell, T. D., Jones, R. G., Lowe, J., Murphy, J. M., Hassell, D., Boorman, P., McDonald, R. and Hill, S. (2002) Climate Change Scenarios for the United Kingdom: The UKCIP02 Scientific Report. Tyndall Centre for Climate Change Research, School of Environmental Sciences, University of East Anglia, Norwich, UK.

IPCC 2013. Climate Change 2013: The Physical Science Basis. Contribution of Working Group I to the Fifth Assessment Report of the Intergovernmental Panel on Climate Change (Stocker, T.F., Qin, D. et al. (eds)). Cambridge University Press, Cambridge.

IPCC 2014. Climate Change 2014: Synthesis Report. Contribution of Working Groups I, II and III to the Fifth Assessment Report of the Intergovernmental Panel on Climate Change (Pachauri, R.K. & Meyer, L.A. (eds)). IPCC, Geneva.

Jenkins, G.J., Perry, M.C. & Prior, M.J. 2008. The Climate of the United Kingdom and Recent Trends. Met Office Hadley Centre, Exeter. Jotisankasa, A. (2005), Collapse behaviour of a compacted silty clay, PhD Thesis, Imperial College.

Jotisankasa, A. (2005). Collapse behaviour of a compacted silty clay (Doctoral dissertation, University of London).

Karube, D., Kato, S., Hamada, K. and Honda, M., (1995). The relationship between the mechanical behaviour and the state of pore water in unsaturated soil. Accepted for publication in JSCE Journal of Geotechnical Engineering.

Khalili, N., Habte, M. A., & Zargarbashi, S. (2008). A fully coupled flow deformation model for cyclic analysis of unsaturated soils including hydraulic and mechanical hystereses. Computers and Geotechnics, 35(6), 872-889.

Koda, E., & Osiński, P. (2015). Application of alternative methods of slope stability improvement on landfills.

König, D., Jessberger, H.L., Bolton, M.D., Phillips, R., Bagge, G., Renzi, R., Garnier, J. 1994. Pore pressure measurement during centrifuge model tests: Experience of five laboratories. In Centrifuge '94. Rotterdam: Balkema, pp. 101–108.

Krahn, J., Fredlund, D. G., & Klassen, M. J. (1989). Effect of soil suction on slope stability at Notch Hill. Canadian Geotechnical Journal, 26(2), 269-278.

Li, X. (1995). Slope Stability in Unsaturated Residual Soils due to Rainfall (Doctoral dissertation, PhD thesis proposal, School of Civil and Structural Engineering, Nanyang Technological University, Singapore).

Leach, B., & Herbert, R. (1982). The genesis of a numerical model for the study of the hydrogeology of a steep hillside in Hong Kong. Quarterly Journal of Engineering Geology and Hydrogeology, 15(3), 243-259.

Lee, H.V., Wray, W.K. (1995). Techniques to evaluate soil suction – a vital unsaturated soil water variable. Unsaturated soils, Alonso and Delage (eds) 2, 615-622.

Leong E. C., He L., and Rahardjo H. (2002) Factors Affecting the Filter Paper Method for

Total and Matric Suction Measurements. J Geotechnical Testing, Vol. 25, No. 3 pp 321-332.

Liew ShawShong, L. S. (2004). Slope failures in tropical residual soils.

Likos, W. J. (2000). Total suction-moisture content characteristics for expansive soils. *2000-2009-Mines Theses & Dissertations*.

Lim, T T (1995) Shear Strength Characteristics and Rainfall-Induced Matric Suction Changes in a Residual Soil Slope, MEng Thesis, School of Civil and Structural Engineering, Nanyang Technological University, Singapore

Lim, T T, Rahardjo, H, Chang, M F and Fredlund, D G (1996) Effect of Rainfall on Matric Suctions in a Residual Soil Slope, Canadian Geotechnical Journal, Vol. 33, pp. 618-628.

Lourenço, S.D.N., Gallipoli, D., Toll, D.G. and Evans, F. D., (2006). Development of a commercial tensiometer for triaxial testing of unsaturated soils. In Fourth International Conference on Unsaturated Soils, Carefree – Arizona – USA, Geotechnical Special Publication No. 14., Reston: ASCE, Vol.2, pp. 1875-1886.

Lourenço, S.D.N. (2008). Suction Measurements and Water retention in unsaturated soils, Phd Dissertation, Durham University

Lourenço, S. D. N., Gallipoli, D., Toll, D. G., Augarde, C. E., & Evans, F. D. (2011). A new procedure for the determination of soil-water retention curves by continuous drying using high-suction tensiometers. Canadian geotechnical journal, 48(2), 327-335.

Low, T. H., Faisal, H. A., & Saravanan, M. (2020). Suction and infiltration measurement on cut slope in highly heterogeneous residual soil. In Unsaturated Soils for Asia (pp. 807-811). CRC Press.

Macari, E. J., Laymon, C. A., & Costes, N. C. (1992). Hydrologic field instrumentation for a small-scale experiment with implications for rain-induced slope stability analyses. In US-Brazil NSF Geotechnical Workshop on Applicability of Classical Soil Mechanics Principles to Structured Soils (pp. 79-88).

Marinho, F.A.M. (1994). Medição de sucção com o método do papel fitro. Proc. X Congresso Brasileiro de Mecanica dos Solos e Engenharia de Fundações. Vol 2, 516522.

Matziaris, V., Marshall, A.M., Yu, H.S. 2015. Centrifuge model tests of rainfall–induced landslides. In Recent Advances in Modeling Landslides and Debris Flows. Cham:

Springer, pp. 73–83.

Matziaris, V., Osinski, P., Vimalan, J., & Koda, E. (2023). Soil water retention curve of silty sand–experimental investigation using different laboratory methods. In E3S Web of Conferences (Vol. 382, p. 25005). EDP Sciences.

Matsui, T., San, K. C., Amano, T., & Otani, Y. (1988). Field measurement on a slope cutting with tensile inclusions.

McQueen, I. S. and Miller, R. F., (1968b) Calibration of a Wide-Range Gravimetric Method for Measuring Moisture Stress, Soil Science, Vol. 106, No. 3, pp. 225–231.

McKeen, R. G., (1980) Field Studies of Airport Pavements on Expansive Soils, 4th International Conference on Expansive Soils, pp. 242–261.

Mendes, J. (2011). Assessment of the impact of climate change on an instrumented embankment: an unsaturated soil mechanics approach (Doctoral dissertation, Durham University).

Mendes, J., & Toll, D. G. (2016). Influence of initial water content on the mechanical behavior of unsaturated sandy clay soil. International journal of geomechanics, 16(6), D4016005.

Nattrass, W. (2009) personal communication

Noguchi, T. (2009) Comparison of Major Suction Measurement Techniques Used to Determine the Soil Water Retention Curves, MEng Final Year Project Report, Durham University.

Oldecop, L.A. and Alonso E.E. (2000), A model for rockfill compressibility, Geotechnique 51, No. 2, 127-139

Osinki, P., Toll, D.G., Koda E. 2016. Comparison of Soil Water Retention Curves for sandy clay, obtained using different laboratory testing methods. In Proceedings of 3rd European Conference on Unsaturated Soils. Paris, France, 12th of September: École des Ponts ParisTech.

Osiński, P., Dobrzelewski, B., Koda, E., & Król, P. (2020). Slope stability analyses incorporating soil improvement methods for valuable urban area. In Geotechnics for Sustainable Infrastructure Development (pp. 803-808). Springer Singapore.

Osinski, P., Matziaris, V., & Koda, E. Soil water retention behaviour of granular soil–modified pore pressure transducer tests. Mendelnet, 2017,edition: vol. 24

Osinski, P., Toll, D., & Koda, E. (2016). Comparison of Soil Water Retention Curves for sandy clay, obtained using different laboratory testing methods. In E3S Web of Conferences (Vol. 9, p. 11008). EDP Sciences.

Osinski, P., Rickson, R. J., Hann, M. J., & Koda, E. (2014). Assessment of slope stability influenced by vegetation coverand additional loads applied. Annals of Warsaw University of Life Sciences-SGGW. Land Reclamation, 46(2).

Öberg, A. L., & Sällfors, G. (1997). Determination of shear strength parameters of unsaturated silts and sands based on the water retention curve. Geotechnical Testing Journal, 20(1), 40-48.

Pitts, J. (1985). An investigation of slope stability on the NTI campus, Singapore.

Polemio, M., & Petrucci, O. (2000). Rainfall as a landslide triggering factor an overview of recent international research. In Landslides in research, theory and practice. Thomas Telford Ltd.

Premchitt, J., Brand, E. W., & Chen, P. Y. M. (1994). Rain-induced landslides in Hong Kong, 1972–1992. Asia Engineer, 43, 51.

Rahardjo, H., Leong, E. C., Gasmo, J. M., & Tang, S. K. (1998). Assessment of rainfall effects on stability of residual soil slopes. In Proceedings of the second international conference on unsaturated soils UNSAT (Vol. 98, pp. 78-83).

Rahardjo, H., Li, X. W., Toll, D. G., & Leong, E. C. (2001). The effect of antecedent rainfall on slope stability. Unsaturated soil concepts and their application in geotechnical practice, 371-399.

Rahardjo, H., & Leong, E. C. (2006). Shear strength and pore-water pressure characteristics during constant water content triaxial tests. Journal of Geotechnical and Geoenvironmental Engineering, *132*(3), 411-419.

Rahim, M.D. Syazwan. (2016). Hydro-mechanical behaviour of a residual soil slope in Malaysia. Doctoral dissertation, Durham University, UK.

Rassam, D. W., & Cook, F. (2002). Predicting the shear strength envelope of unsaturated soils. Geotechnical Testing Journal, 25(2), 215-220.

Ray, R. L., & Jacobs, J. M. (2007). Relationships among remotely sensed soil moisture, precipitation and landslide events. Natural Hazards, 43(2), 211-222.

Ray, R. L., Jacobs, J. M., & Cosh, M. H. (2010). Landslide susceptibility mapping using downscaled AMSR-E soil moisture: A case study from Cleveland Corral, California, US. Remote sensing of environment, 114(11), 2624-2636.

Richards, S.J., (1965). Soil suction measurements with tensiometers. In: Methods of Soil Analysis, Monograph No. 9, American Society of Agronomy, Madison, 153-163.

Ridley, A. M., Dineen, K., Burland, J. B. and Vaughan P. R. (2003). Soil matrix suction: some examples of its measurement and application in geotechnical engineering. Geotechnique 53, No. 2, 241–253

Ridley, A.M. and Burland, J.B., (1993). A new instrument for the measurement of soil moisture suction. Geotechnique, 43, No. 2, 321-324.

Ridley, A. M. and Wray, W. K. (1996). Suction measurement: theory and practice. A state-ofthe-art-review. Proc. 1st Int. Conf. Unsaturated Soils, Paris 3, 1293–1322. Roscoe, K.H. and Burland, J.B., (1968). On the generalised stress-strain behaviour of "wet" clay. Engineering Plasticity (Heyman, J. and Leckie F.A., eds.) Cambridge University Press, Cambride, 535-609.

Roscoe, K. H., and Burland, J. B. (1968). On the generalised stress-strain behaviour of wet clay. Engineering plasticity, J. Heyman and F. A. Leekie, eds., Cambridge University Press, Cambridge, U.K.

Sadrekarimi, A. (2016). Effect of ambient temperature variation on triaxial shear testing of sands. Geotechnical Testing Journal, *39*(4), 624-632.

Sayers, P., Walsh, C. & Dawson, R. 2015. Climate impacts on flood and coastal erosion infrastructure. Infrastructure Asset Management, 2, 69 – 83.

Schofield, A. N. and Wroth, C. P. (1968). Critical state soil mechanics, McGraw Hill, London.

Shull, C. A. (1916). Measurement of the surface forces in soils. The Botanical gazette, vol. LXII, n.1, 1-31.

Schuster, R. L. (1996). Landslides: investigation and mitigation. Chapter 2-socioeconomic significance of landslides, No. 247.

Simmon, R. (2007) http://earthobservatory.nasa.gov/Features/LandslideWarning/.

Sivakumar, V. (1993). A critical state framework for unsaturated soil. Ph.D. thesis, University of Sheffield, UK.

Skempton, A. W. (1953), The colloidal activity of clays, Proc. 3rd ICSMFE, Zurich, 1, 57-61.

SMI Soil Mechanics Instrumentation (2004) Manual for the 12-probe transistor psychrometer. Adelaide, South Australia.

Stenke, F., Toll, D.G., and Gallipoli, D. (2006) Comparison of suction measurement techniques for three clayey soils. Proceeding 4th International Conference on Unsaturated Soils, Phoenix, USA, Geotechnical Special Publication No. 14., Reston: ASCE, Vol.2, pp 1451-1461.

Stephenson, I. B. (2008) Pore water pressures in embankments: soil compaction influencing water infiltration and its effect on pore water pressures, Msc dissertation, School of Civil Engineering and Geosciences, Newcastle University.

Stipanovic-Oslakovic, I., ter Maat, H., Hartmann, A. & Dewulf, G. 2012. Climate change and infrastructure performance: should we worry about? Procedia –Social and Behavioral Sciences, 48, 1775 – 1784.

Stirling, R., & Hen-Jones, R. (2015). Investigating geotechnical/geophysical relationships in unsaturated glacial till. *Short Term Scientific Mission Report, EU COST Action TU1202*.

Tan, S. B., Tan, S. L., & Chin, Y. K. (1988). Soil nailing for slope stabilization in Singapore residual soils. In International Conference on Geomechanics in Tropical Soils, 2nd, 1988, Singapore (Vol. 1).

Tang, A. M., Hughes, P. N., Dijkstra, T. A., Askarinejad, A., Brenčič, M., Cui, Y. J., Osinski, P... & Grossi, G. (2018). Atmosphere–vegetation–soil interactions in a climate change context; impact of changing conditions on engineered transport infrastructure slopes in Europe. Quarterly Journal of Engineering Geology and Hydrogeology, 51(2), 156-168.

Tarantino, A. and Mongiovi, L. (2003) Calibration of tensiometer for direct measurement of matric suction. Geotechnique 53, No.1, 137-141

Tarantino, A. and Tombolato, S. (2005) Coupling of hydraulic and mechanical behaviour in unsaturated compacted clay. Geotechnique 55, No. 4, 307-317

Toll, D.G. (1999) A Data acquisition and control system for geotechnical testing. Computing developments in civil and structural engineering (eds. B. Kumar and B.H.V. Topping), Edinburgh: CivilComp Press, pp 237-242.

Toll, D.G. (2001). Rainfall-induced Landslides in Singapore, Proc. Institution of Civil Engineers: Geotechnical Engineering, Vol. 149, No. 4, pp. 211–216.

Toll, D. G. and Ong, B. H. (2003). Critical-state parameters for an unsaturated residual sandy clay. Geotechnique 53, No. 1, 93–103.

Toll, D.G., Lourenço, S.D., Mendes, J. 2013. Advances in suction measurements using high suction tensiometers. Engineering Geology, 165: 29–37.

Toll, D.G., Asquith, J.D, Fraser, A., Hassan, A.A., Liu, G., Lourenço, S.D.N., Mendes, J., Noguchi, T., Osinski, P., Stirling, R.A. (2015). Tensiometer techniques for determining soil water retention curves. In Proceedings of 6th Asia–Pacific Conf. on Unsaturated Soil. Guilin, China, 23–26 of October. London: Taylor & Francis, pp. 15– 22.

Toll, D. G., Rahim, M. M., Karthikeyan, M., & Tsaparas, I. (2015). Soil atmosphere interactions for analysing slopes in tropical soils. In Computer Methods and Recent Advances in Geomechanics: Proceedings of the 14th International Conference of International Association for Computer Methods and Recent Advances in Geomechanics, 2014 (IACMAG 2014) (pp. 1333-1338). Taylor & Francis Books Ltd.

Toll, D. G., Asquith, J. D., Hughes, P. N., & Osinski, P. (2016). Soil water retention behaviour of a sandy clay fill material. Procedia engineering, 143, 308-314.

Tsaparas, I. (2002). Field measurements and numerical modelling of infiltration and matric suctions within slopes (Doctoral dissertation, University of Durham. School of Engineering).

Tsaparas, I., Rahardjo, H., Toll, D.G., Leong, E. (2003) Infiltration characteristics of two instrumented residua soil slopes. Canadian Geotechnical Journal, 40, pp. 1012-1032.

UN Office for Disaster Risk Reduction, "The Human Cost of Weater Related Disasters 1995-2015," 2016.

US Geological. Landslides 101. 2016. [Online]. Available: http://landslides.usgs.gov/learn/ls101.php.

Vargas, j. E. A., Velloso, R. C., De Campos, T. M. P. & Filho, l. M. C. (1990). Saturated-

Unsaturated Analysis of Water Flow in Slopes of Rio De Janeiro, Brazil,. Computers and Geotechnics, 10, 247-261.

Vanapalli, S. K., Fredlund, D. G., Pufahl, D. E., & Clifton, A. W. (1996). Model for the prediction of shear strength with respect to soil suction. Canadian geotechnical journal, 33(3), 379-392.

Van den Hurk, B., Klein-Tank, A. et al. 2006 KNMI Climate Change Scenarios 2006 for the Netherlands. Royal Netherlands Meteorological Institute, Scientific Report, WR-2006-01.

Van Genuchten, M. T. (1980). A closed-form equation for predicting the hydraulic conductivity of unsaturated soils. Soil Sci. Soc. Am. J., pp. 892-898.

Vaquero, J.L. (2007) Soil suction measurement using the pressure plate technique within the MUSE network, Project report, Durham University.

Vaunat, J., Romero, E. and Jommi, C., (2000). An elastoplastic hydromechanical model for unsaturated soils. Proceedings of the International Workshop on Unsaturated Soils, Trento, 121-138.

Weerasinghe, K. M., Gunaratne, M., Ratnaweera, P., & Arambepola, N. M. S. I. (2011). Upgrading of the subjective landslide hazard evaluation scheme in Sri Lanka. Civil Engineering and Environmental Systems, 28(2), 99-121.

Wei, J., Heng, Y. S., Chow, W. C., & Chong, M. K. (1991, December). Landslide at Bukit Batok sports complex. In Proceedings of the 9th Asian regional/geotechnical conference.

Wheeler, S. J., Sharma, R. J. and Buisson, M. S. R. (2003). Coupling of hydraulic hysteresis and stress–strain behaviour in unsaturated soils. Geotechnique 53, No 1, 41-54

Wheeler, S. J. and Sivakumar, V. (1995). An elastoplastic critical state framework for unsaturated soil. Geotechnique 45, No. 1, pp. 35-53.

Woodburn, J.A. and Lucas, B. (1995) New Approaches to the Laboratory and Field Measurement of Soil Suction, Unsaturated Soils. Alonso, E.E. and Delage, P. (eds) Unsaturated Soils (UNSAT 95) Proc. 1st Int. Conf., Paris, France. Rotterdam: Balkema, Vol. 2, pp 667671.

Yamamuro, J. A., & Wood, F. M. (2004). Effect of depositional method on the undrained behavior and microstructure of sand with silt. Soil Dynamics and Earthquake

Engineering, 24(9-10), 751-760.

Yamamuro, J. A., Wood, F. M., & Lade, P. V. (2008). Effect of depositional method on the microstructure of silty sand. Canadian Geotechnical Journal, 45(11), 1538-1555.

Yang, K. S. & Tang, S. K. (1997). Stabilising the Slope of Bukit Gombak. Proceedings of the 3rd Young Geotechnical Engineers Conference, Singapore, 589–605.

Zur, B. (1966). Osmotic control of the matric soil-water potential. Soil Science. 102, 394-398.

List of figures

161

List of tables

Wyrażam zgodę na udostępnienie mojej pracy w czytelniach Biblioteki SGGW w tym w Archivum Prac Dyplomowych SGGW.

…………………………………………….

(czytelny podpis autora pracy)